

**FEASIBILITY OF BOOTSTRAP AGGREGATING FUSION METHOD  
TO ENHANCE EXTREME LEARNING MACHINE FOR REFERENCE  
EVAPOTRANSPIRATION ESTIMATION**

**LAI LIK SHENG**

**A project report submitted in partial fulfilment of the  
requirements for the award of Bachelor of Engineering  
(Honours) Civil Engineering**

**Lee Kong Chian Faculty of Engineering and Science  
Universiti Tunku Abdul Rahman**

**April 2020**

**DECLARATION**

I hereby declare that this project report is based on my original work except for citations and quotations which have been duly acknowledged. I also declare that it has not been previously and concurrently submitted for any other degree or award at UTAR or other institutions.

Signature :  \_\_\_\_\_

Name : Lai Lik Sheng \_\_\_\_\_

ID No. : 1502286 \_\_\_\_\_

Date : 16/5/2020 \_\_\_\_\_

**APPROVAL FOR SUBMISSION**

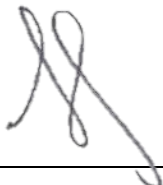
I certify that this project report entitled **“FEASIBILITY OF BOOTSTRAP AGGREGATING FUSION METHOD TO ENHANCE EXTREME LEARNING MACHINE FOR REFERENCE EVAPOTRANSPIRATION ESTIMATION”** was prepared by **LAI LIK SHENG** has met the required standard for submission in partial fulfilment of the requirements for the award of Bachelor of Engineering (Honours) Civil Engineering at Universiti Tunku Abdul Rahman.

Approved by,

Signature :   
\_\_\_\_\_

Supervisor : Ir. Dr. Huang Yuk Feng  
\_\_\_\_\_

Date : 16/5/2020  
\_\_\_\_\_

Signature :   
\_\_\_\_\_

Co-Supervisor : Ir. Dr. Koo Chai Hoon  
\_\_\_\_\_

Date : 16/5/2020  
\_\_\_\_\_

The copyright of this report belongs to the author under the terms of the copyright Act 1987 as qualified by Intellectual Property Policy of Universiti Tunku Abdul Rahman. Due acknowledgement shall always be made of the use of any material contained in, or derived from, this report.

© 2020, LAI LIK SHENG. All right reserved.

## ACKNOWLEDGEMENTS

I would like to thank everyone who had contributed to the successful completion of this project. I would like to express my gratitude to my research supervisor, Ir. Dr. Huang Yuk Feng and co-supervisor, Ir. Dr. Koo Chai Hoon for their invaluable advice, guidance and enormous patience throughout the development of the research.

Next, I would like to express my deepest thanks to my mentor, Mr. Chia Ming Yuan who had offered invaluable comments and unconditional support during my venture. In addition, I would also like to express my gratitude to my loving parents and friends who had helped in one way or another and had given me encouragement through to the final completion of this project.

## ABSTRACT

Evapotranspiration (ET) is a process comprising of both evaporation and transpiration, which plays an important role in the hydrological cycle. A good precise estimation of it is very important in various fields including water resources, agriculture and irrigation systems. The purpose of the study is to estimate the reference evapotranspiration ( $ET_0$ ) in Peninsular Malaysia using extreme learning machine (ELM) and the ELM enhanced with the bootstrap aggregating fusion method, with climatic data as input to the model. The climatic data used to train the model included maximum temperature, mean temperature, minimum temperature, relative humidity, wind speed, and solar radiation. These data were obtained from eight stations in Peninsular Malaysia, which were the Alor Setar, Bayan Lepas, Ipoh, Kuala Lumpur International Airport (KLIA) Sepang, Lubok Merbau, Pulau Langkawi, Sitiawan and Subang stations. The data obtained were arranged into 63 combinations and each of these combination sets was used separately as input in the model estimation. The results generated were interpreted based on the root mean square error (RMSE), Nash-Sutcliffe model efficiency coefficient (NSE), adjusted Nash-Sutcliffe model efficiency coefficient (ANSE), mean bias error (MBE) as well as the mean absolute error (MAE). The results showed the best performance for most of the stations was the combination set with six climatic data as input for the model. Solar radiation was found to be the most important single input data for good model estimation. Bootstrap aggregating, also known as bagging did not improve but had reduced the performance of the model. A large amount of dataset utilized might be the reason for the inability of bagging to improve the performance of the model. Bootstrapping a huge amount of dataset might lead to over-fitting and thus reduce the accuracy in return. The large data size with respect to the low data dimensionality might also contribute to the ineffectiveness of the bagging to improve the model prediction.

## TABLE OF CONTENTS

<b>DECLARATION</b>		<b>i</b>
<b>APPROVAL FOR SUBMISSION</b>		<b>ii</b>
<b>ACKNOWLEDGEMENTS</b>		<b>iv</b>
<b>ABSTRACT</b>		<b>v</b>
<b>TABLE OF CONTENTS</b>		<b>vi</b>
<b>LIST OF TABLES</b>		<b>viii</b>
<b>LIST OF FIGURES</b>		<b>x</b>
<b>LIST OF SYMBOLS / ABBREVIATIONS</b>		<b>xi</b>
<b>LIST OF APPENDICES</b>		<b>xiv</b>
 <b>CHAPTER</b>		
<b>1</b>	<b>INTRODUCTION</b>	<b>1</b>
	1.1 General Introduction	1
	1.2 Importance of the Study	3
	1.3 Problem Statement	4
	1.4 Aim and Objectives	4
	1.5 Scope and Limitation of the Study	5
	1.6 Contribution of the Study	5
	1.7 Outline of the Report	6
<b>2</b>	<b>LITERATURE REVIEW</b>	<b>7</b>
	2.1 FAO-56 Penman-Monteith Equation	7
	2.2 Artificial Neural Network for Evapotranspiration	7
	2.2.1 Multilayer Perceptron	8
	2.2.2 Radial Basis Function	13
	2.2.3 Generalized Regression Neural Network	16
	2.2.4 Back-Propagation Neural Network	18
	2.2.5 Extreme Learning Machine	22
	2.3 Bootstrap Aggregating	34
	2.4 Summary	37

<b>3</b>	<b>METHODOLOGY AND WORK PLAN</b>	<b>38</b>
3.1	Workflow of Study	38
3.2	Mapping, Location of Study and Data Acquisition	38
3.3	FAO-56 Penman-Monteith Method	41
3.4	Normalization of Data	42
3.5	Parameter Tuning	42
3.6	k-Fold Cross Validation	43
3.7	Extreme Learning Machine	43
3.8	Activation Function of Model	44
3.9	Bootstrap Aggregating Fusion Method	45
3.10	Performance Evaluation	45
<b>4</b>	<b>RESULTS AND DISCUSSION</b>	<b>47</b>
4.1	Parameter Tuning of the Model	47
4.1.1	Hidden Node Number	47
4.1.2	Activation function	48
4.2	Result Analysis for Conventional ELM	49
4.3	Result Analysis for Bagged ELM	59
4.4	Conventional and Bagged ELM Comparison	68
<b>5</b>	<b>CONCLUSIONS AND RECOMMENDATIONS</b>	<b>73</b>
5.1	Conclusions	73
5.2	Recommendations for Future Work	74
	<b>REFERENCES</b>	<b>75</b>
	<b>APPENDICES</b>	<b>83</b>

## LIST OF TABLES

Table 2.1:	Summary of Journals Reviewed.	26
Table 3.1:	Combinations of Climatic Data.	40
Table 4.1:	Percentage of the Activation Function giving Best Results in 63 Combinations for Each Station.	49
Table 4.2:	Result Performance at Alor Setar Station using ELM.	50
Table 4.3:	Result Performance at Bayan Lepas Station using ELM.	51
Table 4.4:	Result Performance at Ipoh Station using ELM.	52
Table 4.5:	Result Performance at KLIA Sepang Station using ELM.	53
Table 4.6:	Result Performance at Lubok Merbau Station using ELM.	54
Table 4.7:	Result Performance at Pulau Langkawi Station using ELM.	54
Table 4.8:	Result Performance at Sitiawan Station using ELM.	55
Table 4.9:	Result Performance at Subang Station using ELM.	56
Table 4.10:	Result Performance at Alor Setar Station using Bagged ELM.	60
Table 4.11:	Result Performance at Bayan Lepas Station using Bagged ELM.	61
Table 4.12:	Result Performance at Ipoh Station using Bagged ELM.	62
Table 4.13:	Result Performance at KLIA Sepang Station using Bagged ELM.	63
Table 4.14:	Result Performance at Lubok Merbau Station using Bagged ELM.	64
Table 4.15:	Result Performance at Pulau Langkawi Station using Bagged ELM.	64
Table 4.16:	Result Performance at Sitiawan Station using Bagged ELM.	65

Table 4.17: Result Performance at Subang Station using Bagged ELM.

## LIST OF FIGURES

Figure 2.1:	Structure of an Artificial Neuron (Agatonovic-Kustrin and Beresford, 2000).	8
Figure 2.2:	Typical Architecture of MLP (Traore, Luo and Fipps, 2015).	9
Figure 2.3:	Typical Structure of Radial Basis Function (Partal, 2015).	14
Figure 2.4:	Schematic Diagram of GRNN (Ladlani et al, 2012).	16
Figure 2.5:	Schematic Diagram of BPNN (Pakhale et al., 2015).	19
Figure 2.6:	Typical Structure of ELM (You et al., 2014).	22
Figure 2.7:	Procedure of Bootstrap Aggregating (Lan, 2019).	34
Figure 3.1:	Overall Work Plan.	38
Figure 3.2:	Location of Study.	39
Figure 4.1:	Graph of RMSE against Hidden Node Number (Alor Setar, Sigmoid, C1).	48
Figure 4.2:	Graphs of RMSE against Hidden Node Number for (left) Alor Setar, Sigmoid, C60 and (right) Alor Setar, Sigmoid, C62.	48
Figure 4.3:	Scatter Plots of Best Combinations of Six to One Input Variable (A1-A6) for Conventional ELM and Corresponding Combinations (B1-B6) for Bagged ELM.	71

## LIST OF SYMBOLS / ABBREVIATIONS

$d$	Willmott index of agreement
$e_a$	actual vapour pressure, kPa
$e_s$	saturation vapour pressure, kPa
$E_{pan}$	pan evaporation, mm
$G$	soil heat flux density, MJ m <sup>-2</sup> day <sup>-1</sup>
$h_c$	crop reference height, m
$n$	sunshine duration, h
$P$	rainfall, mm
$R$	correlation coefficient
$R^2$	coefficient of determination
$R_a$	extra-terrestrial radiation, MJ m <sup>-2</sup> day <sup>-1</sup>
$RH$	relative humidity, %
$RH_{max}$	maximum relative humidity, %
$RH_{mean}$	mean relative humidity, %
$RH_{min}$	minimum relative humidity, %
$R_n$	net radiation at the crop surface, MJ m <sup>-2</sup> day <sup>-1</sup>
$R_s$	solar radiation, MJ m <sup>-2</sup> day <sup>-1</sup>
$T$	temperature, °C
$T_a$	air temperature, °C
$T_{max}$	maximum temperature, °C
$T_{mean}$	mean temperature, °C
$T_{min}$	minimum temperature, °C
$T_s$	soil temperature, °C
$U_2$	wind speed, m/s
$\Delta$	slope vapour pressure curve, kPa °C <sup>-1</sup>
$\gamma$	psychrometric constant, kPa °C <sup>-1</sup>
ACC	accuracy
ANFIS	adaptive neuro fuzzy inference system
ANFIS-FCM	fuzzy c-means clustering adaptive neuro fuzzy inference system

ANFIS-GP	grid partition based adaptive neuro fuzzy inference system
ANFIS-SC	subtractive clustering based adaptive neuro fuzzy inference system
ANFIS-GEP	gene expression programming based adaptive neuro fuzzy inference system
ANN	artificial neural network
ANSE	adjusted Nash-Sutcliffe model efficiency coefficient
APE	absolute percentage error
ARIMA	auto regressive integrated moving average model
BCR	Blaney-Criddle
BPNN	back-propagation neural network
C-ELM	complex extreme learning machine
CIMIS	California Irrigation Management Information System
DL-MLP	deep learning multilayer perceptron
E	model efficiency
ELM	extreme learning machine
ET	evapotranspiration
ET <sub>o</sub>	reference crop evapotranspiration
GANN	genetic algorithm neural network
GBM	gradient-boosting machine
GEP	gene expression programming
GFF	generalized feed-forward
GLM	generalized linear model
GP	genetic programming
GRNN	generalized regression neural network
HARG	Hargreaves equation
KLIA	Kuala Lumpur International Airport
LL	log loss
LR	linear regression
LS-SVM	least-square support vector machine
MAD	mean absolute deviation
MAE	mean absolute error
MAPE	mean absolute percentage error
MBE	mean bias error

MCE	mean per-class error
MLP	multilayer perceptron
MLR	multiple linear regression
MSE	mean squared error
MSESS	mean square error skill score
MVRVM	multivariate relevance vector machine
NMSE	normalised mean square error
NRMSE	normalized root mean square error
NSE	Nash-Sutcliffe model efficiency coefficient
OI	overall index
OS-ELM	online sequential extreme learning machine
PE	processing element
PET	potential evapotranspiration
PM	Penman-Monteith equation
PNN	probabilistic neural network
PT	Priestley-Taylor
RBF	radial basis function
RBF-BP	radial basis function with particle swarm optimization
RBF-PSO	radial basis function with back-propagation
RE	relative error
RF	random forest
RMBF	Reference Model of Burkina Faso
RMSD	root mean square difference
RMSE	root mean square error
RMSLE	root mean square logarithmic error
SaE-ELM	self-adaptive evolutionary extreme learning machine
SVM	support vector machine
TS	threshold statistics
WANN	wavelet-based artificial neural network
WELM	wavelet-based extreme learning machine
WMLR	wavelet-based multiple linear regression
WNN	wavelet-based neural network
WRBF	wavelet-based radial basis function

**LIST OF APPENDICES**

APPENDIX A: Result Performance of All Combinations	83
----------------------------------------------------	----

## CHAPTER 1

### INTRODUCTION

#### 1.1 General Introduction

Evapotranspiration (ET), as the name implies, refers to two processes whereby the water is lost back to the atmosphere: the loss of water from the surface of soil through evaporation and the loss of water from the crop through transpiration (Allen et al., 1998). ET plays a main role in the hydrologic cycle. According to Pokorny (2019), about 70% of the yearly precipitation in the United States returns to the atmosphere via ET. The return of precipitation to the atmosphere by ET in the western region of the United States having arid and semiarid climate is even higher at about 90%. According to Traore, Wang and Chung (2014), water shortage problems have led to a shortage of food and constrained economic growth in arid and semiarid regions of Africa. Therefore, a good estimation of ET is very crucial for agriculture, irrigation system management, environmental assessment and water allocation.

The rate of ET process is affected by many factors. The amount of precipitation returns to the atmosphere by ET from a field is dependent on the ability of the plants to draw the water from the soil to the atmosphere during transpiration process and also the water or moisture content of the soil. Thus, the type of plants available in the field will affect the rate of ET. Other than the plants and soil, some of the climatic criteria also have significant impacts on ET. For example, solar radiation, temperature of both the evaporative surface and the air, surrounding vapour pressure and the speed of wind that moves above the evaporative surface. (Pereira, Cordery and Iacovides, 2009).

Potential evapotranspiration (PET) was defined by Dingman (2015) in his book, "Physical Hydrology" as the ET rate of a huge field that is utterly covered with vegetation, having unlimited or abundant soil water and no occurrence of heat advection. Notwithstanding the abundant supply of water, there are still some vegetative-surface-related factors that strongly affect the ET rate, including the albedo of the surface, maximum leaf conductance as well as the atmospheric conductance. Therefore, the concept of PET was then replaced with the reference-crop evapotranspiration. Reference-crop evapotranspiration

( $ET_o$ ) indicates the quantity of water transpired by a short green crop of even height that totally covers the ground surface and is with unlimited water supply.

Due to the significance of  $ET_o$ , a number of studies (Hill et al, 1983; Allen, 1983; Allen et al, 1998) had been carried out in the past few decades with the aim of developing new precise methods to estimate  $ET_o$  and to improve the estimation performance of current methods at the same time. The value of  $ET_o$  can be measured by using lysimeters that work on soil water balance (Xu and Chen, 2005) or by micrometeorological means, for example, eddy covariance or the Bowen ratio energy balance method (Campbell and Williamson, 1997). The downfall of the evapotranspiration measurement using lysimeter is that it is certainly time-consuming. Besides, careful and precise planning is required to carry out the method (Kumar et al., 2002). The  $ET_o$  value also can be calculated using empirical equations which require climatic data. These empirical equations include the Priestley-Taylor (PT) equation, Hargreaves equation (HARG), Thornthwaite equation and the combined method such as the FAO-56 Penman-Monteith or simply known as the Penman-Monteith (PM) equation. Among these methods, the PM method has been described to be better in estimating the  $ET_o$  compared to other empirical equations. This method has always been used as the reference method in a number of studies, such as the studies done by Falamarzi and others in 2014, Gocic and others in 2016 as well as Ladlani and others in 2012.

However, despite all the improvements mentioned above, their applications are difficult when there is only limited climatic data available. Consequently, a more advanced method is introduced, namely the artificial neural network (ANN). It is a non-linear mathematical network that relates the inputs and outputs of a system with complex processes. There are commonly five types of ANN models used to estimate  $ET_o$ : back-propagation neural network (BPNN) (Kuo et al., 2011; Traore, Wang and Chung, 2014; Pakhale et al., 2015), extreme learning machine (ELM) (Patil and Deka, 2016; Gocic et al., 2016; Dou and Yang, 2018), multilayer perceptron (MLP) (Traore, Luo and Fipps, 2015; Yassin, Alazba and Mattar, 2016; Antonopoulos and Antonopoulos, 2017), generalized regression neural network (GRNN) (Traore, Wang and Kerh, 2008; Heddam et al. 2013; Feng et al., 2017) and radial basis function (RBF) (Trajkovic, 2005; Trajkovic, 2009; Goodarzi and Islamian, 2018).

Bootstrap aggregating, also known as bagging, is a type of prediction combination method applied in the machine learning field. In bagging, bootstrap samples regarding training data sets are used to develop base models. The forecasts made by these samples are averaged to minimize the variance of forecasts without bagging. This method has high performance when the model is non-linear and the size of the data sample is not large (Elliott and Timmermann, 2013). Bagging can be used in ANN to improve estimation accuracy.

## **1.2 Importance of the Study**

As the population in the world keeps on expanding, the management of water resources and irrigation needs to be enhanced to a higher level of efficiency to meet the demands all around the world. ET which is one of the most important components in the hydrological cycle greatly influences the volume of runoff, water required in the irrigation system and soil moisture content. Accurate estimation of  $ET_o$  is a vital practice in water resource planning and water budgeting.

A good understanding and accurate estimation of  $ET_o$  can contribute to a greener urbanization process. One of the systems that apply the idea of ET is the green stormwater infrastructure (GSI). GSI mitigates the runoff and pollutants by using hydrological components instead of drainage and sewerage systems.  $ET_o$  plays an influential role in enhancing the ability of GSI systems by restoring the soil pore storage via the reduction of moisture (Ebrahimian, Wadzuk and Traver, 2019).

In tropical countries like Malaysia, hydrological changes are considered as one of the largest potential effects on global climate change (Parry et al., 2007). In tropical regions, climate change leads to an increase in temperatures. The rise in temperature, in turn, induces a higher rate of evapotranspiration which will have an impact on the hydrological system as well as water resources (Shahid, 2011). Therefore, the ability to estimate the  $ET_o$  and to evaluate its changes is very important in managing long-term water resources. Certainly, in the agricultural field, it is crucial to predict the change in ET due to climate change which will affect the amount of water loss (Tukiman, Harun and Shahid, 2012). The significance of estimation on rice crop evapotranspiration was

explained by Lee, Najim and Aminul (2004) as some of the commercial paddy estates in Malaysia constantly find better means to manage crop and irrigation systems in order to enhance the productivity and so their profits. A good estimation of rice crop evapotranspiration will improve the irrigation planning and scheduling as well as crop and irrigation systems for large scale production, while helping in reducing costs of production.

### **1.3 Problem Statement**

The estimation of  $ET_o$  has been approached in various ways and many of them are by direct measurements and empirical methods; with the recommendation by FAO that the PM model as the standard way to obtain the  $ET_o$  (Rahimikhoob and Hosseinzadeh, 2014). However, these methods utilize the climatic data of the respective region of study to calculate the value of  $ET_o$  corresponding to the region but are not reliable when applied to other regions, especially those having distinct differences in climatic patterns. A large amount of data is required for the estimation and this makes it harder in that the data sets are not easily acquired. In many places where relating studies are carried out, hydrologists had to make reasonable assumptions on meteorological information that are not available (Sudheer, Gosain and Ramasastri, 2003).

Much focus has been placed on current methods like ANN, a non-linear and complex mathematical structure to estimate the  $ET_o$ . This modelling structure had been used successfully to model intricate non-linear relationships in other types of application fields. Compared to conventional empirical methods, the ANN's advantages over them is that it does not need well-interpreted information about the complex relationships such as equations to describe the underlying process (Sudheer, Gosain and Ramasastri, 2003). The performance of ANN models was investigated in this study where one type of ANN model, the ELM was used to estimate the  $ET_o$  in Malaysia. Besides, the bootstrap aggregating method was adopted in the modelling to test the effect of it on the accuracy of the results.

### **1.4 Aim and Objectives**

The study is aimed at estimating the potential evapotranspiration using extreme learning machine (ELM) with bootstrap aggregating fusion method.

- (i) To develop an ELM model with various combinations of climatic data for  $ET_o$  estimation.
- (ii) To study the capability of the bootstrap aggregating fusion method to improve the model estimation accuracy.
- (iii) To interpret the performance of the ELM model by referring to the PM method as the reference standard.
- (iv) To determine the combination of climatic data that registers the best accuracy from the model.

### **1.5 Scope and Limitation of the Study**

The focus of the study is to investigate the performance of ANN in the estimation of  $ET_o$ . Extreme learning machine (ELM) is selected for the study to investigate its accuracy in estimating the  $ET_o$ . The value of  $ET_o$  that is calculated using the PM method will be set as a standard for the comparison. Bootstrap aggregating fusion method is incorporated in the modelling to reduce the errors. Climatic data from eight meteorological stations located on the west coast side of Peninsular Malaysia are acquired and used as the input variables for ANN models. These input variables include maximum temperature ( $T_{max}$ ), minimum temperature ( $T_{min}$ ), mean temperature ( $T_{mean}$ ), mean relative humidity ( $RH$ ), mean wind speed ( $U_2$ ) and solar radiation ( $R_s$ ). The accuracy of neural network models is measured in terms of root mean square error (RMSE), mean absolute error (MAE), mean bias error (MBE), Nash-Sutcliffe model efficiency coefficient (NSE) and adjusted NSE.

There are some limitations that may restrict the study to be carried out with the fullest coverage. Only one type of ANN model (ELM) is selected for this study due to the limited study period. Training of the models is time-consuming and thus testing on all types of ANN models is not considered. These data are extracted from eight stations only and the time range of these data is from 2014 to 2018.

### **1.6 Contribution of the Study**

This study aims to exploit the reliability of ANN models in estimating the  $ET_o$ . ANN is viewed as a potential substitute for the empirical PM method which depends strongly on the availability of large amounts of data. It also works on

the different combinations of climatic factors as the inputs of ANN models. It is also one of the priorities to figure out the best data combination that gives the greatest precision. It is hoped that knowledge of ANN will help in enhancing the estimation of  $ET_0$  for the forecasting of ET. In Malaysia, an important part of the economy is contributed by agricultural activities, such as paddy and oil palm plantation, etc. Thus, the ability to estimate evapotranspiration accurately will result in a better economy. Besides, with better methods to estimate evapotranspiration, water resource and management as well as supply can be organized in more sufficient mean and water shortage issues can be reduced.

### **1.7 Outline of the Report**

Chapter 1 provides an explanation of evapotranspiration, methods of estimation and limitations encountered in the study. Chapter 2 reviews the PM method, five types of ANN models which are the MLP, RBF, GRNN, BPNN and ELM. The review on the bootstrap aggregating fusion method is also covered in Chapter 2. Chapter 3 is the methodology part, where the processes of pre-processing, model training, and performance evaluation are described in detail. Data, results of the model estimations and interpretation are focused in Chapter 4 while Chapter 5 presents the conclusions of the study.

## CHAPTER 2

### LITERATURE REVIEW

#### 2.1 FAO-56 Penman-Monteith Equation

Reference evapotranspiration  $ET_0$  is important as it acts as a standard for the comparison of evapotranspiration at different areas or time as well as provides relations for evapotranspiration of other crops. The FAO-56 Penman-Monteith (PM) method is recommended as the standard method to compute the  $ET_0$  by the Food and Agriculture Organization of United Nations (FAO). The PM equation is the result of the combination of the original Penman-Monteith equation, aerodynamic equation and surface resistance equation. This equation requires several climatic variables which are solar radiation, air temperature, wind speed and humidity. The measurement of climatic variables should be carried out at a height of 2 m from a green grass surface covering a large area, shading the ground and without water supply shortage. The PM equation takes into consideration of both physical and physiological factors affecting the evapotranspiration process (Allen et al., 1998).

#### 2.2 Artificial Neural Network for Evapotranspiration

Artificial neural network (ANN) is a computational model which can be thought of as a highly simplified form of biological neural network structure. It consists of numerous interconnected processing elements (PE) or simply known as neurons (Yegnanarayana, 2006). A PE consists of weighted inputs, transfer function, and one output. In each PE, inputs are regulated by the connection weights and combined to produce what so-called the activation function before being propagated across a transfer function to create an output. The sigmoid function is the most common transfer function used (Agatonovic-Kustrin and Beresford, 2000). ANN offers many advantages due to its processing characteristics including nonlinearity which results in a better fit of data, robustness and generalization ability. This allows the model to be applied to unlearned data and learning ability. Besides, the model adaptivity enables it to update internal structure due to the changing environment. (Basheer and

Hajmeer, 2000). ANN has been incorporated in the evapotranspiration estimation and was found to have greater accuracy compared to conventional empirical methods (Trajkovic, 2009; Salim et al., 2013; Antonopoulos and Antonopoulos, 2017).

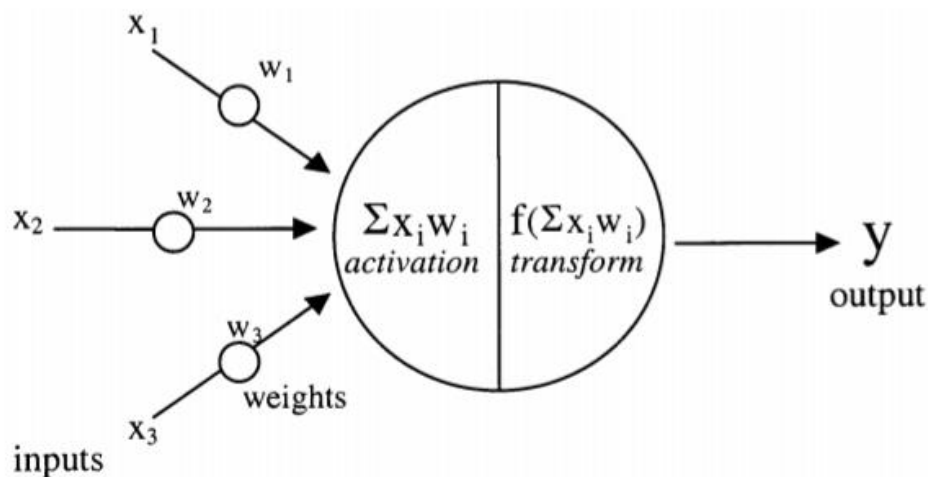


Figure 2.1: Structure of an Artificial Neuron (Agatonovic-Kustrin and Beresford, 2000).

### 2.2.1 Multilayer Perceptron

Multilayer perceptron models are one of the artificial neural networks that have been commonly used by researchers in the study of evapotranspiration estimation. Generally, these models composed of three layers, input layers, hidden layers and output layers. MLPs are classified as feed-forward ANN models which means the inputs transmit from the input layer via the hidden layer to the output layer, in a forward direction manner (Antonopoulos and Antonopoulos, 2017). There are two main stages in the MLP. Firstly, input values are fed forward via the hidden layer to generate output values which then used to compare with initial values to estimate the difference. After that, the best results with the smallest difference are optimized by adjusting the connection weights (Pham et al., 2017).

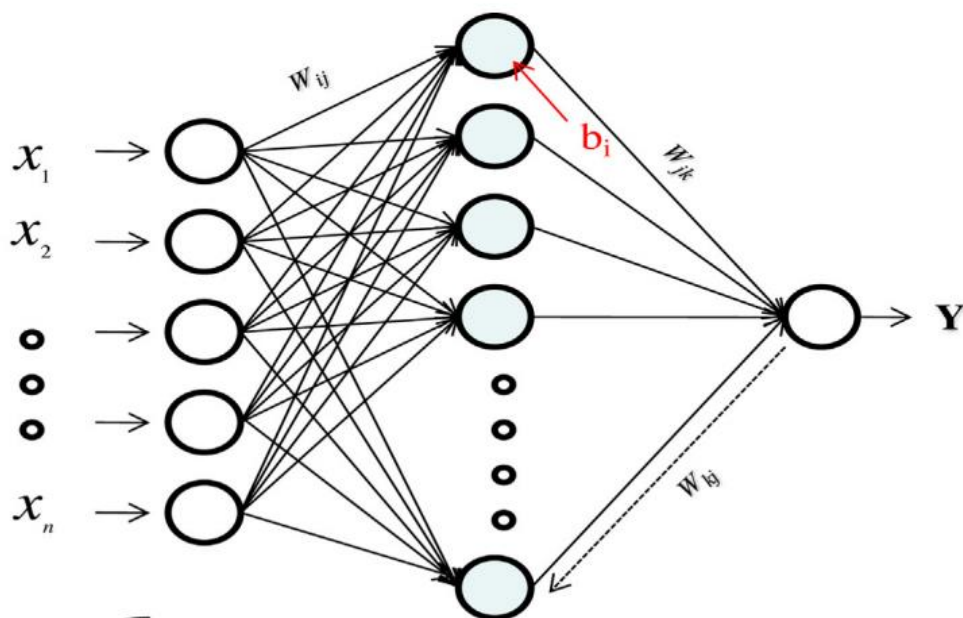


Figure 2.2: Typical Architecture of MLP (Traore, Luo and Fipps, 2015).

Landeras, Ortiz-Barredo and López (2009) studied the weekly evapotranspiration prediction performance of the MLP-type ANN model and the auto regressive integrated moving average model (ARIMA) and compared the results with a model that obtained  $ET_0$  based on weekly averages. The region of study was the Álava located in the Basque Country where its temperature, solar radiation, relative humidity and wind speed were collected for model inputs purpose. The results were compared in terms of root mean square difference (RMSD) and mean absolute deviation (MAD). Compared to the averaged-based model, the MLP and ARIMA model decreased the root mean square differences by 6% to 8% while standard deviation differences by 9% to 16%.

In the study carried out by Rahimikhoob (2010), MLP was used to estimate the  $ET_0$  on the southern coast of the Caspian Sea with maximum temperature, minimum temperature and extra-terrestrial radiation data obtained from eight weather stations as input variables. The estimation of the MLP was compared with the one estimated by the HARG equation and the PM method was set as a benchmark. The coefficient of determination ( $R^2$ ) and RMSE of the estimation using the MLP were 0.95 and 0.41 mm/day respectively while The

$R^2$  and RMSE of the estimation using the HARG were 0.91 and 0.51 mm/day respectively, indicating that MLP was better in performance.

Jadeja (2011) compared the ability of the MLP and  $E_{pan} \times K_p$  equation in converting the pan evaporation data for  $ET_o$  estimation. The climatic data used as inputs were the maximum and minimum temperatures of Sabarmati River in Gujarat. The  $ET_o$  standard for the comparison was calculated using the PM method. The evaluation criteria included the RMSE, correlation coefficient ( $R$ ) and  $R^2$ . It was found that MLP was more accurate in estimating the  $ET_o$ .

Cobaner (2011) tested the effectiveness of two types of adaptive neuro fuzzy inference system (ANFIS) which were the grid partition based ANFIS (ANFIS-GP) and subtractive clustering based ANFIS (ANFIS-SC) in estimating the  $ET_o$  using the climatic data from Santa Monica in Los Angeles, USA. The results of ANFIS models were compared with the estimations of the MLP model as well as the California Irrigation Management Information System (CIMIS) Penman, HARG and Ritchie equations. Four input variables were adopted which were average temperature, solar radiation, relative humidity and wind speed. Their performance was judged using the RMSE, MAE and determination coefficient statistics. ANFIS-SC was shown to be the model with the highest precision among all of these methods. From the perspective of input variable combination, the model having all variables had the top accuracy.

Torres, Walker and McKee (2011) investigated the reliability of multivariate relevance vector machine (MVRVM) in predicting the  $ET_o$  in Sevier River Basin in Central Utah, USA. There were only two climatic data used for the modelling, namely the maximum temperature and minimum temperature. The study was carried out in two scenarios, the first scenario utilized the already computed  $ET_o$  data to forecast  $ET_o$  while the second scenario used the already computed data to forecast other needed climatic variables and subsequently forecast the  $ET_o$ . The evaluation criteria were the NSE and RMSE. The prediction of the MVRVM was compared with the one predicted by the MLP and it was found that the MVRVM was more reliable than the MLP.

Traore, Luo and Fipps (2015) conducted a study on the performance of four ANN models, namely the MLP, generalized feed-forward (GFF),

probabilistic neural network (PNN) and linear regression (LR) in predicting the  $ET_o$  at Dallas. The performance evaluation criteria included the MSE,  $R$ , normalised mean square error (NMSE), MAE and mean square error skill score (MSESS) while the PM method was used to obtain standard  $ET_o$ . Among the combination of four variables, which were maximum temperature, minimum temperature, extra-terrestrial radiation and solar radiation, the combination that contained the maximum temperature, minimum temperature and solar radiation produced results with the greatest precision. The results showed that the MLP had a greater precision than other models. Researchers concluded that maximum temperature was the most important factor in forecasting the  $ET_o$  while the solar radiation accuracy affected the performance the most.

Kisi et al. (2015) tested the performance of five methods, the MLP, ANFIS-GP, ANFIS-SC and gene expression programming ANFIS (ANFIS-GEP) as well as gene expression programming in forecasting the  $ET_o$  hinged on the meteorological data acquired from 50 weather stations in Iran. Input variables for model training included altitude, latitude as well as longitude of the station and periodicity component. The RMSE and  $R^2$  were used to determine the performance of the models. The results showed that the former three models had similar accuracy while the ANFIS-GEP had the lowest accuracy.

The  $ET_o$  forecasting ability of four types of ANN models relying on forecasted temperature data were investigated by Luo et al. (2015). The four models were namely the MLP, generalized feed-forward (GFF), Probabilistic Neural Network (PNN) and Linear Regression (LR) with PM method as benchmark. Maximum temperature and minimum temperature were the input variables and their performances were tested using the NMSE, MAE and  $R^2$ . The results showed that the MLP, PNN and GFF all performed well in the predictions except for the LR.

Yassin, Alazba and Mattar (2016) carried out a study on the comparison of performance of the MLP and GEP models in estimating daily  $ET_o$  in the Kingdom of Saudi Arabia. 30 years of climatic data, from 1980-2010, were obtained from 13 climatic stations and 65% of the data was used for training purpose while the rest were taken for the testing stage. These data included

maximum temperature, minimum temperature, average temperature, maximum relative humidity, minimum relative humidity, average relative humidity, wind speed, solar radiation and crop height. Standard  $ET_o$  values were estimated by using the generalized PM method. Several items were utilized to interpret the estimation performance of the models which were  $R^2$ , overall index of the model performance (OI), RMSE and MAE. Based on the results,  $R^2$  and RMSE of the MLP models were in the range of 67.6% to 99.8% and 0.20 to 2.95 mm/day respectively, which were generally higher than those of the GEP models with values 64.4% to 95.5% and 1.13 to 3.1 mm/day respectively. The models with all variables as inputs had the highest accuracy. The benefits of the ANN model were its flexibility and ability to model nonlinear relationships, as mentioned by the authors.

Antonopoulos and Antonopoulos (2017) applied MLP models to run an estimation on  $ET_o$  based on the five-year-period climatic data collected from a station in northern Greece. Temperature, relative humidity, solar radiation and wind speed were the input variables while RMSE and  $R$  were the evaluation criteria for performance. The PT, HARG, Makkink and mass transfer methods were also adopted for comparison with MLP models, and the PM method as referring standard. It was found that the MLP model with four input variables had the highest accuracy, and the accuracy decreased when the number of variables decreased. Generally, MLP models were better than empirical methods. However, the accuracy of ANN decreases with pooled data due to high non-linearity and less similarity among the data.

In the research done by Ferreira et al. (2019), MLP-type ANN model and support vector machine (SVM) model were adopted to estimate the  $ET_o$  in Brazil and then compared with original as well as calibrated version of empirical methods. These empirical methods included the HARG-Samani, Oudin, Hamon, Valiantzas, Romanenko and Schendel. They carried out the research in two scenarios. In the first scenario, the data of meteorological stations were categorized according to their climatic feature similarities and models were developed for each category. The second scenario incorporated previous climatic data as input variables for the models. In this study, only temperature and relative humidity were used as the input variables while the performance of

the methods in estimating  $ET_o$  was measured using the RMSE, MBE and  $R^2$ . Both, the MLP and SVM models performed better than empirical methods, with MLP models having registered the highest accuracy in both temperature-based as well as temperature and relative humidity-based models. Moreover, models with two input variables estimated  $ET_o$  better than models with one input variable.

Saggi and Jain (2019) used four types of models to estimate the  $ET_o$  in Hoshiapur and Patiala in Punjab, and those were the deep learning MLP, generalized linear model (GLM), random forest (RF) and gradient-boosting machine (GBM). The climatic factors involved were the maximum temperature, minimum temperature, relative humidity, wind speed and sunshine hour. The results were interpreted using the NSE,  $R$ ,  $R^2$ , normalized root mean square error (NRMSE), root mean square logarithmic error (RMSLE), accuracy (ACC), log loss (LL) as well as mean per-class error (MCE). The results showed that deep learning MLP had the highest accuracy, with NSE ranged from 0.95-0.98,  $R^2$  ranged from 0.95-0.99, ACC ranged from 85-95, MSE ranged from 0.0369-0.1215 and RMSE ranged from 0.1921-0.2691. Deep learning MLP thus showed greater robustness than other common methods.

Based on the previous researches, MLP models generally exhibited better performance and higher accuracy compared to conventional methods and many of the machine learning models but some machine learning models outperformed MLP such as MVRVM as shown in study done by Torres, Walker and McKee (2011). The accuracy of the estimation seems to increase with the increase in the number of input variables.

### **2.2.2 Radial Basis Function**

Radial basis function (RBF) neural networks are nonlinear hybrid networks with three layers similar to MLP. The three layers are input layers, hidden layers and output layers. Generally, the Gaussian function is adopted in the hidden layer while the linear function is adopted in the output layer. The RBF process can be separated into unsupervised learning session and supervised learning session. The parameters and basic functions are determined in the first session while the weights between the hidden and output layers are determined in the second

session by applying the linear regression and reduce slope method (Dehghani et al, 2009). This type of model utilizes the trial and error process to obtain the best architecture. This is achieved by varying the number of hidden layers and their neurons along with other components such as transfer function and learning algorithm (Goodarzi and Eslamian, 2018).

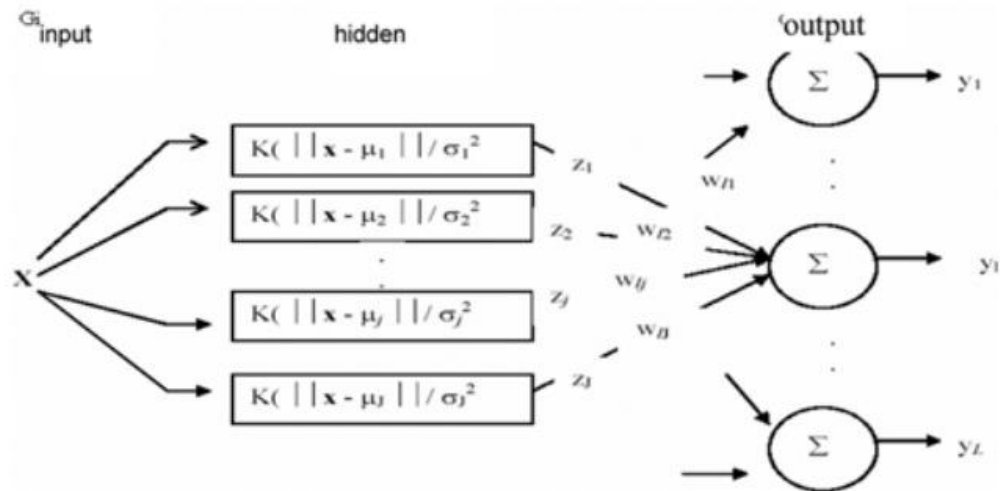


Figure 2.3: Typical Structure of Radial Basis Function (Partal, 2015).

Trajkovic (2009) analysed the reliability of RBF in converting the pan evapotranspiration to  $ET_0$  values. The model was fed with climatic data obtained from Policoro, Italy and the outcomes were compared with the Christiansen, FAO-24 pan, and PM method with measurement using the lysimeter as the benchmark. The input variables provided for the RBF training were pan evaporation and extra-terrestrial radiation. The performance of these methods was tested using RMSE and  $R^2$ . The results indicated that RBF with 0.433 mm/day of RMSE was the lowest among all methods.

In the study by Partal (2015), wavelet transformation technique was incorporated in both the RBF and multiple linear regression (MLR) models to estimate the  $ET_0$  using the climatic data gathered from two weather stations in the US. Four input factors were used in the modelling, and these were solar radiation, temperature, relative humidity and wind speed. Comparison was made between seven models, including the RBF, wavelet-based RBF (WRBF), MLR, wavelet-based MLR (WMLR), HARG, PM method and Turc method.

MAE and  $R^2$  were the criteria used to study the precisions of the methods. The results showed that WRBF performed better than MLR. Besides, involvement of wavelet transformation in the modelling enhanced the performance greatly. They also stated that WRBF learns through the data in one time and is able to generalize from example from the time they are stored.

Petković et al. (2015) compared the performance of two types of RBF networks, one worked with particle swarm optimization (RBF-PSO) while another worked with back-propagation (RBF-BP) in estimating the  $ET_o$  in Serbia using 30-year period of climatic data. Maximum temperature, minimum temperature, sunshine hour, actual vapour pressure and wind speed. The reference equation used was the PM method and the performance of the models was evaluated based on RMSE, MAE and  $R^2$ . RBF with particle swarm optimization was found to be better than RBF with back-propagation in the estimation.

Goodarzi and Eslamian (2018) carried out an analysis of the performance of the RBF and genetic programming (GP) which were non-linear-type models as well as the MLR which represented the linear-type model in estimating the monthly  $ET_o$  in Isfahan. Maximum temperature, minimum temperature, mean temperature, relative humidity, wind speed and solar radiation were the input variables while RMSE and  $R^2$  were the performance evaluation elements. In terms of precision, GP models registered the lowest error with RMSE value of 0.21 but in terms of training speed, RBF turned out to be faster than GP. Both RBF and GP models registered the greater performance when all input variables were utilized compared to less input variables were utilized. It was mentioned by the authors that both RBF and GP are able to filter out noises, outliers and missing data as well as able to update the model with new data.

In a nutshell, RBF showed a better estimation of  $ET_o$  in the former studies, compared to conventional methods which require a large amount of input data. The modified RBF such as with the incorporation of particle swarm optimization can be used to further enhance the performance.

### 2.2.3 Generalized Regression Neural Network

Generalized regression neural network (GRNN) which was proposed by Specht (1991) is an improved version of radial basis function. Similar to feed-forward neural network, it estimates any arbitrary function between inputs and outputs directly from the training data. However, the operation of the GRNN is different from the general feed-forward neural network in the way that it is based on non-linear regression theory to estimate function (Feng et al., 2017). This type of model does not encounter local minima problem and does not require a repetitive training process. The architecture of GRNN model is made up of four layers which comprise input layer, pattern layer, summation layer and output layer. It is a parallel structure with one-pass learning algorithm which allows the transfer of data between layers smoothly even with a huge amount of data (Specht, 1991). There will be a weight connecting each node in the pattern layer to two nodes in the summation layer while each of these summation layer nodes calculates the weighted outputs and un-weighted outputs of the pattern nodes (Ladlani et al, 2012).

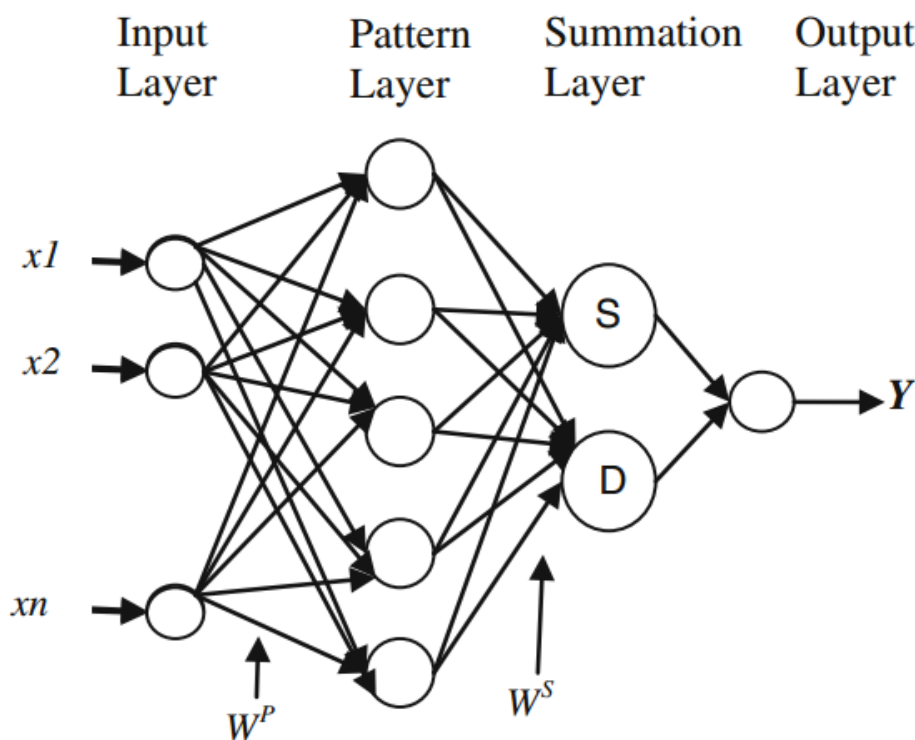


Figure 2.4: Schematic Diagram of GRNN (Ladlani et al, 2012).

Ladlani et al. (2012) investigated the effectiveness of the GRNN and RBF in estimating the  $ET_o$  in Algeria. Meteorological data including maximum temperature, minimum temperature, mean temperature, sunshine duration and relative humidity were used as input variables for the models with  $ET_o$  calculated using the PM method as the standard. Other than these two models, HARG-Samani and PT equations were also adopted for comparison with the neural network models. RMSE, MAE,  $R$  and Willmott index of agreement ( $d$ ) were used to test for their performance. In the study, GRNN showed the highest accuracy in estimating the  $ET_o$ , followed by RBF. When all variables were utilized as inputs of the models, the precision was the best among all types of combinations. The researchers stated that these ANN models are responsive, fast, economical, suitable to be used in real-time and able to simulate possible conditions for both partially and totally available climatic data.

Heddami et al. (2013) compared the ability of both GRNN and MLR in estimating the monthly PET in Guelma, northeast of Algeria. The input variables fed into the models consisted of maximum temperature, minimum temperature, mean temperature, sunshine duration and wind speed and RMSE, MAE,  $R$  and  $d$  were the criteria used for determining the performance of the models. It was found that the GRNN registered more accurate  $ET_o$  than the MLR.

GRNN was also applied by Feng et al. (2017) to estimate the  $ET_o$  hinged on the climatic data acquired from two stations in the southwest of China and then compared with random forests (RF) model. The input variables were maximum temperature, minimum temperature, solar radiation, wind speed, relative humidity and extra-terrestrial radiation. These models were trained using two combinations of input variables. The first combination used all the climatic data whereas the second combination only used temperature and extra-terrestrial radiation as input factors. The performance of the models was rated using RMSE, MAE and NSE with the aid of the k-fold test. For both stations, RF models with the first variable combination were the highest in terms of accuracy. The results showed that both models gave  $ET_o$  estimation at high precision, but RF was slightly higher than GRNN.

Feng et al. (2017) estimated the  $ET_o$  utilizing ELM and GRNN with solely temperature data obtained from six weather stations in Sichuan basin.

There were only three climatic variables used as input variables, namely maximum temperature, minimum temperature and extra-terrestrial radiation while evaluation components were RRMSE, MAE as well as NSE. The results of the two models were compared with HARG and calibrated HARG. They trained the models with two conditions. In the first condition, only local data of each station was used in the training while in the second condition, the data from all stations were used in training and then applied for each station. For the first condition, ELM had a higher accuracy, with a value of 0.198 for RRMSE, 0.267 for MAE and 0.891 for NS. For the second condition, GRNN turned out to be the model that reported higher accuracy, with a value of 0.194 for RRMSE, 0.263 for MAE and 0.895 for NSE. The authors stated that ELM was faster than GRNN in terms of training and testing processes.

As a summary, GRNN also registered desirable performance in terms of  $ET_0$  estimation and is a potential alternative to conventional methods. As stated by Specht (1991), this type of model offers advantages including that it does not need a repetitive training procedure and is a one-pass learning algorithm that enables the smooth transfer of vast data amount through the layers.

#### **2.2.4 Back-Propagation Neural Network**

Back-propagation neural networks (BPNN) are one of the most widely used forward neural networks. These models are multilayer mapping networks that propagate the information forward while minimizing the error backward. Thus, they are also known as error back-propagation networks. In the back-propagation learning algorithm, the network's connection weights and thresholds are initialized by random means. These two components are then adjusted to minimize the errors of the output and actual values through the gradient descent by using training data. The training process is completed when the error reaches the set level and the connection weights as well as the thresholds are determined (Wang, Zeng and Chen, 2015).

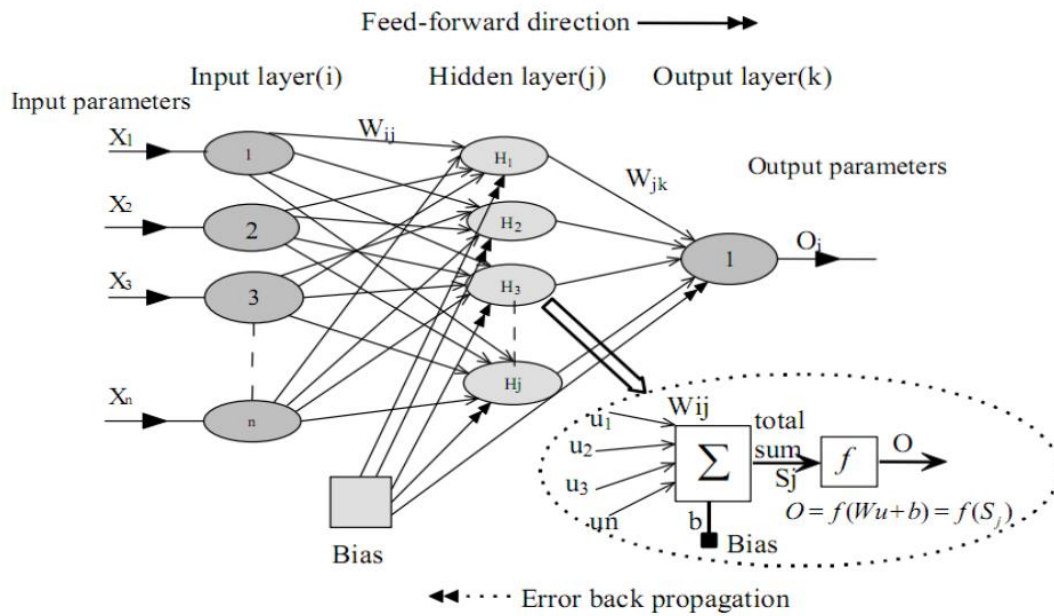


Figure 2.5: Schematic Diagram of BPNN (Pakhale et al., 2015).

Traore, Wang and kerh (2010) carried out a study on the performance of the BPNN in the modelling the  $ET_o$  in the Bobo-Dioulasso region in Sudano-Sahelian zone of Burkina Faso. Temperature data was used as the input variables of the modelling as many of the climatic data was unavailable in the region while sunshine duration, relative humidity and wind speed variables were added as extra variables to test the effects on performance. The result of the BPNN was compared with the result of HARG, by setting PM method as standard reference with RMSE, MAE and  $R^2$  as evaluation criteria. It was shown that BPNN models are more accurate than HARG due to the better generalization ability. The introduction of wind variables into the BPNN models increased the accuracy the most when compared to sunshine duration and relative humidity, rising the  $R^2$  by 9.52%. The input variable combination that offered the highest accuracy was the one that had included all the five variables.

In the study conducted by Kuo et al. (2011), the prediction performance of the BPNN based on PM method was compared to the one based on pan evapotranspiration method. Chia Nan was selected as the area of study and ten weather factors were adopted. Those were maximum temperature, minimum temperature, average temperature, relative humidity, wind speed, solar radiation amount, sunshine duration, dew point, morning ground temperature and

afternoon ground temperature. The evaluation criteria for the prediction performance were the MAE and  $R$ . They found out the forecasted errors were 1.67% and 13.23% for PM method and pan evapotranspiration method respectively, proving that BPNN model is able to predict  $ET_0$  more accurately when it is based on PM method. The model that used all the variables as input variables registered the best accuracy. Besides, they also ranked the ten factors according to their importance in optimizing the degree of correlation between the factors and the predicted  $ET_0$ . It was found that wind speed was the most impactful.

Huo et al. (2012) investigated the performance of BPNN models in estimating the  $ET_0$  utilizing the climatic data from three stations in northwest China. Maximum temperature, minimum temperature, wind speed, relative humidity and sunshine duration were adopted as input variables. Four other methods were adopted to make comparison on the  $ET_0$  estimation of ANN, including multiple linear regressions (MLR), PM equation, PT equation and HARG-Samani equation. The precision of these methods was measured based on RMSE, relative error (RE) and  $R^2$  and results showed that ANN models had the higher accuracy over the other methods. They also found out the ANN model with five input variables was better than three or four input variables only as the model consisted of all five input variables reported the highest accuracy. The effects of climatic variables in terms of accuracy were evaluated using connection weight method. Maximum temperature, minimum temperature and relative humidity were found to be the most important variables. They concluded that the better performance of ANN models is due to the ability to capture the nonlinear input-output relationship.

Falamarzi et al. (2014) tested the ability of both ANN with BPNN type model and wavelet-based neural network (WNN) in estimating the daily  $ET_0$  based on the meteorological data from the Redesdale station in Australia. Maximum and minimum temperature were used as the input variables with wind speed as the extra variable to investigate its effect on the performance of models. The evaluation criteria were the RMSE, absolute percentage error (APE), NSE and  $R$ . The results showed that both models predicted the  $ET_0$  at desirable precision level. The best model was the decomposed time series WNN with two

input variables, six neurons and one output, giving 1.03 mm/day, 0.79, 22% and 0.89 for RMSE, NS, APE and  $R$  respectively.

BPNN is utilized in the study carried by Traore, Wang and Chung (2014) to estimate the ET in Dedougou. The climatic data used as input variables included maximum temperature, minimum temperature, relative humidity, wind speed, extra-terrestrial radiation and sunshine duration. The comparison of accuracy was made between BPNN, Blaney-Criddle (BCR) and Reference Model of Burkina Faso (RMBF) with PM method as standard. RMSE, MAE and  $R^2$  were the evaluation criteria used to measure their precisions. It was shown that BPNN was the most accurate method and the introduction of wind speed as input variables increased the accuracy significantly. Models with all variables showed the lowest error.

Pakhale et al. (2015) applied three types of ANN models, namely BPNN, RBF and GRNN to estimate the daily grass reference crop evapotranspiration in Ameleke watershed with PM method as the standard method. Seven input variables were adopted, namely, maximum temperature, minimum temperature, average temperature, relative humidity, wind speed, rainfall and net radiation. RMSE, model efficiency ( $E$ ) and  $R^2$  were the criteria used to test their performance. In their study, BPNN showed the highest accuracy among the three models. It was explained by the authors that ANN methods are simpler, develop models faster and can be used on minimal data structure compared to PM method.

Panda et al. (2018) tested the performance of BPNN and RBF in estimating the homogenous pine forest daily evapotranspiration flux at Coastal North Carolina, USA. Remote-sensing based estimation tools were adopted by them which required ANN models, ArcGIS-based automated geospatial model and software to forecast the ET flux. Two principal component analysis (PCA) bands were used as input data, namely PC1 and PC2. The performance of the models was determined using average absolute error and average accuracy. BPNN models registered values of 0.18  $\text{Wm}^{-2}$  and 81% of average absolute error and average accuracy respectively, while RBF reported values of 0.15  $\text{Wm}^{-2}$  and 85%.

As one of the most commonly used ANN models in the estimation of  $ET_o$ , many studies were done on the estimation performance of BPNN and showed that it generally proved a higher accuracy compared to the conventional methods. However, it was also shown that there was machine learning algorithm that had a higher estimation precision than the BPNN, for example, RBF. At the same time, it can be seen that the accuracy of the model increased when the number of input variables increased.

### 2.2.5 Extreme Learning Machine

Extreme learning machine (ELM) is a type of learning algorithm applied to the single layer feed-forward neural network (SLFN). This learning algorithm chooses hidden nodes randomly but analytically decides the weights of output of SLFN. ELM has much faster learning speed with conventional feed-forward neural network learning algorithms as comparison and has more favourable generalization capability. It is able to achieve the lowest training error as well as the smallest norm of weights (Huang, Zhu and Siew, 2006). Besides, this algorithm does not need much human intervention as the hidden nodes are chosen randomly (Gocic et al., 2016).

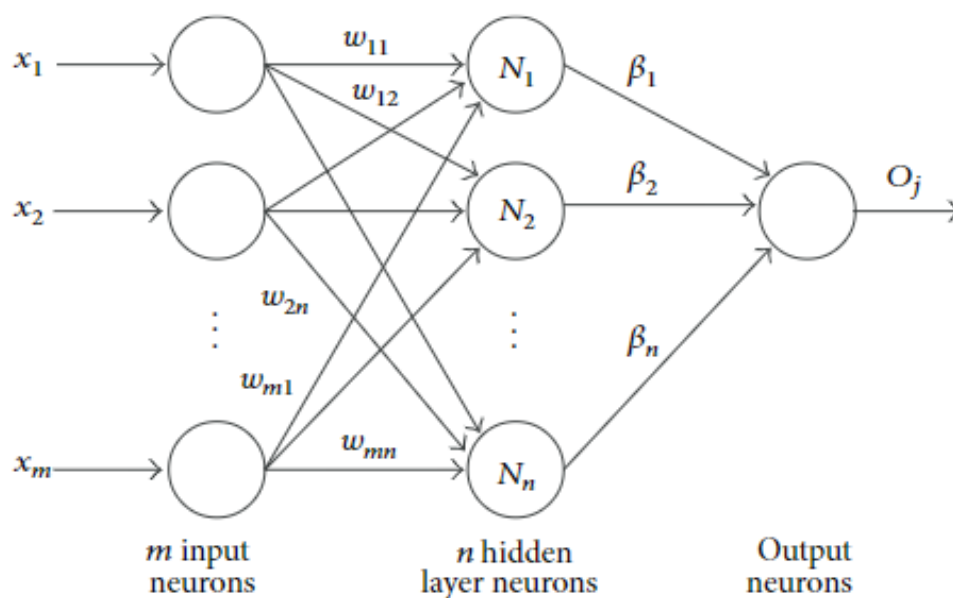


Figure 2.6: Typical Structure of ELM (You et al., 2014).

Weekly reference crop evapotranspiration in Jodhpur and Pali weather stations in Thar Desert, India was estimated using improved ELM in the study done by Patil and Deka (2016). Three ways of input variable combinations were tested: first one consisted only of maximum and minimum temperature data from local stations whereas the other two combinations adopted  $ET_o$  values from other stations together with local temperature data. HARG equation, BPNN type ANN model and least-square support vector machine (LS-SVM) were used to compare the performance with ELM. The climatic data used to train the models included maximum temperature, minimum temperature, maximum relative humidity, minimum relative humidity, wind speed and solar radiation. The estimation performance of the model was measured in terms of RMSE, NSE and threshold statistics (TS). The results indicated that the ELM model was more precise than HARG and ANN models but is almost the same as the LS-SVM model. The model with first type of combination showed the highest accuracy. Besides, they found that the ELM had the fastest training speed among all the models with an average time of 0.004 seconds.

Gocic et al. (2016) analysed the ability of the ELM to estimate the monthly  $ET_o$  in Nis and Belgrade stations in Serbia by using  $ET_o$  values obtained from different equations, namely the Adjusted HARG, PT and Turc equations. Input climatic variables were maximum temperature, minimum temperature, wind speed, actual vapour pressure and sunshine hours while the PM method was used as standard. The precision evaluation criteria included MAD, mean absolute percentage error (MAPE), RMSE,  $R$  and  $R^2$ . ELM model with  $ET_o$  of adjusted HARG reported the greatest accuracy in both stations. It was stated that the advantage of the ELM is that it can estimate the  $ET_o$  with an incomplete data set.

Feng et al. (2016) adopted ELM, genetic algorithm neural network (GANN) and WNN to estimate the  $ET_o$  for region of southwest China. Besides, temperature-based and radiation-based models were developed for the three types of networks and their performance was compared with the HARG and modified HARG for temperature-based models and the Makkink, PT and Ritchie for radiation-based models. Five input variables used were the maximum temperature, minimum temperature, wind speed, relative humidity

and sunshine duration. RMSE and MAE were the criteria determined in order to compare the performance of the methods. Results showed that ELM and GANN were more superior compared to WNN. In terms of temperature-based and radiation-based models, the ELM and GANN models still gave a better accuracy than the others. In terms of variable combination, the one with all variables gave the greatest accuracy. They stated that ELM creates input weights and biases randomly and tuning is not required for the hidden layer, which make it superior to the WNN and BPNN.

The performance of ELM and ANFIS in estimating the  $ET_o$  in four different ecosystems were analysed by Dou and Yang (2018). The mean, maximum, minimum, standard deviation, kurtosis and skewness of four variables including air temperature, net radiation, relative humidity and soil temperature were used as input variables. The effectiveness of the two models were compared with conventional ANN and SVM models. Through the evaluation of accuracy based on  $R^2$ , NSE and RMSE, ELM and ANFIS registered good results. Three types of hybrid ELM, complex ELM (C-ELM), self-adaptive evolutionary ELM (SaE-ELM) and online sequential ELM (OS-ELM) were also developed and it was found that these hybrids were better than the original ELM in estimation. Likewise, the ANFIS-GP, ANFIS-SC and fuzzy c-means clustering ANFIS (ANFIS-FCM) also showed higher accuracy compared to the original ANFIS. They concluded that the better accuracy of both ELM and ANFIS is due to the robustness and feasibility.

Kisi and Alizamir (2018) conducted a study on estimation of  $ET_o$  using wavelet-based ELM (WELM), a model that combines discrete wavelet transform and ELM. Meteorological data including mean temperature, solar radiation, relative humidity and wind speed were obtained from Ankara and Kirikkale stations in central Anatolia, Turkey as input data. Comparison in terms of performance were made between ELM (WELM) and wavelet-based ANN (WANN), single ANN, ELM as well as OS-ELM. The Evaluation criteria used were RMSE, NSE, MAE and  $R^2$ . Models that incorporated wavelet method showed better precisions compared to the other models. Besides, researchers also found out that models with four input variables reported the highest accuracy with solar radiation being the most important variable.

In a nutshell, the performance of ELM for  $ET_0$  estimation was higher than the other comparison methods in the previous researches reviewed. Compared to conventional feed-forward ANN models, the ELM offers much faster learning speed and better generalization ability. Besides, the hidden nodes are selected randomly and therefore require less human monitoring.

Table 2.1: Summary of Journals Reviewed.

No.	Method	Input Variables	Study Area	Best Model and Its Combination Preference	Authors & Years of Publication
1	BPNN, HARG Equation	$T_{max}, T_{min}, R_a, RH, U_2, n$	Bobo-Dioulasso in the Western region of Bukina Faso in Sudano-Sahelian (semi-arid climate)	Model: BPNN 1. $T_{max}, T_{min}, R_a, RH, U_2$ 2. $T_{max}, T_{min}, R_a, U_2$ 3. $T_{max}, T_{min}, RH, U_2$ 4. $T_{max}, T_{min}, U_2$ 5. $T_{max}, T_{min}, RH$ 6. $T_{max}, T_{min}, R_a, RH$ 7. $T_{max}, T_{min}, R_a$ 8. $T_{max}, T_{min}, R_a, n$ 9. $T_{max}, T_{min}$ 10. $T_{max}, T_{min}, n$	(Wang, Traore and Kerh, 2010)
2	BPNN (PM and pan evapotranspiration method as output layer)	$T_{max}, T_{min}, T_{mean}, RH, U_2, n, R_s$ , dew point, morning ground temperature, afternoon ground temperature	Chia Nan irrigated area of Tainan (humid subtropical climate)	Model: BPNN (PM as output layer) 1. $T_{max}, T_{min}$ and $T_{mean}, RH, U_2, n, R_s$ , dew point, morning ground temperature, afternoon ground temperature 2. $T_{max}, T_{min}, RH, U_2, R_s$ , dew point 3. $T_{mean}, RH, U_2, R_s$	(Kuo et al., 2011)
3	BPNN, PM Equation, MLR, PT Equation, HARG-Samani Equation	$T_{max}, T_{min}, RH, n, U_2$	Shiyang River basin in Gansu Province of northwest China (south basin: highly gelid, semi-arid; middle basin: cool	Model: BPNN 1. $T_{max}, T_{min}, RH, n, U_2$ 2. $T_{max}, T_{min}, RH, U_2$ 3. $T_{max}, T_{min}, RH, n$	(Huo et al., 2012)

Table 2.1 (Continued)

			and arid; north basin: warmer and more arid)	4. $T_{max}, T_{min}, RH$ 5. $T_{max}, T_{min}, n, U_2$ 6. $T_{max}, T_{min}, U_2$ 7. $T_{max}, T_{min}, n$ 8. $RH, n, U_2$	
4	ANN, WNN	$T_{max}, T_{min}, U_2$	Redesdale climatology station (oceanic climate)	Model: WNN 1. Decomposed $T_{max}, T_{min}$ 2. Original $T_{max}, T_{min}, U_2$ 3. Original $T_{max}, T_{min}$ 4. Decomposed $T_{max}, T_{min}, U_2$	(Falamarzi et al., 2014)
5	BPNN, RMBF, BCR	$T_{max}, T_{min}, RH, U_2, R_a, n$	Dedougou, western Burkina Faso (semi-arid climate)	Model: BPNN 1. $T_{max}, T_{min}, R_a, RH, n, U_2$ 2. $T_{max}, T_{min}, R_a, U_2$ 3. $T_{max}, T_{min}, R_a$ 4. $T_{max}, T_{min}, R_a, RH$ 5. $T_{max}, T_{min}, R_a, RH, n$	(Wang, Traore and Chung, 2014)
6	BPNN, RBF, GRNN	$T_{max}, T_{min}, T_{mean}, RH, U_2, P, R_s$	Ameleke watershed, Ethiopia (tropical climate)	Model: BPNN 1. $T_{max}, T_{min}$ and $T_{mean}, RH, U_2, P, R_s$	(Pakhale et al., 2015)
7	BPNN, RBF	Remote sensing	Coastal North Carolina, USA (oceanic climate)	Model: RBF 1. PC1, PC2	(Panda et al., 2018)
8	HARG Equation, ELM, LS-SVM	$T_{max}, T_{min}, RH_{max}, RH_{min}, U_2, R_s$	Jodhpur and Pali in Thar Desert, India (arid climate)	Model: ELM 1. $T_{max}, T_{min}$ (local station) 2. $T_{max}, T_{min}$ (others station) 3. $T_{max}$ (others station), $T_{min}$	(Patil and Deka, 2016)

Table 2.1 (Continued)

9	ELM Training: Adjusted HARG Equation, PT Equation, Turc Equation	$T_{max}, T_{min}, U_2, e_a, n$	Belgrade (humid subtropical climate) and Nis (oceanic climate) in Serbia	Model: ELM with adjusted HARG 1. $T_{max}, T_{min}, U_2, e_a, n$	(Gocic et al., 2016)
10	ELM, GANN, WNN, HARG Equation, modified HARG Equation, Makkink Equation, PT Equation, Ritchie Equation	$T_{max}, T_{min}, U_2, RH, n$	Hilly Area of Central Sichuan (HACS), Southwest China (warm and humid climate)	Model: ELM, GANN 1. $T_{max}, T_{min}, U_2, RH, n$ 2. $T_{max}, T_{min}$ 3. $T_{max}, T_{min}, n$	(Feng et al., 2016)
11	ANN, ELM, C-ELM, SaE-ELM, OS-ELM, SVM, ANFIS-GP, ANFIS-SC, ANFIS-FCM	$T_a, R_s, RH, T_s$ (all variables include mean, maximum, minimum, standard deviation, kurtosis, and skewness)	Vaira Ranch in US (Mediterranean climate), Hainich National Park in Germany (oceanic climate), Lonze in Belgium (oceanic climate), Degero-Stromyr in Sweden (Subarctic climate)	Model: ELM, ANFIS 1. $T_a, R_s, RH, T_s,$	(Dou and Yang, 2018)
12	WELM, WANN, ANN, ELM, OS-ELM	$T_{mean}, R_s, RH, U_2$	Ankara and Kirikkale in central Anatolia region of Turkey (semi-arid climate)	Model: WELM, ELM 1. $R_s, T_{mean}, RH, U_2$ 2. $R_s, T_{mean}, RH$ 3. $R_s, T_{mean}$ 4. $R_s$ 5. $T_{mean}$ 6. $RH$ 7. $U_2$	(Kisi and Alizamir, 2018)

Table 2.1 (Continued)

13	GRNN, RBF, HARG Equation, PT Equation	$T_{max}, T_{min}, T_{mean}, RH, U_2, n$	Dar El Beida, Algiers, Algeria (Mediterranean climate)	Model: GRNN 1. $T_{max}, T_{min}, T_{mean}, RH, U_2, n$ 2. $T_{max}, T_{min}, T_{mean}, U_2, n$ 3. $T_{max}, T_{min}, T_{mean}, n$ 4. $T_{max}, T_{min}, T_{mean}$ 5. $T_{max}, T_{mean}$	(Ladlani et al., 2012)
14	GRNN, MLR	$n, T_{max}, T_{min}, T_{mean}, U_2$	Guelma, Algeria (semi-arid climate)	Model: GRNN 1. $n, T_{max}, T_{min}, T_{mean}, U_2$	(Salim et al., 2013)
15	RF, GRNN	$T_{max}, T_{min}, R_s, U_2, RH, R_a$	Chengdu and Nanchong in Sichuan basin, southwest China (humid and warm climate)	Model: RF Chengdu: 1. RF1 ( $T_{max}, T_{min}, R_s, U_2, RH$ ) 2. GRNN1 ( $T_{max}, T_{min}, R_s, U_2, RH$ ) 3. RF2 ( $T_{max}, T_{min}, R_a$ ) 4. GRNN2 ( $T_{max}, T_{min}, R_a$ ) Nanchong: 1. RF1 ( $T_{max}, T_{min}, R_s, U_2, RH$ ) 2. GRNN1 ( $T_{max}, T_{min}, R_s, U_2, RH$ ) 3. RF2 ( $T_{max}, T_{min}, R_a$ ) 4. GRNN2 ( $T_{max}, T_{min}, R_a$ )	(Feng et al., 2017)
16	ELM, GRNN, HARG Equation, Calibrated HARG Equation	$T_{max}, T_{min}, R_a$	Chengdu, Liangping, Mianyang, Nanchong, Neijiang, Shapingba in Sichuan basin, southwest China (warm and humid climate)	Model: GRNN (Pooled), ELM (Individual) 1. $T_{max}, T_{min}, R_a$	(Feng et al., 2017)

Table 2.1 (Continued)

17	MLP, ARIMA	$T, R_s, RH, U_2$	Álava in Basque Country, Northern Spain (oceanic climate)	Model: MLP, ARIMA 1. $T, R_s, RH, U_2$	(Landeras, Ortiz-Barredo and Lopez, 2009)
18	MLP, HARG Equation	$T_{max}, T_{min}, RH, U_2$	Caspian Sea, Iran (humid subtropical climate)	Model: MLP 1. $T_{max}, T_{min}, RH, U_2$	(Rahimikhoob, 2010)
19	MLP, $E_{pan}$ X Kp equation	$T_{max}, T_{min}$	Sabarmati River, Gujarat State (semi-arid climate)	Model: MLP 1. $T_{max}, T_{min}$	(Jadeja, 2011)
20	MLP, CIMIS Penman Equation, HARG Equation, Ritchie Equation, ANFIS-GP, ANFIS-SC	$T_{mean}, RH, R_s, U_2$	Santa Monica in Los Angeles (moderate Mediterranean climate)	Model: S-ANFIS 1. $R_s, T_{mean}, RH, U_2$ 2. $R_s, T_{mean}, RH$ 3. $R_s, T_{mean}, U_2$ 4. $R_s, T_{mean}$ 5. $R_s$ 6. $T_{mean}$ 7. $U_2$ 8. $RH$	(Cobaner, 2011)
21	MLP, HARG Equation, MVRVM	$T_{max}, T_{min}$	Sevier River Basin in Central Utah, USA (semi-desert climate)	Model: MVRVM 1. $T_{max}, T_{min}$	(Torres, Walker and McKee, 2011)
22	MLP, GEP, ANFIS-SC, ANFIS-GP	Longitude and latitude values, station altitude and periodicity component	50 stations in Iran (arid and semi-arid climate)	Model: MLP 1. Longitude and latitude values, station altitude and periodicity component	(Kisi et al., 2015)

Table 2.1 (Continued)

23	MLP, PNN, GFF, LR	$T_{max}, T_{min}$	Jiangsu Province, China (humid subtropical climate)	Model: MLP, PNN, GFF 1. $T_{max}, T_{min}$	(Luo et al., 2015)
24	MLP, GEP	$T_{max}, T_{min}, T_{mean},$ $RH_{max}, RH_{min},$ $RH_{mean}, U_2, R_s, h_c$	Kingdom of Saudi Arabia (arid climate)	Model: MLP 1. $T_{max}, T_{min}, T_{mean}, RH_{max}, RH_{min},$ $RH_{mean}, U_2, R_s, h_c$ 2. $T_{max}, T_{min}, T_{mean}, RH_{max}, RH_{min},$ $RH_{mean}, U_2, h_c$ 3. $T_{max}, T_{min}, T_{mean}, U_2, R_s, h_c$ 4. $T_{max}, T_{min}, T_{mean}, U_2, h_c$ 5. $T_{max}, T_{min}, T_{mean}, RH_{max}, RH_{min},$ $RH_{mean}, R_s, h_c$ 6. $T_{max}, T_{min}, T_{mean}, RH_{max}, RH_{min},$ $RH_{mean}, h_c$ 7. $T_{max}, T_{min}, T_{mean}, R_s, h_c$ 8. $T_{max}, T_{min}, T_{mean}, h_c$	(Yassin, Alazba and Mattar, 2016)
25	MLP, PNN, GFF, LR	$T_{max}, T_{min}, R_a, R_s$	Dallas, State of Texas (humid subtropical climate)	Model: MLP 1. $T_{max}, T_{min}, R_s$ 2. $T_{max}, T_{min}, R_a$ 3. $T_{max}, T_{min}$	(Traore, Luo and Fipps, 2015)
26	PT Equation, HARG Equation, FAO-24 Makkink Equation, mass transfer method, MLP	$T, RH, R_s, U_2$	Aminteo, West Macedonia, of northern Greece (humid subtropical climate)	Model: MLP 1. $T, RH, R_s, U_2$ 2. $T, RH, R_s$ 3. $T, R_s$ 4. $T, RH$ 5. $T$	(Antonopoulos and Antonopoulos, 2017)

Table 2.1 (Continued)

27	MLP, SVM, HARG-Samani Equation, Oudin Equation, Hamon Equation, Valiantzas Equation, Romanenko Equation, Schendel Equation	$T, RH$	Brazil (equatorial, tropical, high altitude tropical, atlantic tropical, semi-arid, subtropical)	Model: MLP 1. $T, RH$ 2. $T$	(Ferreira et al., 2019)
28	DL-MLP, GLM, RF, GBM	$T_{max}, T_{min}, RH, U_2, n$	Hoshiarpur (monsoon-influenced humid subtropical climate) and Patiala (hot semi-arid climate) in Punjab, northern India	Model: DL-MLP 1. $T_{max}, T_{min}, RH, U_2, n$	(Saggi and Jain, 2019)
29	pan-based RBF, Christiansen Equation, FAO-24 pan Equation, PM Equation	$E_{pan}, R_a$	Policoro, Italy; Novi Sad, Serbia and Kimberly, Idaho, USA (Mediterranean semi-arid climate)	Model: RBF 1. $E_{pan}, R_a$	(Trajkovic, 2009)
30	WMLR, MLR, WRBF, PM Equation, HARG Equation and Turc Equation	$T, R_s, U_2, RH$	Otay Lake and Escondido SPA in San Diego, Davis in Yolo (Mediterranean climate)	Model: WRBF 1. $R_s$ 2. $T, R_s$ 3. $T, R_s, U_2$ 4. $T, R_s, RH, U_2$	(Partal, 2015)
31	RBF, GP, MLR	$T_{max}, T_{min}, RH, U_2, R_s$	Isfahan synoptic station in central Iran (hot and dry climate)	Model: RBF (fastest), GP (accuracy) For GP case: 1. $T_{mean}, U_2, R_s$ 2. $T_{mean}, U_2, RH$	(Goodarzi and Eslamian, 2018)

Table 2.1 (Continued)

				3. $T_{mean}, U_2, RH, R_s$	
				4. $T_{mean}, RH, R_s$	
				5. $T_{max}, T_{min}, U_2$	
				6. $T_{max}, T_{min}, R_s$	
				7. $T_{max}, T_{min}, RH$	
				8. $U_2, RH, R_s$	
32	RBF-PSO, RBF-BP, ANN, SVM	$T_{max}, T_{min}, e_a, n, U_2$	Serbia (moderately continental climate)	Model: RBF-PSO 1. $T_{max}, T_{min}, e_a, n, U_2$	(Petkovic et al., 2015)

### 2.3 Bootstrap Aggregating

The bootstrap method is a method that works on data-based simulation for the purpose of statistical inference. It was first introduced by Bradley Efron (1979). According to Efron and Tibshirani (1993), resampling of data is carried out intensively using the replacement method to generate the bootstrap samples and the replicate of each sample is obtained. Through the data resampling, a set of bootstrap samples with a more desirable understanding of the average and the variability of the initial datasets can be reached. This method forms the basis of bootstrap aggregating or also known as bagging which was proposed by Breiman (1996) in order to reduce the estimation error of learning algorithms. In bagging method,  $B$  independent bootstrap samples are drawn from the original sample. Each sample is applied to the learning algorithm and the  $B$  resultant models are then aggregated (Pino-Mejías et al., 2008).

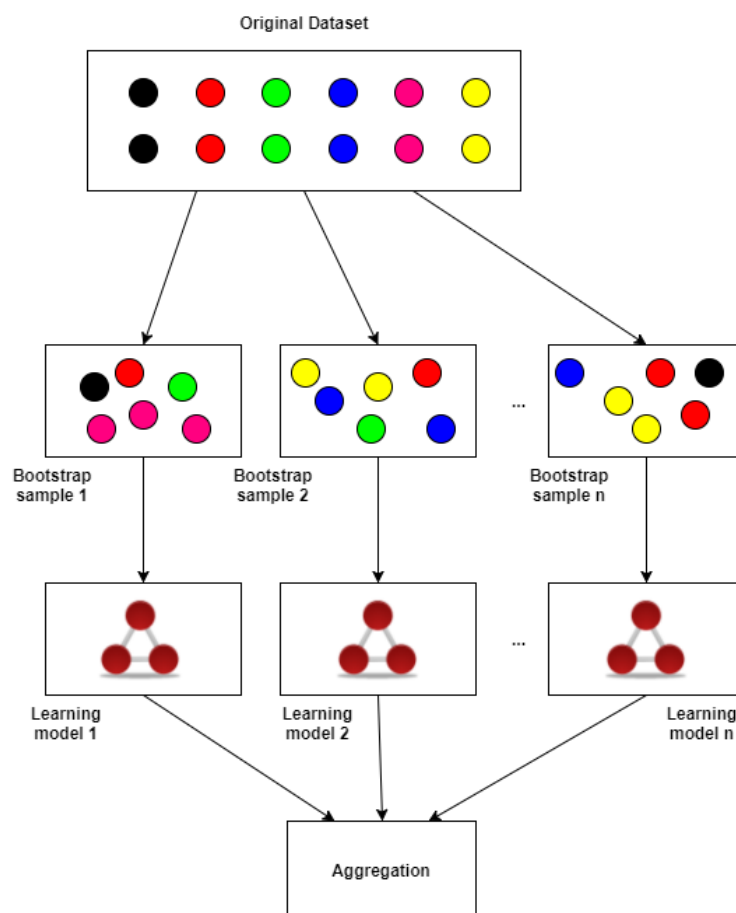


Figure 2.7: Procedure of Bootstrap Aggregating (Lan, 2019).

In the modelling of ANN, estimation tends to be biased between the space of input and output sections due to the underestimation or overestimation of deterministic function, unfitting architecture setting and premature halting of training (Tiwari and Chatterjee, 2010). Due to this reason, bootstrapping method has been incorporated in the neural networks modelling and applied in performing bootstrap aggregation (bagging) for multi-model ensembles. The estimation accuracy of neural network model can be enhanced with data resampling to obtain multiple versions of datasets and aggregating them (Breiman, 1996). Theoretically, a higher accuracy of estimation can be achieved by increasing the number of bootstrap replication but in practice, the increment will not guarantee desired results with the exchange of longer training time (Xu et al., 2017). Therefore, the number of repetitions usually ranges from 50 to 200.

In the study done by Sharma and Tiwari (2009), bagging method had been incorporated in ANN model to predict the monthly runoff in Upper Damodar Valley Catchment. Five input variables were used in the study including standardized monthly rainfall, topography, soil, geomorphology, and normalized difference vegetation index. 188 set of data each having all the five input data were used, with 126 training sets which were obtained by random resampling and the rest of 62 sets as validation. A total of 50 replications of training set were selected randomly for bagging, and the estimates of the bootstrap replicates were averaged to obtain the final output. Maximum number of 100 intervals were set for each estimation of bootstrap replicate. Whenever a minimum value was acquired by the network objective function or the maximum number of intervals was reached, the training of each bootstrap sets would be terminated. The performance of the bootstrap-based ANN (BANN) was tested by comparing with single ANN and multiple regression models. BANN models consistently showed better results than single ANN and multiple regression models for each hierarchy of input variables. They concluded that the performance of BANN is due to its greater generalization ability.

In the research carried out by Tiwari and Chatterjee (2010), BANN was used to analyse the uncertainty of hourly flood forecast. Low, medium and high peak water levels were the input variables. These models were used for forecasting a one to ten hour lead time and the average of the estimation results

represented the final water level forecast. Four BANN models were developed which adopted bootstrap aggregation of multi-model ensembles registered averaged outputs as well as more stable solution with conventional ANN models as a comparison. It was shown that the uncertainty of parameters could be quantified based on the confidence interval of BANN method and thus could improve the prediction reliability.

Another study done by Liu et al. (2014) was to estimate the ice-cover thickness in rivers at two sites, which were the Athabasca River at Fort McMurray and Clear Water River at Draper using bootstrap based artificial neural network (BANN). Comparison was made between BANN models, conventional ANN models and MLR models. Input data used to train the models were water level, accumulated freezing degree days and air temperature. For both ANN and BANN models, architecture of single hidden layer and double hidden layer were also tested respectively. Bootstrap size ranged from 2 to 30 were adopted and found that the performance rose with the increase of size until a certain size, and there was no more performance increase with the increase in bootstrap size. Optimum bootstrap size at Athabasca was 17 for both single and double hidden layers while at Draper, they were 11 and 19 respectively. The results pointed out that the model with the highest performance was the BANN model, followed by ANN model and lastly MLR model. It was mentioned that the BANN model had advantages in terms of ensemble modelling, enhanced model robustness as well as improved reliability.

Bootstrap-based artificial neural network was also adopted in the study of energy efficiency optimization of a crude distillation unit carried out by Osulale and Zhang (2015). In this study, ANN models for energy efficiency and product quality which were developed by simulation of data were used to optimize energy efficiency. Bootstrap sample of 30 neural networks was developed using product flow rate as input variable. It was shown that when neural network was used individually, its performance in training was inconsistent and the unseen validation data was not robust. On the other hand, BANN showed consistent training performance and unseen validation data. Bootstrap method was introduced to improve the accuracy and reliability of the models.

Tahir, Tehzeeb-ul-Hassan and Saqib (2016) compared the performance of both conventional BPNN model and the one with bootstrap aggregating algorithm in simulating the load-shedding in Pakistan. The generated power, load demand, load shed in 24 hours duration and frequency deviation were obtained from Pakistan's power system as input variables. The result showed that the error between the actual and simulated results was reduced significantly when bagging algorithm was used compared to conventional ANN model.

Based on the studies reviewed, it can be seen that the model prediction accuracy with bootstrap aggregating was increased compared to the one without bootstrap aggregating. This is because bootstrap aggregating is able to create more data version by data resampling. As the degree of accuracy of the estimation performed by a model is the main concern, bootstrap aggregating can be applied together to improve the reliability of the estimation.

## **2.4 Summary**

In chapter 2, five types of ANN models including MLP, RBF, GRNN, BPNN and ELM are discussed on their application to the estimation of  $ET_o$  and their degree of accuracy in the estimation. Generally, the ANN models show a higher accuracy compared to conventional methods in estimating the  $ET_o$ , especially when there is not sufficient climatic data available. Besides, bootstrap aggregating can be incorporated to further enhance the performance of ANN models. This method resamples the data into multiple sets of data and aggregates them.

In this study, ELM which can be viewed as the ANN model that needs the shortest training time was selected to study on its ability to provide satisfactory accuracy in estimating the  $ET_o$  values in exchange for its renowned training speed. The effect of the addition of bootstrap aggregating fusion method to the model estimation ability will also be observed.

## CHAPTER 3

### METHODOLOGY AND WORK PLAN

#### 3.1 Workflow of Study

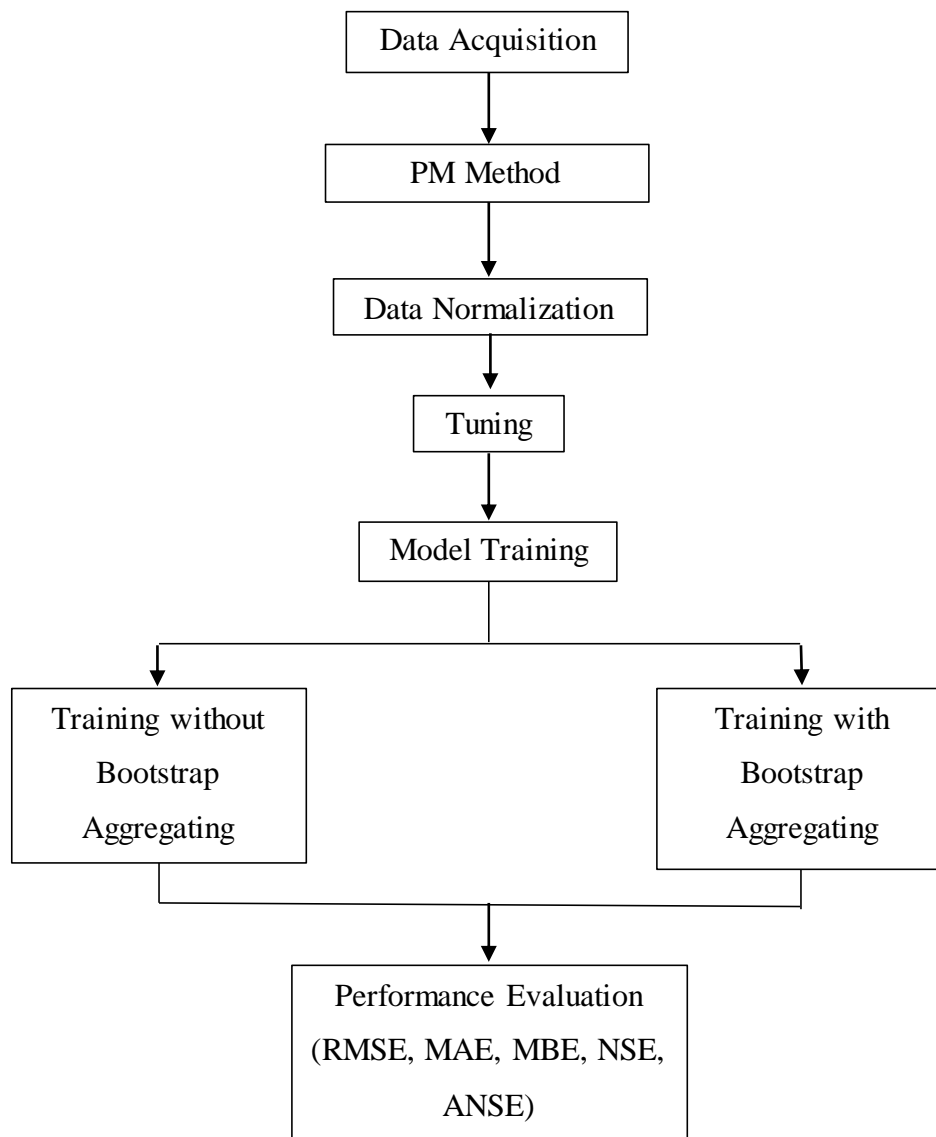


Figure 3.1: Overall Work Plan.

#### 3.2 Mapping, Location of Study and Data Acquisition

Eight stations were selected for study which are positioned in Peninsular Malaysia (Figure 3.2). These eight stations are the Kuala Lumpur International Airport (KLIA) Sepang station which is located at  $2^{\circ}44'N$  latitude and  $101^{\circ}42'E$

longitude, Alor Setar station which is located at  $6^{\circ}12'N$  latitude and  $100^{\circ}24'E$  longitude, Bayan Lepas station which is located at  $5^{\circ}18'N$  latitude and  $100^{\circ}16'E$  longitude, Ipoh station which is located at  $4^{\circ}34'N$  latitude and  $101^{\circ}06'E$  longitude, Lubok Merbau station which is located at  $4^{\circ}48'N$  latitude and  $100^{\circ}54'E$  longitude, Pulau Langkawi station which is located at  $6^{\circ}20'N$  latitude and  $99^{\circ}44'E$  longitude, Sitiawan station which is located at  $4^{\circ}13'N$  latitude and  $100^{\circ}42'E$  longitude and Subang station which is located at  $3^{\circ}08'N$  latitude and  $101^{\circ}33'E$  longitude.

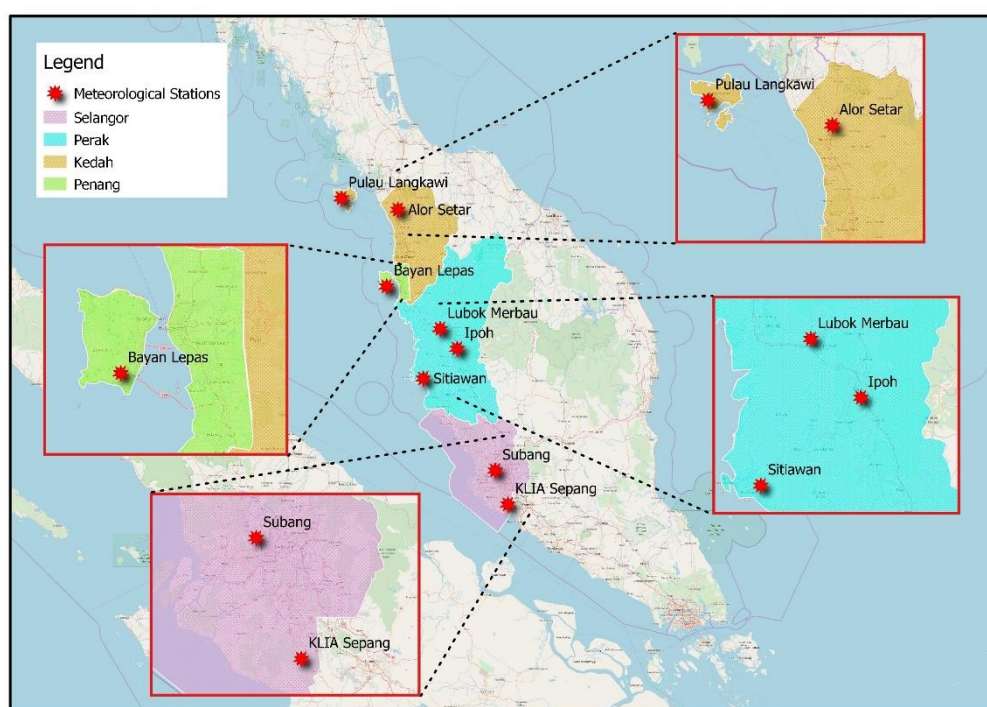


Figure 3.2: Location of Study.

In this study, the daily climatic data used composed of maximum temperature ( $T_{max}$ ), minimum temperature ( $T_{min}$ ), mean temperature ( $T_{mean}$ ), 24 hours mean relative humidity ( $RH$ ), 24 hours mean wind speed ( $U_2$ ), and solar radiation ( $R_s$ ) for the eight stations. The period of these data ranged from 1<sup>st</sup> of January 2014 to 31<sup>st</sup> of December 2018, a period of five years.

Using the six types of climatic data, a total of 63 ways of combinations can be obtained. Each combination was used as input for neural network model training. Table 3.1 shows the climatic data those are included in each of the combinations.

Table 3.1: Combinations of Climatic Data.

<b>Combination</b>	$T_{max}$	$T_{min}$	$T_{mean}$	$RH$	$U_2$	$R_s$
C1	✓	✓	✓	✓	✓	✓
C2		✓	✓	✓	✓	✓
C3	✓		✓	✓	✓	✓
C4	✓	✓		✓	✓	✓
C5	✓	✓	✓		✓	✓
C6	✓	✓	✓	✓		✓
C7	✓	✓	✓	✓	✓	
C8			✓	✓	✓	✓
C9		✓		✓	✓	✓
C10		✓	✓		✓	✓
C11		✓	✓	✓		✓
C12		✓	✓	✓	✓	
C13	✓			✓	✓	✓
C14	✓		✓		✓	✓
C15	✓		✓	✓		✓
C16	✓		✓	✓	✓	
C17	✓	✓			✓	✓
C18	✓	✓		✓		✓
C19	✓	✓		✓	✓	
C20	✓	✓	✓			✓
C21	✓	✓	✓		✓	
C22	✓	✓	✓	✓		
C23				✓	✓	✓
C24			✓		✓	✓
C25			✓	✓		✓
C26			✓	✓	✓	
C27		✓			✓	✓
C28		✓		✓		✓
C29		✓		✓	✓	
C30		✓	✓			✓
C31		✓	✓		✓	
C32		✓	✓	✓		
C33	✓				✓	✓
C34	✓			✓		✓
C35	✓			✓	✓	
C36	✓		✓			✓
C37	✓		✓		✓	
C38	✓		✓	✓		

C39	✓	✓				✓
<u>Table 3.1 (Continued)</u>						
C40	✓	✓			✓	
C41	✓	✓		✓		
C42	✓	✓	✓			
C43					✓	✓
C44				✓		✓
C45				✓	✓	
C46			✓			✓
C47			✓		✓	
C48			✓	✓		
C49		✓				✓
C50		✓			✓	
C51		✓		✓		
C52		✓	✓			
C53	✓					✓
C54	✓				✓	
C55	✓			✓		
C56	✓		✓			
C57	✓	✓				
C58						✓
C59					✓	
C60				✓		
C61			✓			
C62		✓				
C63	✓					

The symbol ✓ indicates that the parameter is involved in the combination.

### 3.3 FAO-56 Penman-Monteith Method

The FAO-56 Penman-Monteith Equation (PM) equation is used as a benchmark in this study to estimate the reference evapotranspiration (Allen et al., 1998):

$$ET_o = \frac{0.408\Delta(R_n - G) + \gamma \frac{900}{T+273} U_2 (e_s - e_a)}{\Delta + \gamma(1 + 0.34 U_2)} \quad (3.1)$$

where

$ET_o$  = reference evapotranspiration (mm day<sup>-1</sup>)

$\Delta$  = slope vapour pressure curve (kPa °C<sup>-1</sup>)

$R_n$  = net radiation at the crop surface (MJ m<sup>-2</sup> day<sup>-1</sup>)

$G$  = soil heat flux density (MJ m<sup>-2</sup> day<sup>-1</sup>)

$\gamma$  = psychrometric constant (kPa °C<sup>-1</sup>)

$T$  = mean daily air temperature at 2 m height (°C)

$U_2$  = wind speed at 2 m height (m s<sup>-1</sup>)

$e_s$  = saturation vapour pressure (kPa)

$e_a$  = actual vapour pressure (kPa)

$e_s - e_a$  = saturation vapour pressure deficit (kPa)

### 3.4 Normalization of Data

The data were normalized before being used to train the ANN models. The aim of normalization is to restrict the values of each data set within the range of 0 and 1. The normalization equation used is as equation 3.2 below (Wang, Traore and Kerh, 2008):

$$X_{norm} = \frac{X_i - X_{min}}{X_{max} - X_{min}} \quad (3.2)$$

where

$X_{norm}$  = normalized value of variable

$X_i$  = observed value of variable

$X_{min}$  = minimum value of the variable

$X_{max}$  = maximum value of variable

### 3.5 Parameter Tuning

The generalization performance of ANN model is dependent of the setting of hyper-parameters such as the number of nodes having in hidden layer, activation function in input layer and output layer and the learning rate. However, long processing time is required to test all the combination of the parameters aforementioned to find the best combination. Parameter tuning is a process of getting the optimum combination of parameters for the learning algorithm (Lahiri and Ghanta, 2009).

### 3.6 k-Fold Cross Validation

k-fold cross-validation is a renowned method for estimating generalization error. In this type of cross-validation, the training data set is separated into k equal mutually exclusive subsets or called folds. The first fold is used as testing data and the rest of the subsets is utilized as training data and the error is calculated. This process is iterated k times and each time different fold is used as the testing data. The generalization error is then obtained by averaging the sum of the test errors with value of k (Duan, Keerthi and Poo, 2003).

### 3.7 Extreme Learning Machine

ELM model architecture comprises of input layer, hidden layer and output layer. A model of this learning algorithm with N arbitrary inputs with L hidden nodes and f(x) activation can be modelled as below:

$$\sum_{i=1}^L \beta_i f(w_i x_i + b_i) = y_i, j = 1, 2, 3, \dots, N \quad (3.3)$$

where

$x_i$  = ith input

$w_i$  = ith input weight

$b_i$  = ith biases

$\beta_i$  = ith output weight

The relation above can be represented in a compact form as (Patil and Deka, 2016):

$$H\beta = Y \quad (3.4)$$

where H is the output matrix for hidden nodes and is written as

$$H = \begin{pmatrix} f(w_1 x_1 + b_1) & \dots & f(w_L x_1 + b_L) \\ \vdots & \ddots & \vdots \\ f(w_1 x_N + b_1) & \dots & f(w_L x_N + b_L) \end{pmatrix} \quad (3.5)$$

$$\beta = (\beta_1 \dots \beta_L)^T \quad (3.6)$$

$$Y = (y_1 \dots y_N)^T \quad (3.7)$$

Before training,  $w$  and  $b$  will be produced randomly. After that, the hidden layer output matrix  $H$  will be first computed and using the  $H$  obtained, output weight matrix  $\beta$  will be calculated. In this model,  $w$  and  $b$  are randomly chosen for hidden nodes and then the output weights are computed by obtaining the least-square solution (Feng et al, 2016).

### 3.8 Activation Function of Model

In neural network, activation function is aimed to convert activation level of a neuron into an output signal (Sibi, Jones and Siddarth, 2013). When the activation function used is infinitely differentiable at any interval, the parameters of the network need no adjustment as long as there is enough number of hidden nodes. Such activation functions include sigmoidal function, radial basis function (RBF), sine, cosine, exponential and some other non-regular functions as indicated by Huang and Babri (1998) in their study. Sigmoidal, RBF and sine functions were more commonly adopted functions in ELM model (Ding et al., 2013) and hence three of them were also used in this study. The expression of the three activation functions are as followed.

Sigmoidal Function:

$$f(x) = \frac{1}{1+e^{-x}} \quad (3.8)$$

where

$x$  = input of the function

Sine Function:

$$f(x) = \sin(x) \quad (3.9)$$

Radial Basis Function (RBF) with function  $g(x)$ :

$$f(x) = g(b_i ||x - a_i ||) \quad (3.10)$$

where

$a_i$  = centre of  $i$ th RBF node

$b_i$  = impact factor of  $i$ th RBF node

### 3.9 Bootstrap Aggregating Fusion Method

In the application of bootstrapping method training datasets, multiple realizations can be simulated from each single dataset by iterating “sampling and replacement” of the original dataset with size of  $N$  to generate  $B$  bootstrap datasets. In this way,  $B$  neural networks are generated as each bootstrap dataset has different data. Each of these bootstrap datasets are provided with a model  $f(x)$  and bootstrapping estimate  $f_{bootstrap}(x)$  is computed (Sharma and Tiwari, 2009):

$$f_{bootstrap}(x) = \frac{1}{B} \sum_{b=1}^B f(x) \quad (3.11)$$

### 3.10 Performance Evaluation

The evaluation of performance of each model is carried out by comparing the models' estimated values with the values estimated with the PM method. There are five evaluation criteria adopted in this study, namely; root mean square error (RMSE), mean absolute error (MAE), mean bias error (MBE), Nash-Sutcliffe model efficiency coefficient (NSE) and adjusted Nash-Sutcliffe model efficiency coefficient (ANSE).

RMSE is the measure of the standard deviation of differences between PM estimated values and model estimated values (Patil and Deka, 2016).

$$RMSE = \sqrt{\frac{\sum_{i=1}^n (X_i - Y_i)^2}{n}} \quad (3.12)$$

where

$X_i$  = PM estimated value

$Y_i$  = model estimated value

$n$  = number of data

MAE is the average of the absolute difference between the PM observed values and the model estimated value (Chai and Draxler, 2014).

$$MAE = \frac{1}{n} \sum_{i=1}^n |X_i - Y_i| \quad (3.13)$$

Similar to MAE, MBE also refers to the average of difference between the PM estimated value and model estimated value. The difference is that the signs of the errors are remained (Willmott and Matsuura, 2006).

$$MBE = \frac{1}{n} \sum_{i=1}^n Y_i - X_i \quad (3.14)$$

Nash-Sutcliffe model efficiency coefficient measures the efficiency of the models and can have value ranged from  $-\infty$  to 1. NSE with value of 1 means that the observed and estimated values are perfectly matched (Patil and Deka, 2016).

$$NSE = 1 - \frac{\sum_{i=1}^n (X_i - Y_i)^2}{\sum_{i=1}^n (X_i - \bar{X})^2} \quad (3.15)$$

ANSE is a modified NSE that has been adjusted for number of terms in the models. The equation is as followed:

$$ANSE = 1 - (1 - NSE) \frac{(n-1)}{(n-k)} \quad (3.16)$$

where

$k$  = number of variables

Results with lower values of RMSE, MAE and MBE values nearer to zero or higher values of NSE and ANSE indicate a better performance and accuracy.

## CHAPTER 4

### RESULTS AND DISCUSSION

#### 4.1 Parameter Tuning of the Model

Unlike other types of ANN which require tuning of various parameters, the ELM model just needs to be tuned for its hidden node number and activation function. The bias of the network needs not to be tuned. In this study, the optimum hidden node number as well as the activation function were found by trial and error. It can be observed that the optimum condition of these two parameters varied from one combination to another.

##### 4.1.1 Hidden Node Number

Although the hidden neuron parameters such as bias need not to be tuned, it is crucial to tune the number of hidden nodes. The hidden node number tested in this study was ranged from 1 to 50. This range of node number was considered because the RMSE of the results for the case of more input variables mostly became stable at around 20 to 50. While for the case of fewer input variables, the RMSE either reached its stability at low node numbers or turned out to be higher as the node number increases. Therefore, the node number higher than 50 was not considered in the training of the model.

The optimum hidden node number for every combination of each station was different from each other. Based on Appendix A, it can be seen that the majority of the combinations with three or more input variables had optimum hidden nodes more than 10. Most combinations that had less than 10 optimum hidden nodes used just one or two climatic variables.

Figure 4.1 is the graph of RMSE against node number for six input variables with the sigmoid function for the Alor Setar station. The graph shows a drop in RMSE with an increase in the number of hidden nodes and the drop in value is very small when the node number reaches around 30. However, when the number of input variables becomes lesser, the increase in node number no longer gives a decrease in RMSE or the RMSE reaches a stable value at a low node number, as shown in Figure 4.2. It was suggested that a higher hidden node

number has a higher possibility to yield more accurate results, but this is only true with sufficient number of climatic variables. The pattern shown by combination with a little number of input variables might not be good because a low number of input variables can hardly establish a good relationship to estimate the result, and therefore the change in node number is not important to help in tuning the result.

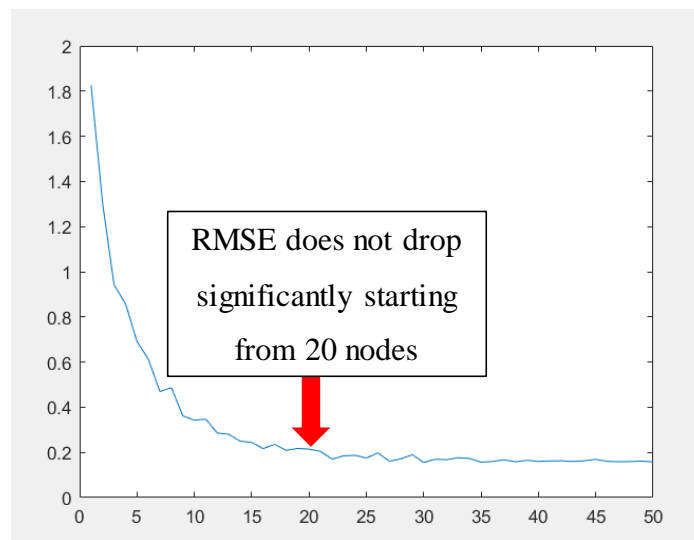


Figure 4.1: Graph of RMSE against Hidden Node Number (Alor Setar, Sigmoid, C1).

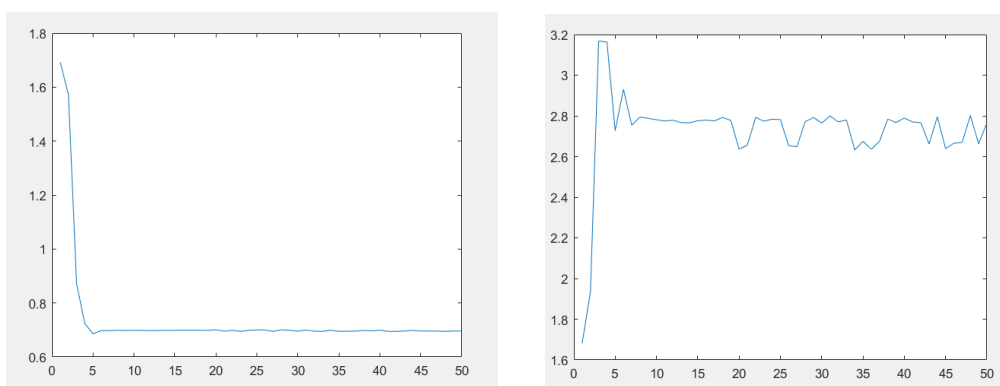


Figure 4.2: Graphs of RMSE against Hidden Node Number for (left) Alor Setar, Sigmoid, C60 and (right) Alor Setar, Sigmoid, C62.

#### 4.1.2 Activation function

Three types of activation functions comprising of sigmoid, RBF and sine functions were utilized to train the ELM and compared for their performance.

Table 4.1 shows the percentage of the lowest RMSE given by each function among three of them for all 63 combinations. The sine function registered the highest percentage of lowest RMSE as well as highest NSE in four of the stations comprising of Bayan Lepas, Ipoh, KLIA Sepang and Langkawi. Sigmoid function showed the highest percentage for Alor Setar station and Subang station while RBF showed the highest percentage for Lubok Merbau station and Sitiawan station.

Table 4.1: Percentage of the Activation Function giving Best Results in 63 Combinations for Each Station.

Stations	Sigmoid (%)	RBF (%)	Sine (%)
Alor Setar	<b>46.03</b>	15.87	38.10
Bayan Lepas	31.75	31.75	<b>36.50</b>
Ipoh	22.22	38.10	<b>39.68</b>
KLIA Sepang	33.33	30.16	<b>36.51</b>
Lubok Merbau	17.46	<b>46.03</b>	36.51
Pulau Langkawi	34.92	23.81	<b>41.27</b>
Sitiawan	28.58	<b>44.44</b>	26.98
Subang	<b>38.10</b>	33.33	28.57

The sine function might be effective in predicting the  $ET_o$  with climate that is affected by airport activities as four of the stations that were well predicted by sine function have airports in the areas. Alor Setar and Subang also have airports nearby the stations but the  $ET_o$  were well predicted using sigmoidal function for the two stations. This might due to the difference that a large field of vegetation exists nearby each of these two stations. On the other hand, RBF function might work well in regions which are not affected by airport activities in that RBF showed the largest percentage of lowest RMSE for Lubok Merbau and Sitiawan stations.

#### 4.2 Result Analysis for Conventional ELM

For the Alor Setar station, C1 which consists of six climatic data had the lowest RMSE and highest NSE among 63 combinations, with values of 0.1530 and 0.9745 respectively. For combinations with five variables, C4 had the best result with RMSE of 0.1642 and NSE of 0.9733 whereas C7 had the worst result with

RMSE of 0.3996 and NSE of 0.8593. For combinations with four variables, C13 had the greatest performance with RMSE of 0.1804 and NSE of 0.9645 while C22 had the worst performance with RMSE of 0.4776 and NSE of 0.8006. For combinations with three variables, C33 had the best performance with RMSE of 0.2290 and NSE of 0.9445 while C42 had the worst performance with RMSE of 0.6619 and NSE of 0.6116. For combinations with two variables, C44 had the best result with RMSE of 0.3219 and NSE of 0.9035 and C50 had the worst result with RMSE of 1.1205 and NSE of -0.1074. Among combinations with only one input variable, C60 showed the highest performance with RMSE of 0.6855 and NSE of 0.5879. The worst combination is C62 with RMSE of 1.6701 and NSE of -1.4412. Based on Table 4.1, by comparing the best combinations selected from each of the variable amount categories, the accuracy of the result decreased as the number of input variables decreased. The performance evaluation of all 63 combinations for all stations is stated in Appendix A.

Table 4.2: Result Performance at Alor Setar Station using ELM.

<b>Number of Variables</b>	<b>Input</b>	<b>Best Activation Function</b>	<b>Best Hidden Nodes</b>	<b>RMSE</b>	<b>NSE</b>	<b>ANSE</b>	<b>MAE</b>	<b>MBE</b>
6	C1	Sine	29	0.1530	0.9745	0.9738	0.1308	0.0979
5	C4	Sine	31	0.1642	0.9733	0.9727	0.1406	0.1114
4	C13	Sigmoid	42	0.1804	0.9645	0.9639	0.1535	0.1158
3	C33	Sigmoid	11	0.2290	0.9445	0.9439	0.1885	0.1164
2	C44	Sine	27	0.3219	0.9035	0.9030	0.2652	0.2186
1	C60	Sigmoid	5	0.6855	0.5879	0.5879	0.5336	0.1254

For the Bayan Lepas station, C1 was the best among all 63 combinations, with RMSE of 0.1259 and NSE of 0.9846. In the case of combinations with five variables, C3 showed the greatest performance with RMSE of 0.1576 and NSE of 0.9765 while C7 showed the worst performance with RMSE of 0.6130 and NSE of 0.6775. For combinations with four variables, C13 had the best result with RMSE of 0.1653 and NSE of 0.9742 whereas C21 had the worst result with RMSE of 0.7340 and NSE of 0.5162. For combinations with three variables, the best result was presented by C23 with RMSE of 0.2034 and NSE of 0.9626 while the worst was presented by C42 with RMSE of 1.2780 and NSE of -

0.4486. For combinations with two variables, C44 had the best performance with RMSE of 0.3065 and NSE of 0.9134 and the worst was given by C52 with RMSE of 1.2562 and NSE of -0.3639. C58 turned out to have the best result among combinations with one variable. The values of RMSE and NSE for C58 are 0.5292 and 0.7489 respectively. C62 with RMSE of 1.4767 and NSE of -0.8756 had the lowest accuracy of all. By comparing the best combinations of one to six input variables, the performance deteriorated as the input variable amount decreased.

Table 4.3: Result Performance at Bayan Lepas Station using ELM.

<b>Number of Variables</b>	<b>Input</b>	<b>Best Activation Function</b>	<b>Best Hidden Nodes</b>	<b>RMSE</b>	<b>NSE</b>	<b>ANSE</b>	<b>MAE</b>	<b>MBE</b>
6	C1	Sigmoid	42	0.1259	0.9846	0.9842	0.1137	-0.0354
5	C3	Sine	35	0.1576	0.9765	0.9759	0.1392	-0.0577
4	C13	Sigmoid	24	0.1653	0.9742	0.9738	0.1446	-0.0501
3	C23	Sine	13	0.2034	0.9626	0.9622	0.1661	0.0153
2	C44	Sine	50	0.3065	0.9134	0.9129	0.2349	0.0831
1	C58	Sigmoid	7	0.5292	0.7489	0.7489	0.4265	0.2399

For the Ipoh station, C1 had the highest degree of accuracy of all, having RMSE of 0.1247 and NSE of 0.9684. In the case of combinations with five variables, C4 had the greatest result with RMSE of 0.1270 and NSE of 0.9671 while C7 had the result with the lowest accuracy, having RMSE of 0.4005 and NSE of 0.7147. For combinations with four variables, C13 was ranked as the highest with RMSE of 0.1434 and NSE of 0.9605 while C12 was ranked as the lowest with RMSE of 0.4563 and NSE of 0.6239. For combinations with three variables, C33 had the greatest performance with RMSE of 0.1550 and NSE of 0.9536 while C29 had the worst performance with RMSE of 0.5311 and NSE of 0.4972. For combinations with two variables, C53 recorded the best result with RMSE of 0.2195 and NSE of 0.9076 while C50 recorded the worst result with RMSE of 0.8896 and NSE of -0.4054. For combinations with one variable, C58 had the best result with RMSE of 0.3134 and NSE of 0.8168, unlike C62 which was also the combination with the lowest performance of all, having RMSE of 1.1716 and NSE of -1.4428. Similar to the previous two stations, the

prediction accuracy dropped with the decrease in the number of input variables, in terms of the best combinations of one to six input variables.

Table 4.4: Result Performance at Ipoh Station using ELM.

<b>Number of Variables</b>	<b>Input</b>	<b>Best Activation Function</b>	<b>Best Hidden Nodes</b>	<b>RMSE</b>	<b>NSE</b>	<b>ANSE</b>	<b>MAE</b>	<b>MBE</b>
6	C1	RBF	41	0.1247	0.9684	0.9675	0.1064	0.0519
5	C4	RBF	30	0.1270	0.9671	0.9664	0.1088	0.0536
4	C13	Sigmoid	49	0.1434	0.9605	0.9599	0.1234	0.0562
3	C33	Sine	8	0.1550	0.9536	0.9531	0.1276	0.0339
2	C53	Sigmoid	8	0.2195	0.9076	0.9071	0.1806	0.1002
1	C58	RBF	29	0.3134	0.8168	0.8168	0.2639	0.1925

For the KLIA Sepang station, among the combinations with five variables, C5 was the best combination with RMSE of 0.4632 and NSE of 0.7876 whereas C7 was the worst combination with RMSE of 0.8367 and NSE of 0.2981. In terms of combinations with four variables, the greatest performance was achieved by C14 with RMSE of 0.4486 and NSE of 0.7988 while the worst performance was given by C22 with RMSE of 0.8968 and NSE of 0.2229. For combinations with three variables, C33 showed the highest accuracy with RMSE of 0.4945 and NSE of 0.7590 while C42 showed the lowest accuracy with RMSE of 1.0853 and NSE of -0.1577. For combinations with two variables, C43 was ranked as the best combination with RMSE of 0.5778 and NSE of 0.6683 while C52 was ranked as the worst combination with RMSE of 1.3929 and NSE of -0.8598. For combinations with only one variable, C58 recorded the best result with RMSE of 0.7046 and NSE of 0.5138 while C61 registered RMSE of 1.6339 and NSE of -1.5011 which made it the worst combination of all. Regarding the comparison between the best combinations of one to six input variables, instead of C1, C14 from the category of four variables turned out to be the best of all combinations with RMSE of 0.4486 and NSE of 0.7988, and this was followed by C5 from the category of five variables and then only C1. From three input variables downwards, the accuracy decreased as the variable number decreased.

Table 4.5: Result Performance at KLIA Sepang Station using ELM.

<b>Number of Variables</b>	<b>Input</b>	<b>Best Activation Function</b>	<b>Best Hidden Nodes</b>	<b>RMSE</b>	<b>NSE</b>	<b>ANSE</b>	<b>MAE</b>	<b>MBE</b>
6	C1	Sine	34	0.4773	0.7726	0.7662	0.4220	0.2718
5	C5	RBF	41	0.4632	0.7876	0.7828	0.4007	0.2431
4	C14	RBF	45	0.4486	0.7988	0.7954	0.3808	0.2739
3	C33	Sine	35	0.4945	0.7590	0.7563	0.4363	0.2866
2	C43	RBF	14	0.5778	0.6683	0.6664	0.4882	0.4382
1	C58	RBF	11	0.7046	0.5138	0.5138	0.5966	0.5277

For the Lubok Merbau station, in the category of five variables, C4 was the combination that yielded the highest performance with RMSE of 0.1499 and NSE of 0.9615 while C7 remained the worst combination with RMSE of 0.3556 and NSE of 0.8036. For combinations with four variables, C13 was ranked as the best combination with RMSE of 0.1428 and NSE of 0.9658 while C12 was ranked as the worst combination with RMSE of 0.4750 and NSE of 0.6416. For combinations with three variables, C25 was the best combination with RMSE of 0.1648 and NSE of 0.9563 while C29 was the worst combination with RMSE of 0.6011 and NSE of 0.4339. In the class of two variables, C53 showed the greatest result with RMSE of 0.1945 and NSE of 0.9394 while C50 showed the worst result with RMSE of 0.8290 and NSE of -0.0675. C58 stood out to be the best combination in the category of one variable, having RMSE of 0.2295 and NSE of 0.9180 whereas C62 was the worst with RMSE of 1.1950 and NSE of -1.2374. In terms of the best combinations of one to six input variables, C13 from the class of four variables held the most accurate result with RMSE of 0.1428 and NSE of 0.9658. The second highest accurate combination was C1 with all input variables and was followed by C4. When the variable number dropped from three to one, it can be seen that the results became worse.

For the Pulau Langkawi station, the combination that had the greatest performance out of all combinations was C1, with RMSE of 0.2127 and NSE of 0.9570. In terms of combinations with five variables, it was C4 that had the best result with RMSE of 0.2176 and NSE of 0.9525 and C7 had the worst one with RMSE of 0.5464 and NSE of 0.7669. In the class of four variables, C13 showed the most accurate result with RMSE of 0.2286 and NSE of 0.9493 while C22

showed the least accurate result with RMSE of 0.6353 and NSE of 0.6836. For combinations with three variables, C33 was the best combination with RMSE of 0.2926 and NSE of 0.9273 while C42 was the worst combination with RMSE of 0.8863 and NSE of 0.3741. For combinations with two variables, C43 had the highest degree of accuracy with RMSE of 0.3573 and NSE of 0.8955 whereas C50 had the lowest degree of accuracy with RMSE of 1.1686 and NSE of -0.0820. In terms of the category of only one input variable, C60 was found to be the best with RMSE of 0.8118 and NSE of 0.4850. C59 from the class of one variable was the worst combination of all 63 combinations, having 1.2784 and -0.3036 for RMSE and NSE. In terms of the best combinations of one to six input variables, the prediction performance dropped with the number of variables.

Table 4.6: Result Performance at Lubok Merbau Station using ELM.

<b>Number of Variables</b>	<b>Input</b>	<b>Best Activation Function</b>	<b>Best Hidden Nodes</b>	<b>RMSE</b>	<b>NSE</b>	<b>ANSE</b>	<b>MAE</b>	<b>MBE</b>
6	C1	Sine	26	0.1488	0.9591	0.9579	0.1268	-0.0728
5	C4	Sigmoid	9	0.1499	0.9615	0.9606	0.1263	-0.0349
4	C13	Sigmoid	8	0.1428	0.9658	0.9652	0.1154	0.0027
3	C25	Sigmoid	13	0.1648	0.9563	0.9558	0.1340	-0.0164
2	C53	Sigmoid	6	0.1945	0.9394	0.9391	0.1533	-0.0194
1	C58	Sigmoid	33	0.2295	0.9180	0.9180	0.1867	0.0707

Table 4.7: Result Performance at Pulau Langkawi Station using ELM.

<b>Number of Variables</b>	<b>Input</b>	<b>Best Activation Function</b>	<b>Best Hidden Nodes</b>	<b>RMSE</b>	<b>NSE</b>	<b>ANSE</b>	<b>MAE</b>	<b>MBE</b>
6	C1	Sigmoid	22	0.2127	0.9570	0.9558	0.1821	0.1568
5	C4	Sine	32	0.2176	0.9525	0.9514	0.1892	0.1507
4	C13	RBF	32	0.2286	0.9493	0.9484	0.1953	0.1571
3	C33	Sine	40	0.2926	0.9273	0.9265	0.2477	0.1737
2	C43	Sine	42	0.3573	0.8955	0.8949	0.2893	0.1706
1	C60	RBF	11	0.8118	0.4850	0.4850	0.6542	0.0401

In the category of five variables for Sitiawan station, C4 was ranked as the best combination with RMSE of 0.2819 and NSE of 0.8529 while C7 was

ranked as the worst one with RMSE of 0.5753 and NSE of 0.4675. For combinations with four variables, C14 was the best combination with RMSE of 0.2884 and NSE of 0.8587 while C22 was the worst combination with RMSE of 0.6357 and NSE of 0.3499. For combinations with three variables, C27 showed the greatest result with RMSE of 0.3072 and NSE of 0.8408 whereas C38 showed the worst result with RMSE of 0.6982 and NSE of 0.2186. For combinations with two variables, C53 had the greatest performance with RMSE of 0.3139 and NSE of 0.8268 while C50 had the worst performance with RMSE of 0.8421 and NSE of -0.1551. In terms of combinations with one variable, C58 held the best result with RMSE of 0.3834 and NSE of 0.7644 while C62 held the worst result with RMSE of 1.1803 and NSE of -1.2129, which was also the worst among all 63 combinations. In terms of the best combinations of one to six input variables, C4 from the class of five variables was found to be the one with the highest degree of performance with RMSE of 0.2819 and NSE of 0.8529. This was followed by C14 from the category of four variables and then C1 with all six data. While from three variables downwards, the results deteriorated as the number of variables decreased.

Table 4.8: Result Performance at Sitiawan Station using ELM.

<b>Number of Variables</b>	<b>Input</b>	<b>Best Activation Function</b>	<b>Best Hidden Nodes</b>	<b>RMSE</b>	<b>NSE</b>	<b>ANSE</b>	<b>MAE</b>	<b>MBE</b>
6	C1	RBF	15	0.3049	0.8410	0.8362	0.2631	0.1706
5	C4	RBF	12	0.2819	0.8529	0.8494	0.2386	0.1444
4	C14	RBF	9	0.2884	0.8587	0.8561	0.2471	0.1330
3	C27	RBF	48	0.3072	0.8408	0.8389	0.2608	0.1305
2	C53	Sine	24	0.3139	0.8268	0.8258	0.2670	0.1823
1	C58	Sigmoid	27	0.3834	0.7644	0.7644	0.3263	0.2387

For the Subang station, in the category of five variables, C2 had the most accurate result with RMSE of 0.2832 and NSE of 0.9085 while C7 has the least accurate result with RMSE of 0.9755 and NSE of -0.0392. For combinations with four variables, C9 had the greatest performance with RMSE of 0.2806 and NSE of 0.9094 while C12 had the worst performance with RMSE of 0.9885 and NSE of -0.0418. For combinations with three variables, C33 was the

combination that yielded the best result with RMSE of 0.2762 and NSE of 0.9098 whereas C37 yielded the worst result with RMSE of 1.1722 and NSE of -0.5961. In the class of two variables, C49 showed the highest degree of accuracy with RMSE of 0.3194 and NSE of 0.8875 while C47 showed the lowest degree of accuracy with RMSE of 1.3169 and NSE of -1.0420. The best combination in the class of one variable was C58 with RMSE of 0.3834 and NSE of 0.8418. C62 from the class of one variable was the worst of all with RMSE of 1.6513 and NSE of -1.9073. C9 from the category of four variables turned out to be the most accurate in the comparison between the best combinations of one to six input variables. C1 and C2 were ranked as second and third, and then C33, C48 and lastly C58.

Table 4.9: Result Performance at Subang Station using ELM.

<b>Number of Variables</b>	<b>Input</b>	<b>Best Activation Function</b>	<b>Best Hidden Nodes</b>	<b>RMSE</b>	<b>NSE</b>	<b>ANSE</b>	<b>MAE</b>	<b>MBE</b>
6	C1	Sine	38	0.2517	0.9207	0.9184	0.2098	0.0555
5	C2	Sigmoid	10	0.2534	0.9270	0.9254	0.2051	0.0464
4	C9	RBF	13	0.2435	0.9317	0.9305	0.1951	0.0558
3	C33	Sigmoid	44	0.2625	0.9194	0.9185	0.2168	0.0226
2	C49	Sigmoid	5	0.2863	0.9118	0.9113	0.2272	0.0168
1	C58	Sine	5	0.3795	0.8466	0.8466	0.3105	0.1288

Out of the eight stations, four of them (Alor Setar, Bayan Lepas, Ipoh and Pulau Langkawi) provided the most accurate results out of all combinations with C1 which consists of all input variables. On the other hand, combinations with five variables showed the best prediction for Sitiawan station while combinations with four variables showed the best prediction for KLIA Sepang, Lubok Merbau and Subang stations. Thus, it can be seen that the application of all six input variables has a greater capability to yield more accurate result for conventional ELM. The results estimated based on four and five climatic data also have high accuracy, depending on the variables used. However, the result would not be the highest among all combinations once the amount of variables is three or lower. This might be because the model becomes harder to develop

a well-defined relationship between the inputs and the outputs when there are no sufficient variables.

For the comparison between six ways of combinations with five variables, C4 having  $T_{max}$ ,  $T_{min}$ ,  $RH$ ,  $U_2$  and  $R_s$  (or without  $T_{mean}$ ) showed a better performance by yielding the most accurate estimation for five out of eight stations. On the other hand, it can be seen that C7 was the worst combination for all stations and this combination does not have  $R_s$  as input variable. This shows that the result will be badly affected if the  $R_s$  is removed.

Among 15 ways of combinations with four variables, C13 which consists of  $T_{max}$ ,  $RH$ ,  $U_2$  and  $R_s$  (or without  $T_{mean}$  and  $T_{min}$ ) registered the highest prediction accuracy for five out of eight stations. On the other hand, from the worst performance point of view, four stations showed that C22 was the worst combination. This combination does not have  $U_2$  and  $R_s$  as input data.

In the case of 20 types of combinations with three variables, C33 having  $T_{max}$ ,  $U_2$  and  $R_s$  (or without  $T_{mean}$ ,  $T_{min}$  and  $RH$ ) was ranked as the best as it gave results with the lowest error for five stations. On the other hand, C42 was found to be the combination that yielded the least accurate result in four of the stations which took the largest percentage compared to other combinations with three variables, and this combination does not incorporate  $RH$ ,  $U_2$  and  $R_s$ .

C53 with  $T_{max}$  and  $R_s$  only turned out to be the best between 15 types of combinations with two variables by having the lowest error of estimation for three stations. From the bad performance viewpoint, C50 which does not include  $T_{max}$ ,  $T_{min}$ ,  $RH$  and  $R_s$  yielded the lowest accuracy for four of the stations.

When only one variable was used to train the model, C58 with  $R_s$  only showed a better performance by having the most accurate results for six out of eight stations. This shows that  $R_s$  is the best variable for a better estimation of  $ET_0$  compared to the other five variables when only one climatic data is used. On the contrary, C62 which consists of  $T_{mean}$  as the only input variable recorded the worst results for six of the stations.

Based on the discussion on the all the combinations with five, four, three, two and one variable, every combination that was found to be the best has a similarity, it is the  $R_s$  must be included as one of the variables. Besides, the results had the lowest accuracy in each category for the combinations not having

$R_s$ . Regarding the condition,  $R_s$  can be said to be the most effective and important input variable to accurately predict the  $ET_o$  in Peninsular Malaysia using ELM.

Besides,  $T_{max}$  and  $U_2$  are also very impactful in the estimation of  $ET_o$ . All the best combinations from categories of six to two variables include  $T_{max}$ . The results became worst for the category of two variables with the absence of  $T_{max}$ . While in the case of  $U_2$ , all the best combinations from six to three variables also include  $U_2$  and the results turned to be the worst for categories of four variables and three variables with the absence of  $U_2$ . Both  $T_{max}$  and  $U_2$ , however, must be accompanied by  $R_s$  to work well. On the other hand,  $T_{mean}$  can be indicated as the least impactful climatic data because starting from combinations with five variables to one variable, the best combinations do not include  $T_{mean}$ . This is followed by  $T_{min}$  which has its absence as an input variable starting from the best combinations of the class of four variables to one variable.

The two processes of ET, evaporation and transpiration both depends on the energy supply, vapour pressure gradient and wind. Hence, solar radiation, air temperature, wind speed and humidity are the main weather parameters determining the magnitude of ET (Allen et al., 1998). In the study, it can be seen that  $R_s$  is the most important climatic data out of all six types of climatic data. The ability of climatic data  $R_s$  to generate a result with high accuracy might due to the fact that energy is required in the conversion of water molecules from liquid to vapour form and the main source of energy is direct solar radiation (Bucur, 2019). Besides, Peninsular Malaysia is located in a tropical region with long sunshine duration and high intensity of solar radiation. According to Hakemzadeh et al. (2013), Peninsular Malaysia averagely receives six hours of sunshine in a day. Solar radiation is closely connected to the sunshine duration. The annual average daily solar radiation in 2009 ranged from  $13.67 \text{ MJ m}^{-2} \text{ day}^{-1}$  to  $17.18 \text{ MJ m}^{-2} \text{ day}^{-1}$  with the highest value recorded at  $19.28 \text{ MJ m}^{-2} \text{ day}^{-1}$ . The high solar radiation might provide a strong correlation between solar radiation and  $ET_o$ .  $T_{max}$  and  $U_2$  are also quite impactful climatic variables. This might because of the fact that high temperature is also one of the energy suppliers for evapotranspiration, just not as critical as solar radiation. On the other hand, wind speed plays an important role in maintaining a low water

saturation on the surrounding air in order to promote ET (Allen et al., 1998). Therefore, the two parameters might have a considerably good correlation with  $ET_o$ . The value of  $T_{mean}$  used in this study was calculated by merely finding the average of  $T_{max}$  and  $T_{min}$  but not the detailed average temperature of one whole day temperature values. This might cause  $T_{mean}$  and  $ET_o$  to have low correlation, and therefore does not show much importance in the estimation.

It is observed that some stations' most accurate results, however, had lower accuracy compared to other stations' most accurate results. The best results registered by KLIA Sepang, Sitiawan and Subang were 0.4486 (by C14), 0.2819 (by C4) and 0.2435 (by C9) respectively, which were relatively less accurate compared to the best results registered by Alor Setar, Bayan Lepas, Ipoh, Lubok Merbau and Pulau Langkawi stations with RMSE of 0.1530 (by C1), 0.1259 (by C1), 0.1247 (by C1) 0.1428 (by C13) and 0.2127 (by C1) respectively. It can be noticed that Alor Setar, Bayan Lepas, Ipoh, Lubok Merbau and Pulau Langkawi stations are all located in the northern area of Peninsular Malaysia while KLIA Sepang, Sitiawan and Subang are located at the middle of Peninsular Malaysia. Therefore, the performance of the estimation might also depend on the location of the station.

By observing the results of conventional ELM from Appendix A, majority of the results predicted at Alor Setar, Ipoh, KLIA Sepang, Pulau Langkawi, Sitiawan and Subang stations had positive MBE values. This indicates that the use of climatic data of these six stations tends to overestimate the  $ET_o$ . However, about one-quarter of all the combinations for Bayan Lepas station and about three-quarter of all the combinations for Lubok Merbau station produced negative MBE values, indicating a higher tendency of underestimation of  $ET_o$  by these combinations.

### **4.3 Result Analysis for Bagged ELM**

In the category of five variables of Alor Setar station, C4 was found to have the best performance with RMSE of 0.1744 and NSE of 0.9689 while C7 had the worst performance with RMSE of 0.4483 and NSE of 0.8190. For combinations with four variables, result of C13 had the highest degree of accuracy with RMSE of 0.1897 and NSE of 0.961 while result of C12 had the lowest accuracy with

RMSE of 0.5264 and NSE of 0.7530. For combinations with three variables, C33 was the combination that had the best result with RMSE of 0.2442 and NSE of 0.9330 whereas C29 had the worst result with RMSE of 0.7784 and NSE of 0.4301. For the class of two variables, C44 had the greatest performance with RMSE of 0.3497 and NSE of 0.8836 while C50 had the worst performance with RMSE of 1.2051 and NSE of -0.3195. In terms of the category of one variable, C60 showed the best result with RMSE of 0.7044 and NSE of 0.5628 while C62 showed the worst result with RMSE of 1.7915 and NSE of -1.8745, which was also the worst of all 63 combinations. By comparing the best combinations of one to six input variables, the result of C4 had the top performance with RMSE of 0.1744 and NSE of 0.9689. This was followed by C1 and then C13, C33, C44 and lastly C60.

Table 4.10: Result Performance at Alor Setar Station using Bagged ELM.

<b>Number of Variables</b>	<b>Input</b>	<b>Best Activation Function</b>	<b>Best Hidden Nodes</b>	<b>RMSE</b>	<b>NSE</b>	<b>ANSE</b>	<b>MAE</b>	<b>MBE</b>
6	C1	Sine	29	0.1789	0.9651	0.9642	0.1566	0.1230
5	C4	Sine	31	0.1744	0.9689	0.9682	0.1511	0.1211
4	C13	Sigmoid	42	0.1897	0.9611	0.9604	0.1628	0.1251
3	C33	Sigmoid	11	0.2442	0.9330	0.9323	0.2077	0.1262
2	C44	Sine	27	0.3497	0.8836	0.8830	0.2932	0.2195
1	C60	Sigmoid	5	0.7044	0.5628	0.5628	0.5503	0.1445

In the case of Bayan Lepas station, the combination that showed the greatest performance of all was C1 with RMSE of 0.1404 and NSE of 0.9805. For combinations with five variables, the best combination was C3 with RMSE of 0.1723 and NSE of 0.9711 while the worst combination was C7 with RMSE of 0.7019 and NSE of 0.5575. For the combinations with four variables, C13 had the most accurate result with RMSE of 0.1832 and NSE of 0.9663 whereas C21 had the least accurate result with RMSE of 0.7954 and NSE of 0.4302. In the category of three variables, C23 had the best performance with RMSE of 0.2290 and NSE of 0.9491 while C42 had the worst performance with RMSE of 1.3166 and NSE of -0.5485. For combinations with two variables, C43 showed the highest degree of accuracy with RMSE of 0.3529 and NSE of 0.8860

while C57 showed the lowest degree of accuracy with RMSE of 1.4407 and NSE of -0.9865. In the class of one variable, C58 was the best combination with RMSE of 0.5444 and NSE of 0.7321. The result of C62 from the class of one variable was the worst out of all 63 combinations, with RMSE of 1.5244 and NSE of -1.0094. By comparing the best combinations of one to six input variables, it can be seen that the performance dropped with the decrease in variable amount.

Table 4.11: Result Performance at Bayan Lepas Station using Bagged ELM.

<b>Number of Variables</b>	<b>Input</b>	<b>Best Activation Function</b>	<b>Best Hidden Nodes</b>	<b>RMSE</b>	<b>NSE</b>	<b>ANSE</b>	<b>MAE</b>	<b>MBE</b>
6	C1	Sigmoid	42	0.1404	0.9805	0.9799	0.1266	-0.0480
5	C3	Sine	35	0.1723	0.9711	0.9704	0.1537	-0.0593
4	C13	Sigmoid	24	0.1832	0.9663	0.9658	0.1635	-0.0654
3	C23	Sine	13	0.2290	0.9491	0.9486	0.1943	-0.0154
2	C43	Sine	16	0.3529	0.8860	0.8853	0.2835	0.0145
1	C58	Sigmoid	7	0.5444	0.7321	0.7321	0.4422	0.2499

For Ipoh station, C1 also held the greatest performance of all with values of 0.1335 and 0.9644 for RMSE and NSE respectively. In terms of combinations with five variables, C4 was the best combination with RMSE of 0.1336 and NSE of 0.9643 while C7 was the worst combination with RMSE of 0.4229 and NSE of 0.6758. For combinations with four variables, C13 showed the most accurate result with RMSE of 0.1526 and NSE of 0.9552 while C22 showed the least accurate result with RMSE of 0.5397 and NSE of 0.3751. In the category of three variables, C33 was the best combination with RMSE of 0.1900 and NSE of 0.9254 while C26 was the worst combination with RMSE of 0.6104 and NSE of 0.2730. In the class of two variables, C53 was the best combination with RMSE of 0.2249 and NSE of 0.9023 while C50 was the worst combination with RMSE of 0.9700 and NSE of -0.6985. For combinations with one variable, C58 was the one that yielded the greatest performance with RMSE of 0.3454 and NSE of 0.7641 while C62 yielded the worst performance with RMSE of 1.2234 and NSE of -1.6912, which was also the worst of all combinations. In terms of

the best combinations of one to six input variables, as the number of variables decreased, the prediction result became less accurate.

Table 4.12: Result Performance at Ipoh Station using Bagged ELM.

<b>Number of Variables</b>	<b>Input</b>	<b>Best Activation Function</b>	<b>Best Hidden Nodes</b>	<b>RMSE</b>	<b>NSE</b>	<b>ANSE</b>	<b>MAE</b>	<b>MBE</b>
6	C1	RBF	41	0.1335	0.9644	0.9634	0.1158	0.0528
5	C4	RBF	30	0.1336	0.9643	0.9635	0.1155	0.0539
4	C13	Sigmoid	49	0.1526	0.9552	0.9544	0.1325	0.0607
3	C33	Sine	8	0.1900	0.9254	0.9245	0.1650	0.0749
2	C53	Sigmoid	8	0.2249	0.9023	0.9017	0.1858	0.1054
1	C58	RBF	29	0.3454	0.7641	0.7641	0.2966	0.2344

Based on the result of KLIA Sepang station, in the category of five variables, C5 was found to be the best combination with RMSE of 0.4784 and NSE of 0.7579 whereas C7 was the worst combination with RMSE of 0.9057 and NSE of 0.1633. For combinations with four variables, C14 showed the greatest result with RMSE of 0.4919 and NSE of 0.7493 whereas C22 showed the worst result with RMSE of 0.9651 and NSE of 0.0797. For combinations with three variables, C33 had the greatest performance with RMSE of 0.5270 and NSE of 0.7184 while C42 had the worst performance with RMSE of 1.2907 and NSE of -0.7781. For the class of two variables, C43 had the best performance with RMSE of 0.6609 and NSE of 0.6227 while C52 had the worst performance with RMSE of 1.8166 and NSE of -2.7513. For combinations with one variable, C58 showed the best result with RMSE of 0.7828 and NSE of 0.3927 while C62 showed the least accurate result. RMSE and NSE of C62 were 1.6355 and -1.5047 respectively, which made it the worst combination of all. In terms of the best combinations of one to six input variables, C5 from the class of five variables turned out to be the top with RMSE of 0.4784 and NSE of 0.7579, and this was followed by C1 and then C14. From three variables downwards, it is clear that the performance deteriorated as the variable amount decreased.

Table 4.13: Result Performance at KLIA Sepang Station using Bagged ELM.

<b>Number of Variables</b>	<b>Input</b>	<b>Best Activation Function</b>	<b>Best Hidden Nodes</b>	<b>RMSE</b>	<b>NSE</b>	<b>ANSE</b>	<b>MAE</b>	<b>MBE</b>
6	C1	Sine	34	0.4859	0.7588	0.7520	0.4314	0.3072
5	C5	RBF	41	0.4784	0.7579	0.7525	0.4196	0.2594
4	C14	RBF	45	0.4919	0.7493	0.7451	0.4320	0.3100
3	C33	Sine	35	0.5270	0.7184	0.7152	0.4670	0.3035
2	C43	RBF	14	0.6099	0.6227	0.6206	0.5272	0.3818
1	C58	RBF	11	0.7828	0.3927	0.3927	0.6757	0.5687

For Lubok Merbau station, among the combinations with five variables, C3 was found to show the best result with RMSE of 0.1604 and NSE of 0.9533 while C7 was found to show the worst result with RMSE of 0.3799 and NSE of 0.7732. For combinations with four variables, C8 yielded the most accurate result with RMSE of 0.1639 and NSE of 0.9549 while C12 yielded the least accurate result with RMSE of 0.4995 and NSE of 0.6000. For combinations with three variables, C25 showed the greatest performance with RMSE of 0.1703 and NSE of 0.9529 while C29 showed the worst performance with RMSE of 0.6615 and NSE of 0.2803. For the class of two variables, C44 was ranked as the best combination with RMSE of 0.2017 and NSE of 0.9353 while C51 was ranked as the worst combination with RMSE of 0.9299 and NSE of -0.8916. For the class of one variable, C58 was the best combination with RMSE of 0.2540 and NSE of 0.8863. On the other hand, C62 was found to have the worst result of all with RMSE of 1.3262 and NSE of -1.8127. In terms of the best combinations of one to six input variables, C3 from the class of five variables was ranked as the best with RMSE of 0.1604 and NSE of 0.9533, followed by C1 and C8. Descending from three variables, the accuracy of results declined with the variable amount.

For combinations with five variables of Pulau Langkawi station, C4 had the greatest performance with RMSE of 0.2298 and NSE of 0.9470 while C7 had the worst performance with RMSE of 0.5849 and NSE of 0.7292. For combinations with four variables, C13 showed the greatest result with RMSE of 0.2400 and NSE of 0.9434 while C22 showed the worst result with RMSE of 0.6900 and NSE of 0.6212. In the category of three variables, the combination

that yielded the best result was C25 with RMSE of 0.3325 and NSE of 0.9087 whereas the combination that yielded the worst result was C42 with RMSE of 0.9569 and NSE of 0.2411. In the class of two variables, C43 showed the highest degree of accuracy with RMSE of 0.4891 and NSE of 0.7532, unlike C50 that showed the lowest degree of accuracy with RMSE of 1.2453 and NSE of -0.2480. In the category of only one input variable, C60 had the best performance with RMSE of 0.8737 and NSE of 0.3728 whereas C62 had the worst performance with RMSE of 1.5638 and NSE of -0.9472. C62 was also the worst combination out of all 63 combinations. In terms of the best combinations of one to six input variables, C4 was ranked as the top with RMSE of 0.2298 and NSE of 0.9470. This was followed by C1, C13, C25, C43 and lastly C60.

Table 4.14: Result Performance at Lubok Merbau Station using Bagged ELM.

<b>Number of Variables</b>	<b>Input</b>	<b>Best Activation Function</b>	<b>Best Hidden Nodes</b>	<b>RMSE</b>	<b>NSE</b>	<b>ANSE</b>	<b>MAE</b>	<b>MBE</b>
6	C1	Sine	26	0.1630	0.9509	0.9494	0.1393	-0.0883
5	C3	Sine	30	0.1604	0.9533	0.9522	0.1374	-0.0845
4	C8	RBF	23	0.1639	0.9549	0.9541	0.1360	-0.0528
3	C25	Sigmoid	13	0.1703	0.9529	0.9523	0.1388	-0.0204
2	C44	Sine	9	0.2017	0.9353	0.9349	0.1634	0.0528
1	C58	Sigmoid	33	0.2540	0.8863	0.8863	0.2111	0.0915

Table 4.15: Result Performance at Pulau Langkawi Station using Bagged ELM.

<b>Number of Variables</b>	<b>Input</b>	<b>Best Activation Function</b>	<b>Best Hidden Nodes</b>	<b>RMSE</b>	<b>NSE</b>	<b>ANSE</b>	<b>MAE</b>	<b>MBE</b>
6	C1	Sigmoid	22	0.2317	0.9477	0.9462	0.2004	0.1518
5	C4	Sine	32	0.2298	0.9470	0.9458	0.2000	0.1568
4	C13	RBF	32	0.2400	0.9434	0.9425	0.2080	0.1550
3	C25	Sigmoid	13	0.3325	0.9087	0.9077	0.2727	0.2076
2	C43	Sine	42	0.4891	0.7532	0.7518	0.4204	0.1338
1	C60	RBF	11	0.8737	0.3728	0.3728	0.7114	0.0537

For Sitiawan station, in the class of five variables, C2 was the best combination with RMSE of 0.3270 and NSE of 0.8208 while C7 was the worst combination with RMSE of 0.5935 and NSE of 0.4104. In the category of four

variables, C10 was found to have the most accurate result with RMSE of 0.3159 and NSE of 0.8297 while C22 was found to have the least accurate result with RMSE of 0.6974 and NSE of 0.2039. For combinations with three variables, C23 showed the best performance with RMSE of 0.3175 and NSE of 0.8333 while C41 showed the worst performance with RMSE of 0.7441 and NSE of 0.0431. For combinations with two variables, C43 was ranked as the best combination with RMSE of 0.3342 and NSE of 0.8127 while C50 was ranked as the worst combination with RMSE of 1.0065 and NSE of -0.8611. C58 stood out as the best combination in the category of one variable with RMSE of 0.4002 and NSE of 0.7331. On the other hand, C62 was the worst from the category of one variable which was also the worst of all, having RMSE of 1.2704 and NSE of -1.6969. In terms of the best combinations of one to six input variables, C10 from the category of four variables held the first place with RMSE of 0.3159 and NSE of 0.8297. C23 from the class of three variables turned out to be the combination that had the second highest accuracy followed by C2 and then only C1.

Table 4.16: Result Performance at Sitiawan Station using Bagged ELM.

<b>Number of Variables</b>	<b>Input</b>	<b>Best Activation Function</b>	<b>Best Hidden Nodes</b>	<b>RMSE</b>	<b>NSE</b>	<b>ANSE</b>	<b>MAE</b>	<b>MBE</b>
6	C1	RBF	15	0.3371	0.8052	0.7993	0.2975	0.1963
5	C2	RBF	19	0.3270	0.8208	0.8165	0.2850	0.1599
4	C10	Sine	49	0.3159	0.8297	0.8266	0.2720	0.1693
3	C23	RBF	15	0.3175	0.8333	0.8313	0.2704	0.1698
2	C43	RBF	10	0.3342	0.8127	0.8116	0.2846	0.1831
1	C58	Sigmoid	27	0.4002	0.7331	0.7331	0.3449	0.2660

For Subang station, C5 was the best combination in the category of five variables with RMSE of 0.2557 and NSE of 0.9207 while C7 was the worst in this category with RMSE of 0.9314 and NSE of 0.0889. For combinations with four variables, C14 had the greatest performance with RMSE of 0.2634 and NSE of 0.9192 while C21 had the worst performance with RMSE of 0.9464 and NSE of 0.0485. For combinations with three variables, C33 showed the most accurate result with RMSE of 0.2625 and NSE of 0.9194 whereas C31 showed

the least accurate result with RMSE of 0.9938 and NSE of -0.0295. For combinations with two variables, C43 was the best combination with RMSE of 0.3107 and NSE of 0.8964 while C56 was the worst combination with RMSE of 1.1346 and NSE of -0.3349. In the class of one variable, C58 was the combination that yielded the best result with RMSE of 0.3795 and NSE of 0.8466. In contrast, C62 yielded the result with RMSE of 1.5384 and NSE of -1.4703, which made it to be the worst combination of all. In terms of the best combinations of one to six input variables, C5 from the class of five variables showed the highest accuracy result with RMSE of 0.2530 and NSE of 0.9193. This is followed by C14 from the class of four variables and then C1 from the class of all input variables. Starting from three variables downwards, the prediction performance dropped with the number of variables.

Table 4.17: Result Performance at Subang Station using Bagged ELM.

<b>Number of Variables</b>	<b>Input</b>	<b>Best Activation Function</b>	<b>Best Hidden Nodes</b>	<b>RMSE</b>	<b>NSE</b>	<b>ANSE</b>	<b>MAE</b>	<b>MBE</b>
6	C1	Sine	38	0.2627	0.9152	0.9128	0.2225	0.0550
5	C5	RBF	45	0.2530	0.9193	0.9174	0.2099	0.0502
4	C14	Sigmoid	48	0.2565	0.9206	0.9193	0.2117	0.0513
3	C33	Sigmoid	44	0.2762	0.9098	0.9088	0.2290	0.0443
2	C43	Sigmoid	4	0.3157	0.8826	0.8819	0.2562	0.0321
1	C58	Sine	5	0.3834	0.8418	0.8418	0.3135	0.1202

Among all eight stations, two of the stations (Bayan Lepas and Ipoh) provided the most accurate results out of all combinations with C1 which applies all input variables. On the other hand, combinations with five variables showed the best prediction accuracy for five of the stations which include Alor Setar, KLIA Sepang, Lubok Merbau, Pulau Langkawi and Subang. In the case of the class of four variables, only Sitiawan station registered the greatest accuracy with the combination in this class. It can be seen that the application of five variables has the greater capability to yield more accurate result for bagged ELM. Nevertheless, the results predicted based on four and six climatic data also can provide high accuracy, depending on the variables adopted. Similar to

the conventional ELM, the result would not be the most accurate among all combinations once the amount of input variables is three or lower.

For the comparison between six types of combinations with five variables, C4 which includes  $T_{max}$ ,  $T_{min}$ ,  $RH$ ,  $U_2$  and  $R_s$  was the one that yielded a better performance for most of the stations, which were three out of eight stations compared to C3 and C5 which yielded better results for two stations respectively. In contrast, it is obvious that all of the stations showed that C7 was the worst combination which does not include  $R_s$  data as input variable.

For combinations with four variables, C13 comprising of  $T_{max}$ ,  $RH$ ,  $U_2$  and  $R_s$  as input variables recorded the highest accuracy for half of the total number of stations. On the other hand, four stations reported the worst result by using C22. C22 is a combination that does not involve  $U_2$  and  $R_s$ . Therefore, it can be said that  $U_2$  and  $R_s$  are very much important in ensuring a good prediction when only four input variables are used.

In between 20 types of combinations with three variables, C33 was ranked as the best as it showed the best results for four of the stations. This combination involves  $T_{max}$ ,  $U_2$  and  $R_s$ . On the other hand, C42 which does not incorporate  $RH$ ,  $U_2$  and  $R_s$  remained as the worst combination by yielding the least accurate result in three of the stations.

In the class of two variables, C43 ( $U_2$  and  $R_s$ ) turned out to be the best by showing the lowest error of estimations for five stations, while from the bad performance point of view, C50 which does not include  $T_{max}$ ,  $T_{min}$ ,  $RH$  and  $R_s$  yielded the lowest accuracy for four of the stations.

C58 which consists of  $R_s$  as the input training data showed the best results for six out of eight stations in the category of one variable, hence making it the top combination in this class. On the contrary, all of the stations recorded the worst performance of estimation when only  $T_{mean}$  was used as climatic input data, which refers to C62.

It can be seen from all the combinations with five, four, three, two and one variable, every combination that was found to be the best contains  $R_s$  as one of the input variables. Likewise, all the worst combinations from each of the variable number categories do not have  $R_s$ . Therefore,  $R_s$  can be concluded as the most effective and important climatic data.

Similar to conventional ELM,  $T_{max}$  and  $U_2$  can be observed to be present in most of the best combinations. All the best combinations from six to three input variables include  $T_{max}$ . The prediction result became the worst for the category of two variables with the absence of  $T_{max}$ . While for  $U_2$ , all the best combinations from six to two variables have it as one of the input data and the performance became the least accurate for categories of four variables and three variables with the absence of  $U_2$ . Both  $T_{max}$  and  $U_2$ , however, require  $R_s$  to be present to work well, as in the case of conventional ELM. On the contrary, the least impactful climatic data is  $T_{mean}$  in that starting from combinations with five variables, all the best combinations determined do not include  $T_{mean}$ .  $T_{min}$  is also can be seen to be less important as it was not included as one of the input data to generate the best performance from the class of four variables to one variable.

#### 4.4 Conventional and Bagged ELM Comparison

Figure 4.3 shows the scatter plots of model estimated  $ET_o$  against PM estimated  $ET_o$  for the best combinations of one to six input variables for the Sitiawan station, both conventional and bagged ELM. The results of Sitiawan were selected for the comparison because there is a large area of palm oil plantation field in the vicinity. It can be observed from the series of scatter plots that the more data points in plots of bagged ELM are further from the line of perfect estimation compared to those in plots of conventional ELM, indicating that they had lower NSE compared to those of conventional ELM. Besides, the data points in plots of bagged ELM are more scattered compared to those in plots of conventional ELM. Moreover, in plots of bagged ELM, more data points are located above the line of perfect estimation compared to plots of conventional one. Since the MBE for all combinations of Sitiawan station had positive values, the observation mentioned previously means higher positive MBE values for the case of bagged ELM. Therefore, it is clear that the results of the bagged ELM were not better than those of the conventional ELM. For all the best combinations with six, five, four, three, two and one input variable, none of the bagged results were more accurate than those predicted by conventional ELM.

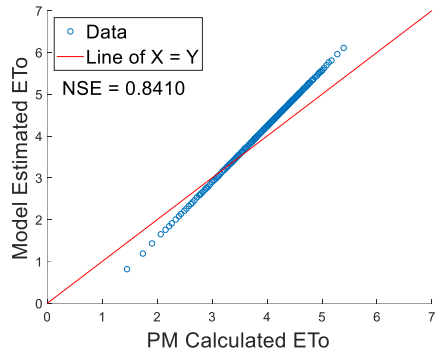
In the study of hierarchical prediction of monthly runoff done by Sharma and Tiwari (2009), bootstrapped ANN was proved to be better than single ANN.

The same result were demonstrated by other researchers such as Tiwari, Song, Chatterjee and Gupta (2013) in their research on river flow forecasting, Wang et al. (2013) in their research on monthly water quality forecasting, Liu et al. (2014) in their study on the estimation of river ice cover thickness as well as Tahir, Tehzeeb-ul-Hassan and Saqib (2016) in their study on the optimal scheduling of electrical power. The amount of dataset used in these studies was small, ranged from 24 to 525. Unlike the research just mentioned, the present study applied a relatively large amount of dataset, ranged from 1729 to 1821. A large amount of dataset utilized might be the reason for the inability of bagging to improve the performance of the model. Bootstrapping a huge amount of dataset might lead to over-fitting and thus reduce the accuracy in return.

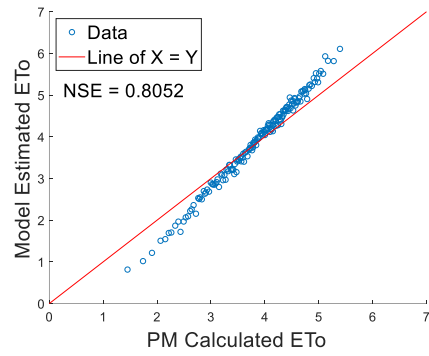
The large amount of data compared to the low data dimensionality might also contribute to the inability of the bagging to improve the model performance. In the study of bagging, Breiman (1996) stated that the efficiency of the method is affected by the stability of the prediction or classification of the model. Bagging can improve the performance of an unstable procedure but can slightly reduce the performance of a stable procedure. In the study on the effect of bagging on linear classifier done by Skurichina and Duin (1998), it was stated that the stability depends on the composition of training dataset. If the size of the training set is comparable to the data dimensionality, then the models are very sensitive to the changes in the dataset or simply known as unstable. On the contrary, if very large data size is used, the models are not sensitive to the data changes or stable. The more stable the model, the less effective the bagging is. In another study carried out by Skurichina, Kuncheva and Duin (2002), it was observed that the bagging is usually useful to deal with critical training sample size, which means the amount of data is comparable with its dimensionality. In the current study, the amount of dataset used is almost 2000, while the data dimensionality is just low at a value of 6. The data size is much larger than its dimensionality. This might result in a relatively high stability for the prediction which in turn cause the bagging to be ineffective.

In the study carried out by Belayneh et al. (2016), ANN with bootstrap was also found to yield a worse result compared to ANN itself. It was explained that the circumstance of the better performance of single ANN compared to

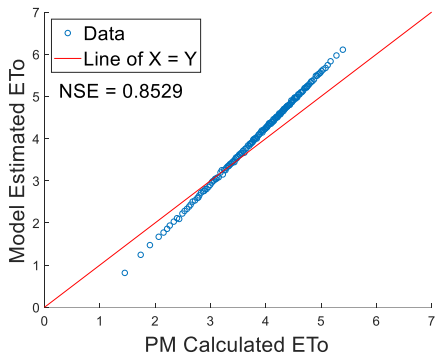
bagged ANN is totally possible since the bagged ANN averages over every ensemble to provide the prediction while single ANN has only one prediction to consider.



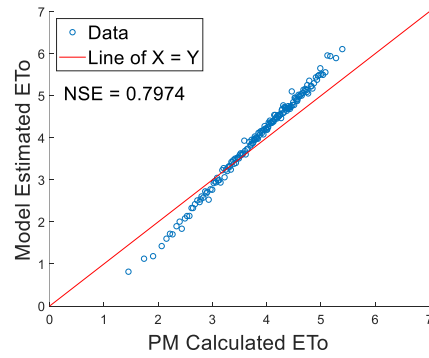
(A1)



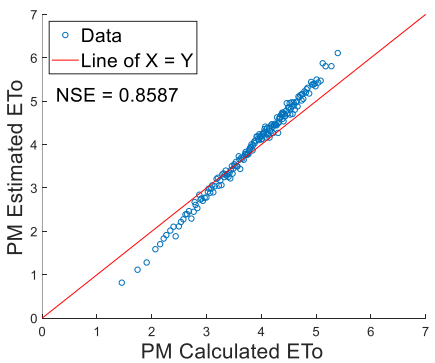
(B1)



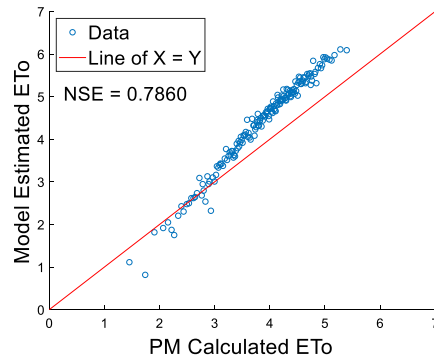
(A2)



(B2)



(A3)



(B3)

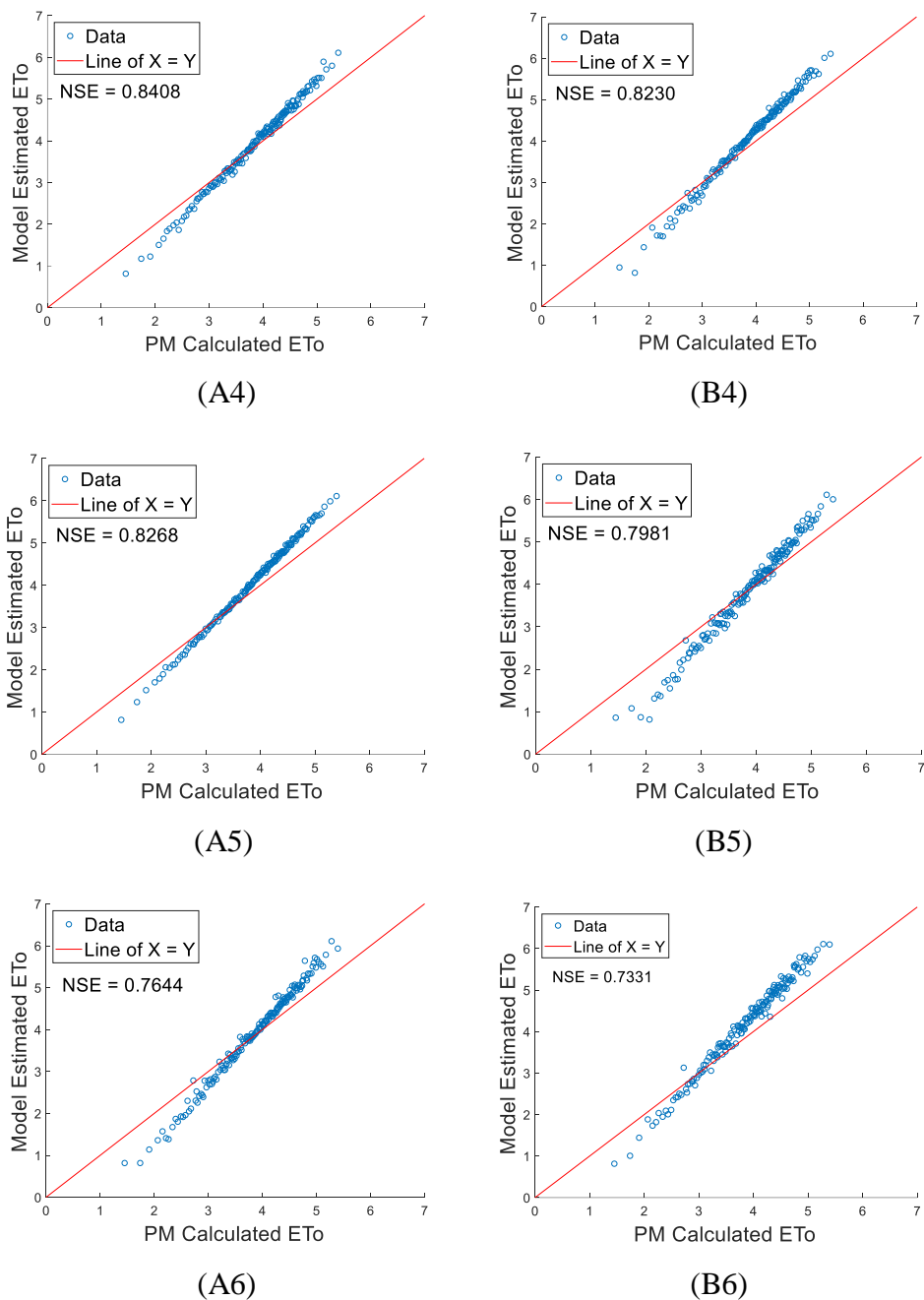


Figure 4.3: Scatter Plots of Best Combinations of Six to One Input Variable (A1-A6) for Conventional ELM and Corresponding Combinations (B1-B6) for Bagged ELM.

All the combinations of Sitiawan station with and without bootstrap yielded positive MBE values. The same condition went to other stations, with the combinations that registered positive MBE values remained positive after bootstrapping while the combinations that registered negative MBE values

remained negative after bootstrapping. Therefore, it can be concluded that in terms of MBE, the trend yielded by conventional ELM persisted even after bootstrapping is adopted into the ELM model.

For the Sitiawan station, four of the best combinations out of all variable amount categories for conventional ELM no longer remained as the best for bagged ELM. This also happened to some other stations, for example, at Bayan Lepas and Pulau Langkawi stations, each with one different best combination as well as at the Lubok Merbau and Subang stations with three different best combinations. This showed that the application of bagging would affect the importance of input parameters. However, based on the interpretation done in sections 4.2 and 4.3 which included all stations, generally,  $R_s$  still turned out to be the most impactful parameter of all. On the other hand, it can be seen that  $T_{mean}$  had the lowest ability to generate better result.

## CHAPTER 5

### CONCLUSIONS AND RECOMMENDATIONS

#### 5.1 Conclusions

The ability of the ELM to estimate the  $ET_0$  in Peninsular Malaysia based on meteorological data was examined in this study. For the study purpose, six types of climatic data comprising of  $T_{max}$ ,  $T_{mean}$ ,  $T_{min}$ ,  $RH$ ,  $U_2$  and  $R_s$ , from the Alor Setar, Bayan Lepas, Ipoh, Klia Sepang, Lubok Merbau, Pulau Langkawi, Sitiawan and Subang stations were adopted as input variables to the ELM model for the  $ET_0$  estimation. 63 sets of climatic data combinations were applied as inputs for the model estimation and each of the combinations was tuned for the optimum hidden neuron number and activation function. Three types of activation functions were used in the model, which include sigmoidal function, radial basis function and sine function. The results predicted by the model were compared with PM equation and its performance was measured in terms of RMSE, NSE, ANSE, MAE and MBE. In the parameter tuning section, the optimum hidden neuron number and activation function varied for every combination.

The model showed the best performance for the majority of the stations when all the six data were used as input variables, while certain combinations with five variables and combinations with four variables also showed great performance, depending on which climatic variables were used. The results revealed that  $R_s$  is the most important input variable to give a high performance of model estimation.  $T_{max}$  and  $U_2$  are also very impactful in giving a good model estimation but they require the presence of  $R_s$ . On the other hand, it can be seen that  $T_{mean}$  is the least impactful data in the performance of the model. Besides, it was found that the results for stations located in the northern region of Peninsular Malaysia were generally better than those located in the middle region.

Furthermore, bootstrap aggregating fusion method was employed in the training of ELM to test for its ability to improve the performance of the neural network. However, the results showed no improvement but deterioration after

the application of bagging. The deterioration could be due to a large data size applied which led to over-fitting. The large amount of data compared to the low data dimensionality could also contribute to the inability of bagging to improve the model performance.

## **5.2 Recommendations for Future Work**

The climatic data used in this study were obtained only from eight stations of Peninsular Malaysia. A trend was observed that the best results generated by the stations located near the northern region were more accurate than the best results generated by the stations located in the middle region. Based on the trend, it can be concluded that the performance of the model estimation might be affected by the location of the station. Thus, data from more stations from northern, middle and even southern regions as well as East Malaysia can be adopted to further examine the effect of the station's location on the model performance.

Besides, the climatic data adopted in this study were of a period of five years only. Estimation based on a longer time period of data such as 10 years can be carried out as the climatic data involving a longer period of time might provide a greater performance in terms of model estimation.

## REFERENCES

- Agatonovic-Kustrin, S. and Beresford, R., 2000. Basic concepts of artificial neural network (ANN) modeling and its application in pharmaceutical research. *Journal of Pharmaceutical and Biomedical Analysis*, 22(5), pp. 717-727.
- Allen, R.G., 1983. New approaches to estimating crop evapotranspiration. *Acta Horticulturae*, 335, pp. 287-294.
- Allen, R.G., Pereira, L.S., Raes, D. and Smith, M., 1998. *Crop evapotranspiration. Guidelines for computing crop water requirements*. Rome, Italy: Food and Agricultural Organization.
- Antonopoulos, V.Z. and Antonopoulos, A.V., 2017. Daily reference evapotranspiration estimates by artificial neural networks technique and empirical equations using limited input climate variables. *Computers and Electronics in Agriculture*, 132, pp. 86-96.
- Basheer, I. and Hajmeer, M., 2000. Artificial neural networks: fundamentals, computing, design, and application. *Journal of Microbiological Methods*, 43(1), pp. 3-31.
- Belayneh, A., Adamowski, J., Khalil, B., and Quilty, J., 2016. Coupling machine learning methods with wavelet transforms and the bootstrap and boosting ensemble approaches for drought prediction. *Atmospheric Research*, 172-173, pp. 37-47.
- Breiman, L., 1996. Bagging predictors. *Machine Learning*, 24, pp. 123-140.
- Bucur, D. ed., 2019. *Advanced Evapotranspiration Methods and Applications*. [e-book] IntechOpen. Available at: Google Scholar <<https://scholar.google.com>> [Accessed on 9 January 2020].
- Campbell, D.I. and Williamson, J.L., 1997. Evaporation from a raised peat bog. *Journal of Hydrology*, 193, pp. 142-160.
- Chai, T. and Draxler, R.R., 2014. Root mean square error (RMSE) or mean absolute error (MAE)? – Arguments against avoiding RMSE in the literature. *Geoscientific Model Development*, 7, pp. 1247-1250.
- Cobaner, M., 2011. Evapotranspiration estimation by two different neuro-fuzzy inference systems. *Journal of Hydrology*, 398, pp. 292-302.
- Dehghani, A.A., Asgari, M. and Mosaedi, A., 2009. Comparison of geostatistics, artificial neural networks and adaptive neuro fuzzy inference system approaches in groundwater level interpolation (case study: Ghazvin aquifer). *Journal of Agricultural Sciences and Natural Resources*, 16(1-b), pp. 517-528.

Dingman, S.L., 2015. *Physical hydrology*. 3<sup>rd</sup> ed. Long Grove, Illinois: Waveland Press, Inc.

Ding, S., Zhao, H., Zhang, Y., Xu, X., and Nie, R., 2013. Extreme learning machine: algorithm, theory and applications. *Artificial Intelligence Review*, 44(1), pp. 103-115.

Dou, X.M. and Yang, Y.G., 2018. Evapotranspiration estimation using four different machine learning approaches in different terrestrial ecosystems. *Computers and Electronics in Agriculture*, 148, pp. 95-106.

Duan, K., Keerthi, S.S., and Poo, A.N., 2003. Evaluation of simple performance measures for tuning SVM hyperparameters. *Neurocomputing*, 51, pp. 41-59.

Ebrahimian, A., Wadzuk, B. and Traver, R., 2019. Evapotranspiration in green stormwater infrastructure systems. *Science of the Total Environment*, 688, pp. 797-810.

Efron, B., 1979. Bootstrap methods: Another look at the jackknife. *The Annals of Statistics*, 7(1), pp. 1-26.

Efron, B. and Tibshirani, R.J., 1993. *An introduction to the bootstrap*. London: Chapman and Hall.

Elliott, G. and Timmermann, A. eds., 2013. *Handbook of economic forecasting*. Oxford: North-Holland.

Falamarzi, Y., Palizdan, N., Huang, Y.F. and Lee, T.S., 2014. Estimating evapotranspiration from temperature and wind speed data using artificial and wavelet neural networks (WNNs). *Agricultural Water Management*, 140, pp. 26-36.

Ferreira, L.B., Fernando, F.C., Rubens, A.O. and Elpídio, I.F.F., 2019. Estimation of reference evapotranspiration in Brazil with limited meteorological data using ANN and SVM – a new approach. *Journal of Hydrology*, 572, pp. 556-570.

Feng, Y., Cui, N.B., Gong, D.Z., Zhang, Q.W. and Zhao, L., 2017. Evaluation of random forests and generalized regression neural networks for daily reference evapotranspiration modelling. *Agricultural Water Management*, 193, pp. 163-173.

Feng, Y., Cui, N.B., Zhao, L., Hu, X.T. and Gong, D.Z., 2016. Comparison of ELM, GANN, WNN and empirical models for estimating reference evapotranspiration in humid region of Southwest China. *Journal of Hydrology*, 536, pp. 376-383.

Feng, Y., Peng, Y., Cui, N., Gong, D. and Zhang, K., 2017. Modeling reference evapotranspiration using extreme learning machine and generalized regression

neural network only with temperature data. *Computers and Electronics in Agriculture*, 136, pp. 71-78.

Gocic, M., Petković, D., Shamshirband, S. and Kamsin, A., 2016. Comparative analysis of reference evapotranspiration equations modelling by extreme learning machine. *Computers and Electronics in Agriculture*, 127, pp. 56-63.

Goodarzi, M. and Eslamian, S., 2018. Performance evaluation of linear and nonlinear models for the estimation of reference evapotranspiration. *International Journal of Hydrology Science and Technology*, 8(1), pp. 1-15.

Hakemzadeh, M.H., Shavalipour, A., Sopian, K., Haris, S.M., and Zaidi, S.H., 2013. New formulation for the estimation of monthly average daily solar irradiation for the tropics: A case study of Peninsular Malaysia. *International Journal of Photoenergy*, 2013, pp. 1-6.

Heddami, S., Ladlani, I., Houichi, L. and Djemili, L., 2013. Modelling monthly potential evapotranspiration (ETP) using generalized regression neural networks (GRNN): Case study of the semi-arid region of Guelma Northeast of Algeria. *Proceeding du Séminaire International sur l'Hydrogéologie et l'Environnement SIHE 2013 Ouargla*, pp. 226-229.

Hill R.W., Johns, E.L. and Frevert. D.K., 1983. *Comparison of equations used for estimating agricultural crop evapotranspiration with field research*. Denver: Bureau of Reclamation, U.S Department of the Interior, Engineering and Research Center.

Huang, G.B., and Babri, H.A., 1998. Upper bounds on the number of hidden neurons in feedforward networks with arbitrary bounded nonlinear activation functions. *IEEE Trans. Neural Networks*, 9(1), pp. 224-229.

Huang, G.B., Zhu, Q.Y. and Siew, C.K., 2006. Extreme learning machine: Theory and applications. *Neurocomputing*, 70, pp. 489-501.

Huo, Z., Feng, S., Kang, S. and Dai, X., 2012. Artificial neural network models for reference evapotranspiration in an arid area of northwest China. *Journal of Arid Environments*, 82, pp. 81-90.

Jackson, S.L., 2009. *Statistics: Plain and simple*. 2<sup>nd</sup> ed. California: Wadsworth.

Jadeja, V., 2011. *Artificial neural network estimation of reference evapotranspiration from pan evaporation in a semiarid environment*. In: B.V.M Engineering College, National Conference on Recent Trends in Engineering & Technology. V.V.Nagar, Gujarat, India, 13-14 May 2011. Bhavnagar, India: Shantilal Shah Engineering College.

Kisi, O. and Alizamir, M., 2018. Modelling reference evapotranspiration using a new wavelet conjunction heuristic method: Wavelet extreme learning machine vs wavelet neural networks. *Agricultural and Forest Meteorology*, 263, pp. 41-48.

- Kisi, O., Sanikhani, H., Zounemat-Kermani, M. and Niazi, F., 2015. Long-term monthly evapotranspiration modeling by several data-driven methods without climatic data. *Computers and Electronics in Agriculture*, 115, pp. 66-77.
- Kumar, M., Raghuwanshi, N.S., Singh, R., Wallender, W.W. and Pruitt, W.O., 2002. Estimating evapotranspiration using artificial neural network. *Journal of Irrigation and Drainage Engineering*. 128, pp. 224-233.
- Kuo, S.F., Chen, F.W., Liao, P.Y. and Liu, C.W., 2011. A comparative study on the estimation of evapotranspiration using backpropagation neural network: Penman-Monteith method versus pan evaporation method. *Paddy and Water Environment*, 9(4), pp. 413-424.
- Ladlani, I., Houichi, L., Djemili, L., Heddami, S. and Belouz, K., 2012. Modeling daily reference evapotranspiration (ET<sub>0</sub>) in the north of Algeria using generalized regression neural networks (GRNN) and radial basis function neural networks (RBFNN): A comparative study. *Meteorology and Atmospheric Physics*, 118(3-4), pp. 163-178.
- Lahiri, S.K. and Ghanta, K.C., 2009. Artificial neural network model with parameter tuning assisted by genetic algorithm technique: study of critical velocity of slurry flow in pipeline. *Asia-Pacific Journal of Chemical Engineering*, 5, pp. 763-777.
- Lan, H., 2019. *Decision Trees and Random Forests for Classification and Regression pt.2*. [online] Towards Data Science. Available at: <https://towardsdatascience.com/decision-trees-and-random-forests-for-classification-and-regression-pt-2-2b1fcd03e342> [Accessed 18 August 2019].
- Landeras, G., Ortiz-Barredo, A. and López, J.J., 2009. Forecasting weekly evapotranspiration with ARIMA and artificial neural network models. *Journal of Irrigation and Drainage Engineering*, 135(3), pp. 323-334.
- Lee, T.S., Najim, M.M.M. and Aminul, M.H., 2004. Estimating evapotranspiration of irrigated rice at the West Coast of the Peninsular of Malaysia. *Journal of Applied Irrigation Science*, 39, pp. 104-117.
- Luo, Y., Traore, S., Lyu, X., Wang, W., Wang, Y., Xie, Y., Jiao, X. and Fipps, G., 2015. Medium range daily reference evapotranspiration forecasting by using ann and public weather forecasts. *Water Resources Management*, 29(10), pp. 3863-3876.
- Osuolale, F.N., and Zhang, J., 2015. Multi-objective optimisation of atmospheric crude distillation system operations based on bootstrap aggregated neural network models. *Computer Aided Chemical Engineering*, pp. 671-676.
- Pakhale, G.K., Nale, J.P., Temesgen, W.B. and Muluneh, W.D., 2015. Modelling reference evapotranspiration using artificial neural network: A case

study of Ameleke watershed, Ethiopia. *International Journal of Scientific and Research Publications*, 5(1), pp. 2250-3153.

Panda, S., Amatya, D.M., Jackson, R., Sun, G. and Noormets, A., 2018. Automated geospatial models of varying complexities for pine forest evapotranspiration estimation with advanced data mining. *Water*, 10(11), 1687.

Parry, M.L., Canziani, O.F., Palutikof, J.P., van der Linden, P.J. and Hanson, C.E. eds., 2007. *Climate Change 2007: Impacts, Adaptation and Vulnerability*. Cambridge, UK: Cambridge University Press.

Partal, T., 2015. Comparison of wavelet based hybrid models for daily evapotranspiration estimation using meteorological data. *KSCE Journal of Civil Engineering*, 20(5), pp. 2050-2058.

Patil, A.P. and Deka, P.C., 2016. An extreme learning machine approach for modeling evapotranspiration using extrinsic inputs. *Computers and Electronics in Agriculture*, 121, pp. 385-392.

Pereira, L.S., Cordery, I. and Iacovides, I., 2009. *Coping with water scarcity: addressing the challenges*. Berlin: Springer Science + BuSiness Media 2009.

Petković, D., Gocic, M., Shamsirband, S., Qasem, S.N. and Trajkovic, S., 2015. Particle swarm optimization-based radial basis function network for estimation of reference evapotranspiration. *Theoretical and Applied Climatology*, 125(3-4), pp. 555-563.

Pham, B.T., Bui, D.T., Prakash, I. and Dholakia, M.B., 2017. Hybrid integration of multilayer perceptron neural networks and machine learning ensembles for landslide susceptibility assessment at Himalayan area (India) using GIS. *CATENA*, 149, pp. 52-63.

Pino-Mejías, R., Jiménez-Gamero, M.-D., Cubiles-de-la-Vega, M.-D., and Pascual-Acosta, A., 2008. Reduced bootstrap aggregating of learning algorithms. *Pattern Recognition Letters*, 29(3), pp. 265-271.

Pokorny, J., 2019. Evapotranspiration. *Encyclopedia of Ecology, 2<sup>nd</sup> Edition*, 2, pp. 292-303.

Rahimikhoob, A., 2010. Estimation of evapotranspiration based on only air temperature data using artificial neural networks for a subtropical climate in Iran. *Theoretical and Applied Climatology*, 101, pp. 83-91.

Rahimikhoob, A. and Hosseinzadeh, M., 2014. Assessment of Blaney-Criddle equation for calculating reference evapotranspiration with NOAA/AVHRR data. *Water Resources Management*, 28(10), pp. 3365-3375.

Saggi, M.K. and Jain, S., 2019. Reference evapotranspiration estimation and modeling of the Punjab Northern India using deep learning. *Computers and Electronics in Agriculture*, 156, pp. 387-398.

- Shahid, S., 2011. Impacts of climate change on irrigation water demand in northwestern Bangladesh. *Climatic Change*, 105(3-4), pp. 433-453.
- Sharma, S.K. and Tiwari, K.N., 2009. Bootstrap based artificial neural network (BANN) analysis for hierarchical prediction of monthly runoff in Upper Damodar Valley Catchment. *Journal of Hydrology*, 374(3-4), pp. 209-222.
- Sibi, P., Jones, S.A., and Siddarth, P., 2013. Analysis of different activation functions using back propagation neural networks. *Journal of Theoretical and Applied Information Technology*, 47(3), pp. 1264-1268.
- Skurichina, M., and Duin, R.P.W., 1998. Bagging for linear classifiers. *Pattern Recognition*, 31(7), pp. 909-930.
- Skurichina, M., Kuncheva, L., and Duin, R.P.W., 2002. Bagging and boosting for the nearest mean classifier: Effects of sample size on diversity and accuracy. *Lecture Notes in Computer Science*, pp. 1-10.
- Specht, D.F., 1991. A general regression neural network. *IEEE Transactions on Neural Networks*, 2(6), pp. 568-576.
- Sudheer, K.P., Gosain, A.K. and Ramasastri, K.S., 2003. Estimating actual evapotranspiration from limited climatic data using neural computing technique. *Journal of Irrigation and Drainage Engineering*, 129(3), pp. 214-218.
- Tiwari, M.K., and Chatterjee, C., 2010. Uncertainty assessment and ensemble flood forecasting using bootstrap based artificial neural networks (BANNs). *Journal of Hydrology*, 382(1-4), pp. 20-33.
- Tahir, M.F., Tehzeeb-ul-Hassan and Saqib, M.A., 2016. Optimal scheduling of electrical power in energy-deficient scenarios using artificial neural network and Bootstrap aggregating. *International Journal of Electrical Power & Energy Systems*, 83, pp. 49-57.
- Tiwari, M.K., Song, K.Y., Chatterjee, C., and Gupta, M.M., 2013. Improving reliability of river flow forecasting using neural networks, wavelets and self-organising maps. *Journal of Hydroinformatics*, 15(2), pp. 486-502.
- Trajkovic, S., 2009. Comparison of radial basis function networks and empirical equations for converting from pan evaporation to reference evapotranspiration. *Hydrological Processes*, 23(6), pp. 874-880.
- Trajkovic, S., 2009. Temperature-based approaches for estimating reference evapotranspiration. *Journal of Irrigation and Drainage Engineering*, 131, pp. 316-323.
- Traore, S., Luo, Y. and Fipps, G., 2015. Deployment of artificial neural network for short-term forecasting of evapotranspiration using public weather forecast restricted messages. *Agricultural Water Management*, 163, pp. 363-379.

- Traore, S., Wang, Y.M. and Chung, W.G., 2014. Predictive accuracy of backpropagation neural network methodology in evapotranspiration forecasting in Dédougou region, western Burkina Faso. *Journal of Earth System Science*, 123(2), pp. 307-318.
- Traore, S., Wang, Y.M. and Kerh, T., 2008. Modeling reference evapotranspiration by generalized regression neural network in semiarid zone of Africa. *WSEAS Transactions on Information Science and Applications*, 5(6), pp. 991-1000.
- Traore, S., Wang, Y.M. and Kerh, T., 2010. Artificial neural network for modeling reference evapotranspiration complex process in Sudano-Sahelian zone. *Agricultural Water Management*, 97(5), pp. 707-714.
- Torres, A.F., Walker, W.R. and McKee, M., 2011. Forecasting daily potential evapotranspiration using machine learning and limited climatic data. *Agricultural Water Management*, 98(4), pp. 553-562.
- Tukimat, N.N. A, Harun, S. and Shahid, S., 2012. Comparison of different methods in estimating potential evapotranspiration at Muda Irrigation Scheme of Malaysia. *Journal of Agriculture and Rural Development in the Tropics and Subtropics*, 113(1), pp. 77-85.
- Wang, L., Zeng, Y. and Chen, T., 2015. Back propagation neural network with adaptive differential evolution algorithm for time series forecasting. *Expert Systems with Applications*, 42(2), pp. 855-863.
- Wang, Y.M., Traore, S. and Kerh, T.F., 2008. Neural network approach for estimating reference evapotranspiration from limited climatic data in Burkina Faso. *WSEAS Transaction on Computers*, 7(6), pp. 704-713.
- Wang, Y., Zheng, T., Zhao, Y., Jiang, J., Wang, Y., Guo, L., and Wang, P., 2013. Monthly water quality forecasting and uncertainty assessment via bootstrapped wavelet neural networks under missing data for Harbin, China. *Environmental Science and Pollution Research*, 20(12), pp. 8909-8923.
- Watson, P.K. and Teelucksingh, S.S., 2002. *A practical introduction to econometric methods: classical and modern*. Mona, Kingston 7, Jamaica: The University of the Indies Press.
- Willmott, C.J. and Matsuura, K., 2006. On the use of dimensioned measures of error to evaluate the performance of spatial interpolators. *International Journal of Geographical Information Science*, 20(1), pp. 89-102.
- Xu, C.Y. and Chen, D., 2005. Comparison of seven models for estimation of evapotranspiration and groundwater recharge using lysimeter measurement data in Germany. *Hydrological Processes*, 19(18), pp. 3717-3734.

Yassin, M.A., Alazba, A.A. and Mattar, M.A., 2016. Artificial neural networks versus gene expression programming for estimating reference evapotranspiration in arid climate. *Agricultural Water Management*, 163, pp. 110-124.

Yegnanarayana, B., 2006. *Artificial neural network*. New Delhi: Prentice Hall of India.

You, Z.H., Li, S., Gao, X., Luo, X. and Ji, Z., 2014. Large-scale protein-protein interactions detection by integrating big biosensing data with computational model. *BioMed Research International*, 2014, pp. 1-9.

## APPENDICES

### APPENDIX A: Result Performance of All Combinations

Table A-1: Full Result Performance at Alor Setar station using ELM.

<b>Input</b>	<b>Best Activation Function</b>	<b>Best Hidden Neurons</b>	<b>RMSE</b>	<b>NSE</b>	<b>ANSE</b>	<b>MAE</b>	<b>MBE</b>
C1	Sine	29	0.1530	0.9745	0.9738	0.1308	0.0979
C2	RBF	35	0.1978	0.9633	0.9625	0.1653	0.1145
C3	RBF	33	0.1800	0.9664	0.9657	0.1539	0.1164
C4	Sine	31	0.1642	0.9733	0.9727	0.1406	0.1114
C5	Sine	22	0.2321	0.9423	0.9410	0.1922	0.1141
C6	Sigmoid	24	0.2354	0.9460	0.9448	0.1957	0.1515
C7	Sigmoid	48	0.3996	0.8593	0.8561	0.3152	0.0216
C8	Sine	16	0.2068	0.9611	0.9605	0.1727	0.1051
C9	RBF	19	0.2083	0.9587	0.9580	0.1709	0.1070
C10	Sine	49	0.2662	0.9331	0.9320	0.2165	0.1319
C11	Sine	17	0.2565	0.9392	0.9382	0.2143	0.1211
C12	Sine	49	0.4694	0.8069	0.8036	0.3692	0.0975
C13	Sigmoid	42	0.1804	0.9645	0.9639	0.1535	0.1158
C14	Sigmoid	34	0.2281	0.9427	0.9418	0.1904	0.1221
C15	Sine	17	0.3028	0.9092	0.9077	0.2571	0.2154
C16	Sigmoid	40	0.4321	0.8372	0.8344	0.3443	-0.0033
C17	Sigmoid	25	0.2196	0.9491	0.9482	0.1824	0.0718
C18	Sine	17	0.2512	0.9379	0.9368	0.2113	0.1470
C19	Sigmoid	43	0.4285	0.8395	0.8368	0.3441	0.0148
C20	RBF	14	0.4759	0.7947	0.7912	0.4170	0.3534
C21	RBF	49	0.4729	0.8006	0.7973	0.3801	0.0716
C22	Sigmoid	49	0.4776	0.8006	0.7972	0.3794	0.0786
C23	RBF	50	0.2835	0.9230	0.9222	0.2326	0.1593
C24	Sigmoid	27	0.2605	0.9364	0.9357	0.2067	0.1079
C25	Sine	11	0.2990	0.9124	0.9114	0.2519	0.1880
C26	Sine	47	0.5818	0.7028	0.6995	0.4512	0.0758
C27	Sine	27	0.3430	0.8942	0.8930	0.2733	0.1659
C28	Sine	11	0.2604	0.9365	0.9358	0.2149	0.1401
C29	Sine	46	0.6588	0.6195	0.6152	0.5107	0.0593
C30	Sigmoid	49	0.4948	0.7805	0.7780	0.4280	0.3650
C31	Sine	39	0.4988	0.7822	0.7798	0.3842	0.1117
C32	Sine	25	0.5373	0.7440	0.7411	0.4281	0.1222

Table A-1 (Continued)

C33	Sigmoid	11	0.2290	0.9445	0.9439	0.1885	0.1164
C34	Sigmoid	13	0.3380	0.8907	0.8895	0.2870	0.2555
C35	RBF	25	0.4421	0.8287	0.8268	0.3518	-0.0258
C36	Sine	10	0.4913	0.7781	0.7757	0.4214	0.3406
C37	Sigmoid	48	0.4855	0.7927	0.7904	0.3891	0.0993
C38	Sine	41	0.4956	0.7853	0.7829	0.3949	0.1032
C39	Sigmoid	13	0.4870	0.7834	0.7810	0.4245	0.3642
C40	Sigmoid	31	0.5063	0.7729	0.7703	0.4057	0.1329
C41	Sigmoid	41	0.5057	0.7759	0.7734	0.4051	0.1253
C42	Sigmoid	42	0.6619	0.6116	0.6073	0.5368	0.3506
C43	Sigmoid	26	0.3710	0.8746	0.8739	0.2978	0.2290
C44	Sine	27	0.3219	0.9035	0.9030	0.2652	0.2186
C45	Sigmoid	21	0.6438	0.6353	0.6333	0.4917	0.1278
C46	Sigmoid	47	0.5355	0.7332	0.7317	0.4528	0.3734
C47	Sigmoid	18	0.6715	0.6059	0.6037	0.5297	0.0807
C48	Sigmoid	35	0.6127	0.6711	0.6692	0.4831	0.1258
C49	RBF	23	0.6840	0.5818	0.5794	0.5931	0.5495
C50	RBF	14	1.1205	-0.1074	-0.1135	0.9225	-0.3470
C51	Sigmoid	16	0.6967	0.5759	0.5735	0.5406	0.1689
C52	Sigmoid	4	0.6568	0.6218	0.6197	0.5160	0.2031
C53	Sigmoid	8	0.4814	0.7866	0.7854	0.4237	0.3647
C54	Sigmoid	18	0.5040	0.7769	0.7756	0.4022	0.1032
C55	Sine	24	0.5310	0.7525	0.7511	0.4229	0.1437
C56	RBF	36	0.7326	0.5229	0.5202	0.5970	0.2573
C57	Sigmoid	3	0.6783	0.5895	0.5872	0.5468	0.2354
C58	Sine	10	0.7252	0.5353	0.5353	0.6308	0.5935
C59	Sine	7	1.1765	-0.2119	-0.2119	0.9719	-0.4170
C60	Sigmoid	5	0.6855	0.5879	0.5879	0.5336	0.1254
C61	Sine	2	0.8890	0.3111	0.3111	0.6901	0.0864
C62	Sine	1	1.6701	-1.4412	-1.4412	1.3534	0.4734
C63	Sigmoid	6	0.7745	0.4729	0.4729	0.6308	0.4406

Table A-2: Full Result Performance at Bayan Lepas station using ELM.

<b>Input</b>	<b>Best Activation Function</b>	<b>Best Hidden Neurons</b>	<b>RMSE</b>	<b>NSE</b>	<b>ANSE</b>	<b>MAE</b>	<b>MBE</b>
C1	Sigmoid	42	0.1259	0.9846	0.9842	0.1137	-0.0354
C2	Sine	38	0.1898	0.9638	0.9629	0.1619	-0.0234
C3	Sine	35	0.1576	0.9765	0.9759	0.1392	-0.0577
C4	Sine	16	0.1727	0.9728	0.9722	0.1485	0.0298

Table A-2 (Continued)

C5	Sigmoid	29	0.2251	0.9550	0.9540	0.1805	-0.0513
C6	Sigmoid	38	0.2744	0.9302	0.9286	0.2279	0.0385
C7	RBF	8	0.6130	0.6775	0.6702	0.4937	0.1114
C8	RBF	18	0.1836	0.9702	0.9697	0.1490	-0.0006
C9	Sigmoid	14	0.1877	0.9688	0.9683	0.1558	-0.0197
C10	Sine	49	0.2593	0.9394	0.9384	0.2071	-0.0471
C11	Sine	14	0.2830	0.9283	0.9271	0.2249	0.0915
C12	RBF	10	0.6607	0.6256	0.6193	0.5266	0.1995
C13	Sigmoid	24	0.1653	0.9742	0.9738	0.1446	-0.0501
C14	Sigmoid	28	0.2427	0.9480	0.9471	0.2043	-0.0665
C15	Sigmoid	16	0.2876	0.9180	0.9166	0.2311	0.0431
C16	Sine	50	0.6227	0.6641	0.6585	0.4953	0.1126
C17	Sine	35	0.2211	0.9567	0.9560	0.1776	-0.0420
C18	Sine	46	0.2599	0.9396	0.9385	0.2119	0.0297
C19	Sine	45	0.6234	0.6587	0.6530	0.5037	0.1629
C20	Sine	45	0.4631	0.8012	0.7978	0.3650	0.2038
C21	Sigmoid	23	0.7340	0.5162	0.5081	0.5976	0.2712
C22	Sigmoid	36	0.6485	0.6372	0.6310	0.5195	0.2056
C23	Sine	13	0.2034	0.9626	0.9622	0.1661	0.0153
C24	Sigmoid	29	0.2686	0.9366	0.9358	0.2126	0.0122
C25	Sigmoid	6	0.3057	0.9150	0.9141	0.2465	0.0981
C26	Sine	12	0.6963	0.5834	0.5787	0.5541	0.1448
C27	Sine	33	0.3047	0.9152	0.9142	0.2375	0.0523
C28	Sine	19	0.2858	0.9265	0.9257	0.2345	0.0486
C29	RBF	9	0.7236	0.5522	0.5472	0.5670	0.1303
C30	Sine	43	0.5742	0.7119	0.7086	0.4851	0.3207
C31	RBF	27	0.7711	0.4882	0.4825	0.6134	0.1153
C32	RBF	29	0.6909	0.5896	0.5851	0.5517	0.1347
C33	RBF	45	0.2403	0.9477	0.9471	0.1970	-0.0931
C34	RBF	13	0.3087	0.9084	0.9074	0.2549	0.0882
C35	RBF	31	0.6214	0.6679	0.6642	0.4942	0.0808
C36	RBF	41	0.4455	0.8230	0.8210	0.3439	0.1298
C37	Sine	40	0.7311	0.5384	0.5332	0.5916	0.1753
C38	RBF	46	0.6452	0.6440	0.6400	0.5170	0.0586
C39	RBF	32	0.4632	0.8126	0.8105	0.3742	0.1960
C40	RBF	48	0.7598	0.4977	0.4921	0.6083	0.1806
C41	RBF	41	0.6576	0.6272	0.6231	0.5252	0.1149
C42	Sine	27	1.2780	-0.4486	-0.4648	1.0953	0.9241
C43	Sine	16	0.3229	0.9083	0.9078	0.2498	0.0261
C44	Sine	50	0.3065	0.9134	0.9129	0.2349	0.0831

Table A-2 (Continued)

C45	RBF	14	0.6952	0.5856	0.5833	0.5472	-0.0372
C46	Sine	32	0.5143	0.7632	0.7619	0.4252	0.2621
C47	Sigmoid	14	0.8370	0.4004	0.3971	0.6515	-0.0657
C48	Sine	30	0.7067	0.5721	0.5698	0.5616	0.1189
C49	Sigmoid	41	0.4917	0.7859	0.7847	0.3908	0.1872
C50	RBF	25	1.0579	0.0342	0.0288	0.8354	-0.2846
C51	Sigmoid	10	0.7500	0.5185	0.5158	0.5965	0.2309
C52	Sine	4	1.2562	-0.3639	-0.3715	1.0417	0.7476
C53	RBF	35	0.4269	0.8348	0.8339	0.3155	0.1066
C54	Sigmoid	15	0.8001	0.4394	0.4363	0.6452	0.2168
C55	Sigmoid	28	0.6580	0.6287	0.6267	0.5238	0.1819
C56	RBF	29	1.2008	-0.3153	-0.3226	1.0180	0.6835
C57	RBF	34	1.1571	-0.1600	-0.1664	0.9636	0.6226
C58	Sigmoid	7	0.5292	0.7489	0.7489	0.4265	0.2399
C59	Sine	7	1.0906	-0.0318	-0.0318	0.8771	-0.4238
C60	Sigmoid	7	0.7186	0.5577	0.5577	0.5748	0.1133
C61	Sigmoid	2	1.3384	-0.5414	-0.5414	1.0928	0.6341
C62	Sigmoid	2	1.4767	-0.8756	-0.8756	1.1882	0.1813
C63	RBF	8	1.3987	-0.7144	-0.7144	1.2067	1.0018

Table A-3: Full Result Performance at Ipoh station using ELM.

<b>Input</b>	<b>Best Activation Function</b>	<b>Best Hidden Neurons</b>	<b>RMSE</b>	<b>NSE</b>	<b>ANSE</b>	<b>MAE</b>	<b>MBE</b>
C1	RBF	41	0.1247	0.9684	0.9675	0.1064	0.0519
C2	RBF	42	0.1606	0.9510	0.9499	0.1359	0.0718
C3	Sigmoid	25	0.1362	0.9646	0.9637	0.1168	0.0552
C4	RBF	30	0.1270	0.9671	0.9664	0.1088	0.0536
C5	Sine	18	0.1535	0.9554	0.9544	0.1291	0.0510
C6	RBF	28	0.1896	0.9270	0.9253	0.1559	0.0934
C7	RBF	34	0.4005	0.7147	0.7083	0.3202	0.1538
C8	Sine	49	0.1485	0.9582	0.9575	0.1238	0.0549
C9	Sine	44	0.1901	0.9303	0.9292	0.1641	0.0786
C10	Sine	47	0.1833	0.9385	0.9375	0.1535	0.0720
C11	RBF	48	0.2176	0.9091	0.9076	0.1793	0.1261
C12	Sigmoid	19	0.4563	0.6239	0.6175	0.3588	0.0721
C13	Sigmoid	49	0.1434	0.9605	0.9599	0.1234	0.0562
C14	Sine	18	0.1533	0.9527	0.9519	0.1306	0.0533
C15	RBF	10	0.2066	0.9197	0.9183	0.1708	0.1133
C16	Sine	41	0.4167	0.6913	0.6861	0.3334	0.0760

Table A-3 (Continued)

C17	Sine	23	0.1476	0.9575	0.9568	0.1248	0.0293
C18	Sigmoid	47	0.1962	0.9261	0.9249	0.1608	0.1115
C19	Sine	39	0.3991	0.7162	0.7114	0.3191	0.1168
C20	Sigmoid	34	0.2232	0.9034	0.9018	0.1849	0.1091
C21	RBF	20	0.4142	0.6950	0.6899	0.3312	0.1761
C22	RBF	43	0.4253	0.6760	0.6706	0.3379	0.0950
C23	Sigmoid	43	0.2246	0.9046	0.9035	0.1909	0.1194
C24	Sine	36	0.1897	0.9343	0.9336	0.1596	0.0692
C25	Sine	37	0.2331	0.8952	0.8940	0.1939	0.1169
C26	Sine	41	0.4867	0.5765	0.5717	0.3859	0.0072
C27	RBF	32	0.2565	0.8807	0.8793	0.2208	0.1160
C28	Sigmoid	30	0.2229	0.9027	0.9016	0.1853	0.1000
C29	Sigmoid	27	0.5311	0.4972	0.4916	0.4220	-0.0391
C30	Sine	36	0.2689	0.8654	0.8639	0.2245	0.1640
C31	RBF	13	0.4779	0.5914	0.5868	0.3775	0.1032
C32	RBF	19	0.5226	0.5148	0.5094	0.4182	0.1172
C33	Sine	8	0.1550	0.9536	0.9531	0.1276	0.0339
C34	Sine	14	0.2015	0.9229	0.9220	0.1657	0.1116
C35	RBF	45	0.4121	0.6971	0.6937	0.3283	0.0798
C36	Sine	43	0.2322	0.8997	0.8985	0.1962	0.1284
C37	Sine	29	0.4574	0.6251	0.6209	0.3661	0.1673
C38	RBF	28	0.4531	0.6327	0.6285	0.3589	0.1406
C39	Sine	42	0.2173	0.9110	0.9100	0.1807	0.1054
C40	Sigmoid	18	0.4669	0.6104	0.6061	0.3739	0.1774
C41	RBF	24	0.4509	0.6311	0.6270	0.3628	0.1399
C42	Sine	38	0.4832	0.5813	0.5766	0.3901	0.1862
C43	RBF	24	0.2723	0.8629	0.8622	0.2312	0.1436
C44	Sine	35	0.2764	0.8619	0.8611	0.2333	0.1433
C45	Sine	22	0.5370	0.4884	0.4855	0.4250	0.0778
C46	Sine	14	0.2767	0.8538	0.8530	0.2334	0.1760
C47	RBF	14	0.5915	0.3727	0.3692	0.4716	0.1499
C48	RBF	24	0.5497	0.4611	0.4581	0.4347	0.1342
C49	RBF	16	0.2989	0.8362	0.8353	0.2529	0.1925
C50	RBF	8	0.8896	-0.4054	-0.4132	0.6976	0.0100
C51	Sine	10	0.5960	0.3662	0.3627	0.4695	0.0543
C52	Sine	4	0.5668	0.4234	0.4202	0.4491	0.0717
C53	Sigmoid	8	0.2195	0.9076	0.9071	0.1806	0.1002
C54	Sine	11	0.4747	0.5980	0.5958	0.3801	0.1788
C55	RBF	16	0.4531	0.6316	0.6295	0.3601	0.1584
C56	Sigmoid	5	0.5800	0.3958	0.3925	0.4747	0.3179

Table A-3 (Continued)

C57	Sigmoid	8	0.5511	0.4548	0.4518	0.4476	0.2561
C58	RBF	29	0.3134	0.8168	0.8168	0.2639	0.1925
C59	Sigmoid	3	0.9422	-0.5753	-0.5753	0.7296	0.1314
C60	Sine	7	0.6028	0.3531	0.3531	0.4745	0.1547
C61	RBF	8	0.7415	0.0134	0.0134	0.6033	0.3764
C62	Sigmoid	2	1.1716	-1.4428	-1.4428	0.9269	-0.1747
C63	RBF	3	0.5928	0.3691	0.3691	0.4847	0.3412

Table A-4: Full Result Performance at KLIA Sepang station using ELM.

<b>Input</b>	<b>Best Activation Function</b>	<b>Best Hidden Neurons</b>	<b>RMSE</b>	<b>NSE</b>	<b>ANSE</b>	<b>MAE</b>	<b>MBE</b>
C1	Sine	34	0.4773	0.7726	0.7662	0.4220	0.2718
C2	RBF	43	0.5074	0.7442	0.7384	0.4454	0.3086
C3	Sine	32	0.4865	0.7574	0.7519	0.4311	0.2972
C4	Sigmoid	49	0.4813	0.7683	0.7631	0.4255	0.3089
C5	RBF	41	0.4632	0.7876	0.7828	0.4007	0.2431
C6	Sine	50	0.5583	0.6964	0.6896	0.4852	0.3744
C7	Sine	35	0.8367	0.2981	0.2822	0.7056	0.4263
C8	Sigmoid	47	0.5085	0.7410	0.7367	0.4435	0.3610
C9	Sine	43	0.5250	0.7253	0.7207	0.4628	0.3548
C10	Sine	43	0.5271	0.7070	0.7021	0.4530	0.4014
C11	RBF	22	0.5741	0.6711	0.6655	0.4932	0.3667
C12	RBF	28	0.7686	0.4413	0.4319	0.6204	0.0848
C13	Sine	44	0.4954	0.7540	0.7499	0.4388	0.2985
C14	RBF	45	0.4486	0.7988	0.7954	0.3808	0.2739
C15	Sine	39	0.5989	0.6336	0.6274	0.5182	0.3984
C16	RBF	36	0.8306	0.3526	0.3417	0.6824	0.3301
C17	Sine	16	0.4770	0.7765	0.7728	0.4066	0.2581
C18	Sigmoid	43	0.5621	0.6860	0.6808	0.4853	0.3741
C19	RBF	31	0.8641	0.2898	0.2779	0.7187	0.3306
C20	Sigmoid	43	0.6737	0.5570	0.5495	0.5869	0.5440
C21	Sigmoid	48	0.7740	0.4205	0.4108	0.6277	0.3204
C22	Sine	24	0.8968	0.2229	0.2098	0.7456	0.4392
C23	Sigmoid	7	0.5155	0.7225	0.7194	0.4423	0.3183
C24	Sine	21	0.5499	0.7027	0.6994	0.4768	0.3562
C25	Sine	47	0.5988	0.6169	0.6127	0.5179	0.4490
C26	RBF	17	0.8311	0.3528	0.3455	0.6723	0.0660
C27	Sine	25	0.5496	0.6950	0.6916	0.4731	0.3573
C28	RBF	49	0.5767	0.6682	0.6645	0.5054	0.3898

Table A-4 (Continued)

C29	Sine	18	0.8397	0.3420	0.3347	0.6578	0.0937
C30	Sigmoid	43	0.7614	0.4170	0.4105	0.6575	0.6095
C31	Sine	9	0.8693	0.2886	0.2806	0.7097	0.2647
C32	RBF	9	0.8756	0.2859	0.2779	0.7009	0.2372
C33	Sine	35	0.4945	0.7590	0.7563	0.4363	0.2866
C34	Sine	29	0.6217	0.5746	0.5699	0.5368	0.4712
C35	RBF	33	0.8150	0.3737	0.3667	0.6656	0.2741
C36	Sine	47	0.6885	0.5286	0.5234	0.5999	0.5568
C37	Sigmoid	37	0.8177	0.3646	0.3575	0.6730	0.0669
C38	Sigmoid	38	0.8307	0.3364	0.3290	0.6778	0.3076
C39	Sine	26	0.7076	0.5031	0.4975	0.6110	0.5675
C40	RBF	35	0.8122	0.3714	0.3644	0.6635	0.1553
C41	RBF	24	0.8620	0.2814	0.2734	0.7092	0.4320
C42	RBF	41	1.0853	-0.1577	-0.1706	0.9039	0.6690
C43	RBF	14	0.5778	0.6683	0.6664	0.4882	0.4382
C44	Sine	34	0.6584	0.5537	0.5512	0.5616	0.5141
C45	Sigmoid	9	0.8809	0.2772	0.2731	0.6936	0.1764
C46	Sigmoid	32	0.6748	0.5215	0.5188	0.5742	0.4442
C47	Sigmoid	14	0.8990	0.2464	0.2423	0.7290	0.3074
C48	Sigmoid	8	0.8966	0.2465	0.2423	0.7325	0.1566
C49	Sigmoid	39	0.7231	0.4566	0.4536	0.6169	0.4453
C50	Sigmoid	21	1.1046	-0.1321	-0.1384	0.8807	-0.2177
C51	Sigmoid	18	0.8668	0.3031	0.2992	0.6917	0.0539
C52	Sine	38	1.3929	-0.8598	-0.8701	1.1547	0.9275
C53	Sine	16	0.7479	0.4523	0.4493	0.6506	0.6053
C54	RBF	14	0.7917	0.4062	0.4029	0.6504	0.2796
C55	Sigmoid	23	0.8424	0.3015	0.2976	0.6947	0.2925
C56	RBF	24	1.0025	0.0188	0.0134	0.8240	0.4462
C57	RBF	33	1.1006	-0.1810	-0.1876	0.9012	0.5913
C58	RBF	11	0.7046	0.5138	0.5138	0.5966	0.5277
C59	Sigmoid	6	1.1081	-0.1452	-0.1452	0.8878	-0.2387
C60	Sine	4	0.9101	0.2164	0.2164	0.7334	0.1677
C61	Sigmoid	4	1.6339	-1.5011	-1.5011	1.3912	1.2306
C62	Sigmoid	4	1.5236	-1.1459	-1.1459	1.2126	-0.2377
C63	Sigmoid	11	1.1338	-0.2846	-0.2846	0.9458	0.6241

Table A-5: Full Result Performance at Lubok Merbau station using ELM.

<b>Input</b>	<b>Best Activation Function</b>	<b>Best Hidden Neurons</b>	<b>RMSE</b>	<b>NSE</b>	<b>ANSE</b>	<b>MAE</b>	<b>MBE</b>
--------------	-----------------------------------------	------------------------------------	-------------	------------	-------------	------------	------------

Table A-5 (Continued)

C1	Sine	26	0.1488	0.9591	0.9579	0.1268	-0.0728
C2	Sine	30	0.1631	0.9568	0.9557	0.1349	-0.0388
C3	Sine	30	0.1507	0.9590	0.9580	0.1269	-0.0688
C4	Sigmoid	9	0.1499	0.9615	0.9606	0.1263	-0.0349
C5	RBF	19	0.1571	0.9556	0.9546	0.1315	-0.0604
C6	Sine	19	0.1511	0.9604	0.9595	0.1206	-0.0509
C7	Sine	26	0.3556	0.8036	0.7989	0.2823	0.0112
C8	RBF	23	0.1627	0.9565	0.9557	0.1345	-0.0548
C9	RBF	17	0.1657	0.9555	0.9547	0.1381	-0.0275
C10	RBF	23	0.1608	0.9573	0.9566	0.1322	-0.0246
C11	RBF	31	0.1658	0.9559	0.9551	0.1348	-0.0300
C12	Sine	23	0.4750	0.6416	0.6352	0.3811	-0.0857
C13	Sigmoid	8	0.1428	0.9658	0.9652	0.1154	0.0027
C14	RBF	25	0.1569	0.9541	0.9532	0.1327	-0.0674
C15	Sine	17	0.1624	0.9553	0.9545	0.1310	-0.0453
C16	Sine	24	0.3710	0.7854	0.7816	0.2950	-0.0241
C17	Sine	14	0.1595	0.9539	0.9531	0.1337	-0.0734
C18	Sigmoid	7	0.1555	0.9604	0.9597	0.1207	-0.0109
C19	RBF	21	0.3643	0.7938	0.7902	0.2898	-0.0061
C20	RBF	38	0.1842	0.9447	0.9437	0.1470	-0.0402
C21	RBF	19	0.3643	0.7932	0.7896	0.2901	0.0144
C22	Sigmoid	19	0.4210	0.7235	0.7186	0.3336	0.0172
C23	Sine	26	0.1869	0.9455	0.9448	0.1533	0.0028
C24	RBF	15	0.1659	0.9542	0.9537	0.1370	-0.0397
C25	Sigmoid	13	0.1648	0.9563	0.9558	0.1340	-0.0164
C26	RBF	13	0.5140	0.5831	0.5782	0.4117	-0.1017
C27	RBF	23	0.1808	0.9467	0.9461	0.1483	-0.0336
C28	Sigmoid	20	0.1774	0.9502	0.9496	0.1461	-0.0369
C29	RBF	18	0.6011	0.4339	0.4272	0.4733	-0.1463
C30	RBF	48	0.1920	0.9416	0.9409	0.1540	-0.0243
C31	RBF	12	0.4820	0.6324	0.6280	0.3880	-0.0070
C32	RBF	25	0.5395	0.5414	0.5360	0.4358	-0.0727
C33	Sine	8	0.1664	0.9518	0.9513	0.1375	-0.0562
C34	Sine	12	0.1826	0.9458	0.9452	0.1494	-0.0245
C35	Sine	16	0.3710	0.7853	0.7828	0.2962	-0.0371
C36	Sine	36	0.1908	0.9411	0.9404	0.1531	-0.0503
C37	Sigmoid	24	0.3869	0.7667	0.7640	0.3107	-0.0147
C38	Sigmoid	17	0.4305	0.7110	0.7076	0.3408	0.0326
C39	Sine	8	0.1821	0.9471	0.9464	0.1426	-0.0359
C40	RBF	15	0.3710	0.7856	0.7830	0.2954	-0.0315

Table A-5 (Continued)

C41	RBF	18	0.4271	0.7153	0.7120	0.3355	-0.0141
C42	RBF	19	0.4505	0.6793	0.6755	0.3576	0.0039
C43	RBF	20	0.1984	0.9377	0.9373	0.1642	-0.0140
C44	Sine	9	0.2022	0.9357	0.9353	0.1642	0.0549
C45	Sine	10	0.5996	0.4363	0.4330	0.4631	-0.1089
C46	RBF	44	0.2037	0.9340	0.9336	0.1663	-0.0183
C47	RBF	8	0.5485	0.5258	0.5231	0.4312	-0.0104
C48	RBF	23	0.5666	0.4926	0.4896	0.4578	-0.1323
C49	RBF	31	0.2056	0.9319	0.9315	0.1660	0.0264
C50	RBF	8	0.8290	-0.0675	-0.0737	0.6533	-0.2841
C51	RBF	35	0.6586	0.3124	0.3083	0.5215	0.0474
C52	RBF	23	0.5486	0.5214	0.5186	0.4436	0.0227
C53	Sigmoid	6	0.1945	0.9394	0.9391	0.1533	-0.0194
C54	Sigmoid	7	0.3981	0.7532	0.7518	0.3203	-0.0411
C55	RBF	8	0.4413	0.6967	0.6949	0.3508	0.0242
C56	Sine	11	0.4868	0.6315	0.6293	0.3890	0.0575
C57	Sine	13	0.4914	0.6224	0.6201	0.3912	0.0207
C58	Sigmoid	33	0.2295	0.9180	0.9180	0.1867	0.0707
C59	Sine	4	0.8559	-0.1435	-0.1435	0.6758	-0.3954
C60	Sine	21	0.6509	0.3373	0.3373	0.5158	0.0373
C61	RBF	8	0.6356	0.3627	0.3627	0.5081	0.0236
C62	Sine	1	1.1950	-1.2374	-1.2374	0.9293	-0.1035
C63	Sine	5	0.5005	0.6073	0.6073	0.3985	0.0216

Table A-6: Full Result Performance at Pulau Langkawi station using ELM.

<b>Input</b>	<b>Best Activation Function</b>	<b>Best Hidden Neurons</b>	<b>RMSE</b>	<b>NSE</b>	<b>ANSE</b>	<b>MAE</b>	<b>MBE</b>
C1	Sigmoid	22	0.2127	0.9570	0.9558	0.1821	0.1568
C2	Sigmoid	19	0.2445	0.9458	0.9446	0.2041	0.1240
C3	Sigmoid	23	0.2183	0.9539	0.9529	0.1883	0.1438
C4	Sine	32	0.2176	0.9525	0.9514	0.1892	0.1507
C5	Sigmoid	21	0.2654	0.9399	0.9385	0.2223	0.1129
C6	Sigmoid	37	0.3402	0.9033	0.9011	0.2843	0.2463
C7	Sine	39	0.5464	0.7669	0.7617	0.4295	0.0912
C8	Sine	13	0.2457	0.9474	0.9465	0.2041	0.1304
C9	Sigmoid	34	0.2499	0.9449	0.9439	0.2111	0.1565
C10	Sine	48	0.2943	0.9278	0.9266	0.2392	0.1704
C11	Sigmoid	18	0.3306	0.9111	0.9096	0.2738	0.2047
C12	RBF	33	0.5978	0.7210	0.7163	0.4737	0.0651

Table A-6 (Continued)

C13	RBF	32	0.2286	0.9493	0.9484	0.1953	0.1571
C14	Sine	19	0.2989	0.9251	0.9238	0.2556	0.1234
C15	Sine	37	0.3328	0.9093	0.9078	0.2708	0.2259
C16	Sine	41	0.5733	0.7436	0.7392	0.4539	0.0618
C17	Sine	45	0.2876	0.9305	0.9293	0.2426	0.1731
C18	Sine	21	0.3525	0.8943	0.8925	0.2935	0.2528
C19	Sine	44	0.5641	0.7522	0.7481	0.4463	0.0636
C20	Sine	21	0.6343	0.6712	0.6657	0.5395	0.4661
C21	Sigmoid	50	0.6033	0.7160	0.7112	0.4758	0.0054
C22	Sigmoid	35	0.6353	0.6836	0.6783	0.5092	0.2587
C23	Sine	42	0.3303	0.8999	0.8987	0.2805	0.1915
C24	Sine	28	0.3172	0.9158	0.9149	0.2600	0.1666
C25	Sigmoid	13	0.3203	0.9162	0.9153	0.2619	0.2053
C26	Sine	17	0.6534	0.6657	0.6619	0.5260	-0.0356
C27	Sine	26	0.3397	0.9046	0.9035	0.2794	0.1935
C28	Sigmoid	19	0.3467	0.8987	0.8976	0.2884	0.2370
C29	Sine	30	0.7082	0.6091	0.6047	0.5619	-0.0661
C30	Sigmoid	16	0.8650	0.3990	0.3923	0.7476	0.6837
C31	Sigmoid	44	0.6569	0.6629	0.6592	0.5038	-0.0002
C32	RBF	30	0.6428	0.6782	0.6746	0.5083	0.0794
C33	Sine	40	0.2926	0.9273	0.9265	0.2477	0.1737
C34	Sigmoid	15	0.3856	0.8744	0.8730	0.3202	0.2752
C35	RBF	38	0.5793	0.7379	0.7350	0.4616	0.0847
C36	RBF	40	0.6418	0.6708	0.6672	0.5543	0.4865
C37	Sigmoid	28	0.6233	0.6959	0.6925	0.5000	0.0742
C38	RBF	34	0.6348	0.6839	0.6804	0.5059	0.1738
C39	Sine	14	0.6077	0.6899	0.6864	0.5184	0.4255
C40	Sigmoid	42	0.6390	0.6803	0.6767	0.5033	0.0661
C41	Sigmoid	38	0.6125	0.7067	0.7034	0.4922	0.1254
C42	Sigmoid	34	0.8863	0.3741	0.3671	0.7163	0.3736
C43	Sine	42	0.3573	0.8955	0.8949	0.2893	0.1706
C44	Sine	32	0.4205	0.8373	0.8364	0.3410	0.2661
C45	Sine	13	0.7360	0.5774	0.5750	0.5903	0.0131
C46	Sigmoid	38	0.9849	0.2389	0.2347	0.8601	0.8160
C47	Sigmoid	44	0.8194	0.4729	0.4700	0.6336	0.2364
C48	RBF	17	0.6489	0.6719	0.6700	0.5215	0.0124
C49	Sine	7	1.1333	-0.0110	-0.0167	0.9870	0.9541
C50	RBF	15	1.1686	-0.0820	-0.0880	0.9599	-0.4402
C51	Sine	24	0.7735	0.5334	0.5308	0.6191	-0.0511
C52	RBF	15	1.0265	0.1648	0.1602	0.8308	0.5512

Table A-6 (Continued)

C53	Sine	31	0.6517	0.6600	0.6581	0.5606	0.4845
C54	Sine	15	0.6536	0.6658	0.6640	0.5210	0.1414
C55	Sigmoid	18	0.6346	0.6843	0.6826	0.5132	0.2087
C56	RBF	22	0.9081	0.3478	0.3442	0.7391	0.4706
C57	Sigmoid	23	0.8969	0.3522	0.3486	0.7251	0.4139
C58	RBF	41	1.2229	-0.1679	-0.1679	1.0780	1.0437
C59	Sine	5	1.2784	-0.3036	-0.3036	1.0812	-0.6258
C60	RBF	11	0.8118	0.4850	0.4850	0.6542	0.0401
C61	RBF	6	1.1844	-0.1144	-0.1144	0.9738	0.6754
C62	RBF	3	1.4544	-0.6515	-0.6515	1.1589	0.0233
C63	RBF	7	0.9137	0.3403	0.3403	0.7438	0.4809

Table A-7: Full Result Performance at Sitiawan station using ELM.

<b>Input</b>	<b>Best Activation Function</b>	<b>Best Hidden Neurons</b>	<b>RMSE</b>	<b>NSE</b>	<b>ANSE</b>	<b>MAE</b>	<b>MBE</b>
C1	RBF	15	0.3049	0.8410	0.8362	0.2631	0.1706
C2	RBF	19	0.3153	0.8339	0.8300	0.2721	0.1505
C3	Sigmoid	22	0.3220	0.8243	0.8201	0.2817	0.1807
C4	RBF	12	0.2819	0.8529	0.8494	0.2386	0.1444
C5	RBF	12	0.3127	0.8334	0.8294	0.2693	0.1459
C6	Sine	16	0.3278	0.8197	0.8154	0.2806	0.1979
C7	Sine	17	0.5753	0.4675	0.4548	0.4842	0.4158
C8	RBF	46	0.3249	0.8240	0.8209	0.2833	0.1665
C9	Sigmoid	50	0.3214	0.8292	0.8261	0.2812	0.1590
C10	Sine	49	0.3052	0.8435	0.8407	0.2618	0.1603
C11	RBF	14	0.3265	0.8223	0.8191	0.2774	0.1704
C12	RBF	16	0.5554	0.5055	0.4967	0.4557	0.2458
C13	RBF	22	0.3197	0.8224	0.8193	0.2779	0.1869
C14	RBF	9	0.2884	0.8587	0.8561	0.2471	0.1330
C15	RBF	12	0.3201	0.8314	0.8284	0.2712	0.1752
C16	Sigmoid	5	0.4868	0.6111	0.6042	0.3907	0.1886
C17	Sine	22	0.3165	0.8306	0.8276	0.2747	0.1664
C18	RBF	12	0.3506	0.7987	0.7951	0.3016	0.2320
C19	RBF	19	0.5321	0.5432	0.5350	0.4351	0.3306
C20	Sigmoid	41	0.3209	0.8239	0.8207	0.2732	0.1820
C21	Sine	6	0.5040	0.5875	0.5801	0.4084	0.2398
C22	RBF	11	0.6357	0.3499	0.3383	0.5229	0.3931
C23	RBF	15	0.3145	0.8372	0.8353	0.2678	0.1786
C24	Sine	13	0.3188	0.8305	0.8285	0.2753	0.1590

Table A-7 (Continued)

C25	RBF	9	0.3222	0.8290	0.8270	0.2730	0.1616
C26	RBF	6	0.6204	0.3792	0.3719	0.5110	0.2958
C27	RBF	48	0.3072	0.8408	0.8389	0.2608	0.1305
C28	Sigmoid	50	0.3300	0.8200	0.8179	0.2841	0.2017
C29	Sigmoid	5	0.5761	0.4647	0.4584	0.4596	0.0305
C30	Sine	21	0.3261	0.8182	0.8160	0.2791	0.1793
C31	Sine	10	0.5517	0.5107	0.5050	0.4470	0.2957
C32	Sigmoid	5	0.6105	0.3995	0.3924	0.4904	0.1760
C33	Sine	10	0.3264	0.8175	0.8153	0.2805	0.1717
C34	Sigmoid	8	0.3258	0.8228	0.8207	0.2791	0.1958
C35	RBF	13	0.6081	0.4026	0.3955	0.5059	0.4131
C36	RBF	38	0.3281	0.8222	0.8201	0.2837	0.1672
C37	RBF	19	0.6365	0.3337	0.3258	0.5306	0.3331
C38	Sigmoid	23	0.6982	0.2186	0.2094	0.5788	0.3833
C39	RBF	42	0.3100	0.8410	0.8391	0.2639	0.1624
C40	RBF	14	0.5560	0.4909	0.4849	0.4525	0.3425
C41	Sigmoid	47	0.6167	0.3779	0.3706	0.5008	0.3142
C42	RBF	8	0.6621	0.2877	0.2793	0.5513	0.4306
C43	RBF	10	0.3351	0.8148	0.8137	0.2848	0.1903
C44	Sine	6	0.3492	0.8042	0.8030	0.2982	0.2188
C45	Sine	4	0.6473	0.3301	0.3262	0.5245	0.0800
C46	RBF	38	0.3260	0.8162	0.8151	0.2778	0.1425
C47	Sine	12	0.6931	0.2174	0.2128	0.5703	0.3482
C48	Sine	11	0.7562	0.0889	0.0835	0.6179	0.4511
C49	Sigmoid	25	0.3382	0.8094	0.8083	0.2891	0.2034
C50	Sigmoid	21	0.8421	-0.1551	-0.1619	0.6653	0.0869
C51	RBF	16	0.7445	0.1098	0.1046	0.5954	0.3907
C52	Sine	3	0.6477	0.3292	0.3253	0.5218	0.2839
C53	Sine	24	0.3139	0.8268	0.8258	0.2670	0.1823
C54	Sigmoid	12	0.6220	0.3741	0.3704	0.5125	0.3913
C55	Sigmoid	3	0.6623	0.2982	0.2941	0.5435	0.3120
C56	Sigmoid	28	0.7592	0.0547	0.0491	0.6303	0.4829
C57	Sigmoid	6	0.6791	0.2343	0.2298	0.5621	0.4265
C58	Sigmoid	27	0.3834	0.7644	0.7644	0.3263	0.2387
C59	RBF	7	0.8529	-0.1887	-0.1887	0.6715	0.1967
C60	Sine	5	0.8076	-0.0557	-0.0557	0.6580	0.4720
C61	Sine	2	0.7409	0.1248	0.1248	0.5857	0.0689
C62	Sigmoid	2	1.1803	-1.2129	-1.2129	0.9386	0.1388
C63	RBF	3	0.7818	-0.0130	-0.0130	0.6553	0.5358

Table A-8: Full Result Performance at Subang station using ELM.

<b>Input</b>	<b>Best Activation Function</b>	<b>Best Hidden Neurons</b>	<b>RMSE</b>	<b>NSE</b>	<b>ANSE</b>	<b>MAE</b>	<b>MBE</b>
C1	Sine	38	0.2627	0.9152	0.9128	0.2225	0.0550
C2	Sigmoid	10	0.2832	0.9085	0.9064	0.2353	0.0364
C3	Sine	41	0.2698	0.9131	0.9112	0.2292	0.0565
C4	RBF	45	0.2594	0.9171	0.9152	0.2201	0.0497
C5	RBF	45	0.2530	0.9193	0.9174	0.2099	0.0502
C6	Sine	18	0.2879	0.9071	0.9050	0.2335	0.0626
C7	RBF	47	0.9755	-0.0392	-0.0627	0.8275	0.5752
C8	Sine	19	0.2797	0.9101	0.9086	0.2317	0.0751
C9	RBF	13	0.2806	0.9094	0.9079	0.2312	0.0694
C10	RBF	16	0.2887	0.9059	0.9043	0.2397	0.0652
C11	RBF	21	0.2894	0.9081	0.9066	0.2356	0.0647
C12	RBF	26	0.9885	-0.0418	-0.0594	0.8227	0.4438
C13	RBF	15	0.2999	0.8927	0.8908	0.2544	0.0811
C14	Sigmoid	48	0.2565	0.9206	0.9193	0.2117	0.0513
C15	Sigmoid	9	0.3071	0.8943	0.8925	0.2511	0.1073
C16	Sigmoid	38	0.9807	-0.0559	-0.0737	0.8335	0.5878
C17	RBF	15	0.2891	0.9019	0.9003	0.2450	0.0332
C18	RBF	24	0.2807	0.9116	0.9101	0.2272	0.0303
C19	Sigmoid	47	0.9318	0.0462	0.0301	0.7795	0.4865
C20	Sigmoid	13	0.2883	0.9078	0.9063	0.2352	0.0565
C21	Sigmoid	29	0.9883	-0.0558	-0.0737	0.8324	0.5729
C22	RBF	7	1.0615	-0.2179	-0.2385	0.9128	0.7043
C23	Sigmoid	10	0.3090	0.8922	0.8910	0.2556	0.1008
C24	RBF	22	0.2771	0.9121	0.9111	0.2285	0.0630
C25	RBF	17	0.3034	0.8985	0.8973	0.2477	0.0844
C26	Sigmoid	47	1.1405	-0.4944	-0.5111	0.9666	0.3438
C27	Sigmoid	6	0.2776	0.9135	0.9125	0.2247	0.0184
C28	Sine	7	0.3156	0.8864	0.8851	0.2592	0.0476
C29	Sine	32	1.0667	-0.2196	-0.2333	0.8865	0.3605
C30	Sigmoid	6	0.3101	0.8929	0.8917	0.2559	0.0730
C31	Sigmoid	9	1.0492	-0.1590	-0.1720	0.8714	0.5193
C32	RBF	5	1.0914	-0.2635	-0.2777	0.9086	0.3372
C33	Sigmoid	44	0.2762	0.9098	0.9088	0.2290	0.0443
C34	Sigmoid	38	0.3474	0.8621	0.8605	0.2893	0.0889
C35	RBF	48	1.0151	-0.1844	-0.1976	0.8680	0.5106
C36	RBF	15	0.3031	0.8979	0.8967	0.2479	0.0835
C37	RBF	42	1.1722	-0.5961	-0.6139	1.0219	0.5408

Table A-8 (Continued)

C38	Sine	6	1.0423	-0.1495	-0.1623	0.8861	0.6989
C39	RBF	12	0.3016	0.9003	0.8992	0.2458	0.0334
C40	Sine	15	0.9722	-0.0025	-0.0137	0.8237	0.5772
C41	Sigmoid	4	0.9893	-0.0482	-0.0600	0.8367	0.5800
C42	Sine	9	1.1218	-0.3271	-0.3420	0.9672	0.8071
C43	Sigmoid	4	0.3157	0.8826	0.8819	0.2562	0.0321
C44	Sigmoid	6	0.3451	0.8708	0.8701	0.2806	0.1555
C45	Sine	12	0.9996	-0.0452	-0.0511	0.8105	0.2890
C46	RBF	6	0.3274	0.8831	0.8825	0.2680	0.0889
C47	Sigmoid	34	1.3169	-1.0420	-1.0534	1.1354	0.1499
C48	Sigmoid	3	0.9912	-0.0212	-0.0269	0.8046	0.1310
C49	Sigmoid	5	0.3194	0.8875	0.8869	0.2633	0.0224
C50	RBF	28	1.3146	-0.8720	-0.8824	1.0953	-0.1086
C51	Sigmoid	4	1.0566	-0.1701	-0.1767	0.8572	-0.0871
C52	Sine	5	1.0796	-0.2163	-0.2230	0.8872	0.5718
C53	Sine	18	0.3529	0.8613	0.8605	0.2911	0.0793
C54	RBF	15	0.9644	-0.0001	-0.0057	0.8079	0.4813
C55	Sigmoid	3	1.0428	-0.2031	-0.2098	0.8907	0.6823
C56	Sine	5	1.1776	-0.4542	-0.4623	1.0164	0.8397
C57	Sine	40	1.5055	-1.7710	-1.7864	1.3359	0.5656
C58	Sine	5	0.3834	0.8418	0.8418	0.3135	0.1202
C59	Sine	4	1.3396	-0.8662	-0.8662	1.0780	0.2590
C60	Sine	2	1.2302	-0.7813	-0.7813	1.0367	-0.1959
C61	Sigmoid	5	1.2576	-0.6663	-0.6663	1.0505	0.7907
C62	Sine	2	1.6513	-1.9073	-1.9073	1.3709	0.4939
C63	Sigmoid	3	1.1975	-0.5028	-0.5028	1.0360	0.8467

Table A-9: Full Result Performance at Alor Setar station using Bagged ELM.

<b>Input</b>	<b>Best Activation Function</b>	<b>Best Hidden Neurons</b>	<b>RMSE</b>	<b>NSE</b>	<b>ANSE</b>	<b>MAE</b>	<b>MBE</b>
C1	Sine	29	0.1789	0.9651	0.9642	0.1566	0.1230
C2	RBF	35	0.2125	0.9559	0.9549	0.1797	0.1281
C3	RBF	33	0.1850	0.9638	0.9630	0.1584	0.1184
C4	Sine	31	0.1744	0.9689	0.9682	0.1511	0.1211
C5	Sine	22	0.2547	0.9298	0.9282	0.2181	0.1324
C6	Sigmoid	24	0.2495	0.9390	0.9377	0.2108	0.1489
C7	Sigmoid	48	0.4483	0.8190	0.8149	0.3598	0.0808
C8	Sine	16	0.2105	0.9575	0.9568	0.1770	0.1154
C9	RBF	19	0.2269	0.9512	0.9504	0.1889	0.1333

Table A-9 (Continued)

C10	Sine	49	0.2939	0.9128	0.9114	0.2429	0.1505
C11	Sine	17	0.2749	0.9277	0.9264	0.2309	0.1465
C12	Sine	49	0.5264	0.7530	0.7488	0.4209	0.0984
C13	Sigmoid	42	0.1897	0.9611	0.9604	0.1628	0.1251
C14	Sigmoid	34	0.2406	0.9344	0.9333	0.2039	0.1307
C15	Sine	17	0.3231	0.8974	0.8956	0.2773	0.2298
C16	Sigmoid	40	0.4706	0.8030	0.7997	0.3778	0.0455
C17	Sigmoid	25	0.2329	0.9392	0.9382	0.1961	0.1114
C18	Sine	17	0.2641	0.9313	0.9302	0.2235	0.1568
C19	Sigmoid	43	0.4812	0.7912	0.7877	0.3896	0.0483
C20	RBF	14	0.5030	0.7636	0.7596	0.4421	0.3796
C21	RBF	49	0.5009	0.7722	0.7684	0.4068	0.0786
C22	Sigmoid	49	0.5235	0.7550	0.7509	0.4226	0.0842
C23	RBF	50	0.3048	0.9103	0.9093	0.2541	0.1302
C24	Sigmoid	27	0.2826	0.9249	0.9241	0.2271	0.1258
C25	Sine	11	0.3197	0.9007	0.8996	0.2714	0.2040
C26	Sine	47	0.6460	0.6240	0.6198	0.5137	0.0907
C27	Sine	27	0.3578	0.8814	0.8801	0.2902	0.2056
C28	Sine	11	0.2643	0.9337	0.9330	0.2210	0.1291
C29	Sine	46	0.7784	0.4301	0.4238	0.6325	-0.0886
C30	Sigmoid	49	0.5344	0.7420	0.7391	0.4677	0.4030
C31	Sine	39	0.5602	0.7180	0.7149	0.4411	0.0978
C32	Sine	25	0.5800	0.6951	0.6917	0.4725	0.0697
C33	Sigmoid	11	0.2442	0.9330	0.9323	0.2077	0.1262
C34	Sigmoid	13	0.3528	0.8798	0.8785	0.3033	0.2690
C35	RBF	25	0.4836	0.7922	0.7898	0.3885	0.0598
C36	Sine	10	0.5107	0.7603	0.7576	0.4451	0.3777
C37	Sigmoid	48	0.5344	0.7407	0.7378	0.4300	0.1440
C38	Sine	41	0.5404	0.7378	0.7348	0.4358	0.0614
C39	Sigmoid	13	0.4969	0.7704	0.7679	0.4346	0.3696
C40	Sigmoid	31	0.5315	0.7484	0.7456	0.4296	0.1024
C41	Sigmoid	41	0.5386	0.7418	0.7389	0.4369	0.0750
C42	Sigmoid	42	0.6946	0.5616	0.5567	0.5695	0.3379
C43	Sigmoid	26	0.3964	0.8308	0.8298	0.3220	0.1930
C44	Sine	27	0.3497	0.8836	0.8830	0.2932	0.2195
C45	Sigmoid	21	0.7155	0.5303	0.5277	0.5603	0.0710
C46	Sigmoid	47	0.6606	0.5355	0.5329	0.5803	0.4413
C47	Sigmoid	18	0.7193	0.5399	0.5373	0.5735	0.1015
C48	Sigmoid	35	0.7785	0.3539	0.3503	0.6480	0.0129
C49	RBF	23	0.6765	0.5826	0.5803	0.5860	0.5257

Table A-9 (Continued)

C50	RBF	14	1.2051	-0.3195	-0.3268	1.0052	-0.4337
C51	Sigmoid	16	0.7327	0.5237	0.5210	0.5823	0.0325
C52	Sigmoid	4	0.6873	0.5801	0.5778	0.5466	0.2073
C53	Sigmoid	8	0.4832	0.7848	0.7836	0.4235	0.3608
C54	Sigmoid	18	0.5341	0.7463	0.7449	0.4306	0.0867
C55	Sine	24	0.5858	0.6878	0.6861	0.4751	0.1868
C56	RBF	36	0.8392	0.2840	0.2801	0.7025	0.3298
C57	Sigmoid	3	0.7934	0.3908	0.3874	0.6580	0.2779
C58	Sine	10	0.7250	0.5264	0.5264	0.6333	0.5914
C59	Sine	7	1.2629	-0.4577	-0.4577	1.0556	-0.2675
C60	Sigmoid	5	0.7044	0.5628	0.5628	0.5503	0.1445
C61	Sine	2	0.9750	0.1392	0.1392	0.7795	0.1891
C62	Sine	1	1.7915	-1.8745	-1.8745	1.4876	0.4318
C63	Sigmoid	6	0.7843	0.4564	0.4564	0.6406	0.4406

Table A-10: Full Result Performance at Bayan Lepas station using Bagged ELM.

<b>Input</b>	<b>Best Activation Function</b>	<b>Best Hidden Neurons</b>	<b>RMSE</b>	<b>NSE</b>	<b>ANSE</b>	<b>MAE</b>	<b>MBE</b>
C1	Sigmoid	42	0.1404	0.9805	0.9799	0.1266	-0.0480
C2	Sine	38	0.2062	0.9553	0.9543	0.1783	-0.0113
C3	Sine	35	0.1723	0.9711	0.9704	0.1537	-0.0593
C4	Sine	16	0.2056	0.9556	0.9546	0.1792	-0.0143
C5	Sigmoid	29	0.3091	0.8979	0.8955	0.2676	-0.1373
C6	Sigmoid	38	0.3029	0.9120	0.9101	0.2589	0.0464
C7	RBF	8	0.7019	0.5575	0.5475	0.5753	0.2413
C8	RBF	18	0.2228	0.9514	0.9506	0.1913	-0.0163
C9	Sigmoid	14	0.2254	0.9490	0.9481	0.1948	-0.0270
C10	Sine	49	0.3132	0.9084	0.9068	0.2582	-0.0396
C11	Sine	14	0.3262	0.8986	0.8969	0.2711	0.0702
C12	RBF	10	0.7145	0.5555	0.5480	0.5700	0.1830
C13	Sigmoid	24	0.1832	0.9663	0.9658	0.1635	-0.0654
C14	Sigmoid	28	0.2664	0.9339	0.9328	0.2257	-0.0900
C15	Sigmoid	16	0.3317	0.8886	0.8867	0.2815	0.0546
C16	Sine	50	0.7237	0.5224	0.5143	0.5960	0.1361
C17	Sine	35	0.2724	0.9313	0.9301	0.2308	-0.0905
C18	Sine	46	0.2849	0.9249	0.9237	0.2339	0.0565
C19	Sine	45	0.7358	0.5183	0.5101	0.6045	0.1747
C20	Sine	45	0.5157	0.7467	0.7424	0.4262	0.2689
C21	Sigmoid	23	0.7954	0.4302	0.4206	0.6583	0.3466

Table A-10 (Continued)

C22	Sigmoid	36	0.7191	0.5455	0.5379	0.5809	0.2696
C23	Sine	13	0.2290	0.9491	0.9486	0.1943	-0.0154
C24	Sigmoid	29	0.3215	0.8999	0.8988	0.2632	0.0555
C25	Sigmoid	6	0.3867	0.8542	0.8525	0.3246	0.1698
C26	Sine	12	0.7582	0.5013	0.4958	0.6091	0.1740
C27	Sine	33	0.3509	0.8834	0.8821	0.2840	0.0538
C28	Sine	19	0.3083	0.9115	0.9105	0.2591	0.0551
C29	RBF	9	0.7861	0.4658	0.4598	0.6222	0.2188
C30	Sine	43	0.6179	0.6472	0.6433	0.5288	0.3813
C31	RBF	27	0.8504	0.3617	0.3545	0.6897	0.1728
C32	RBF	29	0.7731	0.4635	0.4575	0.6253	0.1407
C33	RBF	45	0.2836	0.9233	0.9225	0.2357	-0.0412
C34	RBF	13	0.3411	0.8854	0.8841	0.2878	0.0843
C35	RBF	31	0.6876	0.5854	0.5807	0.5558	0.1397
C36	RBF	41	0.5082	0.7505	0.7478	0.4120	0.2157
C37	Sine	40	0.8947	0.2588	0.2506	0.7423	0.2352
C38	RBF	46	0.7538	0.4865	0.4808	0.6137	0.2027
C39	RBF	32	0.5192	0.7503	0.7475	0.4321	0.2769
C40	RBF	48	0.9245	0.2149	0.2061	0.7654	0.1406
C41	RBF	41	0.7639	0.4682	0.4623	0.6222	0.1382
C42	Sine	27	1.3166	-0.5485	-0.5658	1.1311	0.9458
C43	Sine	16	0.3529	0.8860	0.8853	0.2835	0.0145
C44	Sine	50	0.5871	0.4444	0.4413	0.5082	0.0060
C45	RBF	14	0.7880	0.4383	0.4352	0.6368	0.0862
C46	Sine	32	0.5809	0.6844	0.6827	0.4949	0.3411
C47	Sigmoid	14	0.9140	0.2744	0.2703	0.7254	-0.0385
C48	Sine	30	0.9991	-0.0843	-0.0904	0.8444	0.2415
C49	Sigmoid	41	0.5678	0.6887	0.6870	0.4649	0.2018
C50	RBF	25	1.2058	-0.3607	-0.3682	0.9866	-0.3857
C51	Sigmoid	10	0.7670	0.4933	0.4905	0.6116	0.1945
C52	Sine	4	1.3738	-0.6689	-0.6782	1.1619	0.8980
C53	RBF	35	0.5030	0.7513	0.7499	0.4033	0.1700
C54	Sigmoid	15	0.8312	0.3861	0.3827	0.6760	0.2187
C55	Sigmoid	28	0.8964	0.1211	0.1162	0.7544	0.2129
C56	RBF	29	1.3866	-0.7731	-0.7830	1.2018	0.8996
C57	RBF	34	1.4407	-0.9865	-0.9976	1.2516	0.6482
C58	Sigmoid	7	0.5444	0.7321	0.7321	0.4422	0.2499
C59	Sine	7	1.1696	-0.2269	-0.2269	0.9503	-0.4309
C60	Sigmoid	7	0.7838	0.4445	0.4445	0.6323	0.0805
C61	Sigmoid	2	1.3804	-0.6765	-0.6765	1.1351	0.6313

Table A-10 (Continued)

C62	Sigmoid	2	1.5244	-1.0094	-1.0094	1.2323	0.1660
C63	RBF	8	1.4601	-0.8698	-0.8698	1.2669	1.0000

Table A-11: Full Result Performance at Ipoh station using Bagged ELM.

<b>Input</b>	<b>Best Activation Function</b>	<b>Best Hidden Neurons</b>	<b>RMSE</b>	<b>NSE</b>	<b>ANSE</b>	<b>MAE</b>	<b>MBE</b>
C1	RBF	41	0.1335	0.9644	0.9634	0.1158	0.0528
C2	RBF	42	0.1675	0.9444	0.9432	0.1426	0.0706
C3	Sigmoid	25	0.1434	0.9601	0.9591	0.1240	0.0613
C4	RBF	30	0.1336	0.9643	0.9635	0.1155	0.0539
C5	Sine	18	0.1612	0.9494	0.9482	0.1375	0.0548
C6	RBF	28	0.2117	0.9090	0.9069	0.1794	0.1076
C7	RBF	34	0.4229	0.6758	0.6685	0.3421	0.1317
C8	Sine	49	0.1558	0.9522	0.9514	0.1309	0.0531
C9	Sine	44	0.1891	0.9279	0.9267	0.1633	0.0836
C10	Sine	47	0.1973	0.9272	0.9260	0.1681	0.0616
C11	RBF	48	0.2539	0.8652	0.8629	0.2164	0.1202
C12	Sigmoid	19	0.5125	0.5104	0.5021	0.4162	0.1100
C13	Sigmoid	49	0.1526	0.9552	0.9544	0.1325	0.0607
C14	Sine	18	0.1566	0.9520	0.9512	0.1339	0.0469
C15	RBF	10	0.2163	0.9099	0.9083	0.1792	0.0982
C16	Sine	41	0.4492	0.6310	0.6248	0.3624	0.0326
C17	Sine	23	0.1539	0.9526	0.9518	0.1311	0.0404
C18	Sigmoid	47	0.2215	0.9042	0.9026	0.1864	0.1121
C19	Sine	39	0.4434	0.6369	0.6308	0.3581	0.0839
C20	Sigmoid	34	0.2401	0.8890	0.8871	0.2014	0.1239
C21	RBF	20	0.4234	0.6762	0.6707	0.3392	0.1618
C22	RBF	43	0.5397	0.3751	0.3645	0.4503	0.0585
C23	Sigmoid	43	0.2464	0.8822	0.8809	0.2137	0.1187
C24	Sine	36	0.2134	0.9117	0.9107	0.1841	0.0610
C25	Sine	37	0.2705	0.8547	0.8530	0.2310	0.1275
C26	Sine	41	0.6104	0.2730	0.2648	0.5019	0.0557
C27	RBF	32	0.2630	0.8661	0.8646	0.2275	0.1000
C28	Sigmoid	30	0.2522	0.8738	0.8724	0.2151	0.1328
C29	Sigmoid	27	0.5990	0.2984	0.2905	0.4858	-0.0661
C30	Sine	36	0.2952	0.8266	0.8247	0.2509	0.1338
C31	RBF	13	0.5058	0.5355	0.5303	0.4036	0.1123
C32	RBF	19	0.5671	0.3829	0.3760	0.4624	0.1138
C33	Sine	8	0.1900	0.9254	0.9245	0.1650	0.0749

Table A-11 (Continued)

C34	Sine	14	0.2062	0.9179	0.9169	0.1712	0.1134
C35	RBF	45	0.4810	0.5540	0.5490	0.3934	0.0115
C36	Sine	43	0.2808	0.8360	0.8342	0.2439	0.1639
C37	Sine	29	0.5032	0.5369	0.5317	0.4074	0.1537
C38	RBF	28	0.5120	0.5115	0.5061	0.4159	0.1590
C39	Sine	42	0.2667	0.8469	0.8452	0.2279	0.0911
C40	Sigmoid	18	0.4836	0.5768	0.5721	0.3898	0.1524
C41	RBF	24	0.5006	0.5160	0.5106	0.4074	0.1404
C42	Sine	38	0.5976	0.2420	0.2335	0.5047	0.1281
C43	RBF	24	0.3613	0.7043	0.7026	0.3198	0.0709
C44	Sine	35	0.3100	0.7967	0.7955	0.2673	0.1567
C45	Sine	22	0.6609	0.1741	0.1695	0.5441	0.1307
C46	Sine	14	0.3020	0.8240	0.8230	0.2603	0.2082
C47	RBF	14	0.6361	0.2619	0.2578	0.5160	0.1702
C48	RBF	24	0.6400	0.2136	0.2092	0.5214	0.1774
C49	RBF	16	0.3310	0.7885	0.7873	0.2852	0.1993
C50	RBF	8	0.9700	-0.6985	-0.7080	0.7805	-0.1373
C51	Sine	10	0.6164	0.3178	0.3140	0.4897	0.0248
C52	Sine	4	0.5920	0.3709	0.3674	0.4745	0.0566
C53	Sigmoid	8	0.2249	0.9023	0.9017	0.1858	0.1054
C54	Sine	11	0.4881	0.5699	0.5675	0.3922	0.1791
C55	RBF	16	0.4858	0.5705	0.5681	0.3907	0.1653
C56	Sigmoid	5	0.6149	0.3080	0.3041	0.5091	0.3801
C57	Sigmoid	8	0.5772	0.4004	0.3970	0.4731	0.2876
C58	RBF	29	0.3454	0.7641	0.7641	0.2966	0.2344
C59	Sigmoid	3	0.9901	-0.7630	-0.7630	0.7818	0.0560
C60	Sine	7	0.6251	0.2961	0.2961	0.4956	0.1695
C61	RBF	8	0.8404	-0.3808	-0.3808	0.7029	0.3265
C62	Sigmoid	2	1.2234	-1.6912	-1.6912	0.9784	-0.2840
C63	RBF	3	0.6209	0.2946	0.2946	0.5131	0.3739

Table A-12: Full Result Performance at KLIA Sepang station using Bagged ELM.

<b>Input</b>	<b>Best Activation Function</b>	<b>Best Hidden Neurons</b>	<b>RMSE</b>	<b>NSE</b>	<b>ANSE</b>	<b>MAE</b>	<b>MBE</b>
C1	Sine	34	0.4859	0.7588	0.7520	0.4314	0.3072
C2	RBF	43	0.5249	0.7219	0.7157	0.4625	0.3555
C3	Sine	32	0.5016	0.7384	0.7325	0.4451	0.3257

Table A-12 (Continued)

C4	Sigmoid	49	0.4914	0.7556	0.7501	0.4363	0.3238
C5	RBF	41	0.4784	0.7579	0.7525	0.4196	0.2594
C6	Sine	50	0.6000	0.6395	0.6313	0.5290	0.3806
C7	Sine	35	0.9057	0.1633	0.1444	0.7736	0.5112
C8	Sigmoid	47	0.5091	0.7318	0.7272	0.4458	0.3730
C9	Sine	43	0.5252	0.7200	0.7153	0.4614	0.3788
C10	Sine	43	0.5630	0.6717	0.6662	0.4941	0.3707
C11	RBF	22	0.6249	0.6078	0.6012	0.5495	0.4240
C12	RBF	28	0.8823	0.2446	0.2318	0.7288	0.2219
C13	Sine	44	0.4986	0.7479	0.7436	0.4407	0.3115
C14	RBF	45	0.4919	0.7493	0.7451	0.4320	0.3100
C15	Sine	39	0.6519	0.5568	0.5493	0.5732	0.4655
C16	RBF	36	0.9263	0.1372	0.1227	0.7881	0.2733
C17	Sine	16	0.5077	0.7376	0.7332	0.4464	0.3074
C18	Sigmoid	43	0.5990	0.6345	0.6283	0.5238	0.3873
C19	RBF	31	0.9126	0.1792	0.1654	0.7751	0.3194
C20	Sigmoid	43	0.7130	0.4942	0.4857	0.6214	0.5634
C21	Sigmoid	48	0.9151	0.1562	0.1420	0.7717	0.2886
C22	Sine	24	0.9651	0.0797	0.0642	0.8162	0.5172
C23	Sigmoid	7	0.5387	0.6980	0.6947	0.4627	0.3294
C24	Sine	21	0.5791	0.6670	0.6633	0.5071	0.3738
C25	Sine	47	0.6380	0.5631	0.5582	0.5555	0.4519
C26	RBF	17	0.8978	0.2314	0.2228	0.7389	0.0980
C27	Sine	25	0.5849	0.6583	0.6544	0.5062	0.3818
C28	RBF	49	0.5811	0.6477	0.6437	0.5049	0.3330
C29	Sine	18	0.8912	0.2526	0.2443	0.7074	0.0447
C30	Sigmoid	43	0.8171	0.3197	0.3121	0.7223	0.6570
C31	Sine	9	0.8790	0.2603	0.2520	0.7209	0.2647
C32	RBF	9	0.9194	0.1974	0.1885	0.7480	0.2083
C33	Sine	35	0.5270	0.7184	0.7152	0.4670	0.3035
C34	Sine	29	0.6652	0.5237	0.5183	0.5811	0.4991
C35	RBF	33	0.9399	0.0903	0.0802	0.8036	0.2266
C36	Sine	47	0.7165	0.4751	0.4693	0.6203	0.5364
C37	Sigmoid	37	1.0087	-0.1298	-0.1424	0.8682	0.3391
C38	Sigmoid	38	1.0864	-0.2584	-0.2725	0.9407	0.3534
C39	Sine	26	0.7279	0.4656	0.4597	0.6305	0.5655
C40	RBF	35	0.9615	0.0663	0.0558	0.8103	0.2904
C41	RBF	24	0.9340	0.1319	0.1222	0.7831	0.4261
C42	RBF	41	1.2907	-0.7781	-0.7979	1.1214	0.7764
C43	RBF	14	0.6099	0.6227	0.6206	0.5272	0.3818

Table A-12 (Continued)

C44	Sine	34	0.7249	0.3121	0.3083	0.6278	0.5479
C45	Sigmoid	9	0.9256	0.1946	0.1902	0.7376	0.1888
C46	Sigmoid	32	0.8172	0.2283	0.2240	0.7234	0.4877
C47	Sigmoid	14	0.9735	0.0702	0.0650	0.8042	0.2836
C48	Sigmoid	8	0.9524	0.1299	0.1251	0.7888	0.1823
C49	Sigmoid	39	0.9552	-0.1893	-0.1959	0.8575	0.6025
C50	Sigmoid	21	1.2843	-0.7138	-0.7234	1.0651	-0.1672
C51	Sigmoid	18	0.9503	0.1284	0.1236	0.7742	-0.0455
C52	Sine	38	1.8166	-2.7513	-2.7722	1.6122	1.1807
C53	Sine	16	0.7496	0.4356	0.4325	0.6512	0.5759
C54	RBF	14	0.8852	0.2306	0.2263	0.7398	0.2119
C55	Sigmoid	23	1.0483	-0.2221	-0.2289	0.8934	0.4912
C56	RBF	24	1.3061	-0.9325	-0.9432	1.1324	0.6003
C57	RBF	33	1.5318	-1.7996	-1.8151	1.3507	0.9104
C58	RBF	11	0.7828	0.3927	0.3927	0.6757	0.5687
C59	Sigmoid	6	1.3167	-0.8029	-0.8029	1.0993	-0.1888
C60	Sine	4	0.9214	0.1997	0.1997	0.7434	0.1411
C61	Sigmoid	4	1.6342	-1.5132	-1.5132	1.3898	1.2222
C62	Sigmoid	4	1.6355	-1.5047	-1.5047	1.3237	-0.3071
C63	Sigmoid	11	1.1953	-0.4449	-0.4449	1.0023	0.6774

Table A-13: Full Result Performance at Lubok Merbau station using Bagged ELM.

<b>Input</b>	<b>Best Activation Function</b>	<b>Best Hidden Neurons</b>	<b>RMSE</b>	<b>NSE</b>	<b>ANSE</b>	<b>MAE</b>	<b>MBE</b>
C1	Sine	26	0.1630	0.9509	0.9494	0.1393	-0.0883
C2	Sine	30	0.1694	0.9521	0.9510	0.1414	-0.0488
C3	Sine	30	0.1604	0.9533	0.9522	0.1374	-0.0845
C4	Sigmoid	9	0.1662	0.9509	0.9498	0.1400	-0.0380
C5	RBF	19	0.1755	0.9425	0.9412	0.1516	-0.0834
C6	Sine	19	0.1795	0.9442	0.9429	0.1490	-0.0755
C7	Sine	26	0.3799	0.7732	0.7678	0.3030	-0.0078
C8	RBF	23	0.1639	0.9549	0.9541	0.1360	-0.0528
C9	RBF	17	0.1735	0.9511	0.9502	0.1455	-0.0386
C10	RBF	23	0.1848	0.9352	0.9340	0.1557	-0.0470
C11	RBF	31	0.1685	0.9529	0.9521	0.1370	-0.0393
C12	Sine	23	0.4995	0.6000	0.5929	0.4006	-0.0620
C13	Sigmoid	8	0.1733	0.9480	0.9471	0.1443	-0.0449

Table A-13 (Continued)

C14	RBF	25	0.1891	0.9151	0.9136	0.1650	-0.1015
C15	Sine	17	0.1717	0.9511	0.9502	0.1399	-0.0370
C16	Sine	24	0.3899	0.7616	0.7574	0.3090	-0.0181
C17	Sine	14	0.1802	0.9381	0.9370	0.1539	-0.1013
C18	Sigmoid	7	0.1820	0.9435	0.9425	0.1508	0.0018
C19	RBF	21	0.3843	0.7665	0.7623	0.3068	-0.0347
C20	RBF	38	0.1972	0.9359	0.9347	0.1604	-0.0566
C21	RBF	19	0.3723	0.7817	0.7779	0.2968	-0.0110
C22	Sigmoid	19	0.4488	0.6830	0.6773	0.3574	0.0133
C23	Sine	26	0.2115	0.9075	0.9064	0.1770	-0.0191
C24	RBF	15	0.1946	0.9208	0.9199	0.1661	-0.0564
C25	Sigmoid	13	0.1703	0.9529	0.9523	0.1388	-0.0204
C26	RBF	13	0.5260	0.5609	0.5557	0.4185	-0.0726
C27	RBF	23	0.2182	0.8928	0.8916	0.1880	-0.0712
C28	Sigmoid	20	0.1734	0.9510	0.9504	0.1422	-0.0374
C29	RBF	18	0.6615	0.2830	0.2745	0.5330	-0.1501
C30	RBF	48	0.2357	0.8900	0.8887	0.1947	-0.0080
C31	RBF	12	0.4957	0.6087	0.6041	0.3985	0.0066
C32	RBF	25	0.6007	0.3787	0.3714	0.4924	-0.1529
C33	Sine	8	0.1743	0.9458	0.9452	0.1447	-0.0678
C34	Sine	12	0.1840	0.9438	0.9431	0.1512	-0.0287
C35	Sine	16	0.4029	0.7284	0.7252	0.3225	-0.0041
C36	Sine	36	0.1928	0.9391	0.9384	0.1550	-0.0588
C37	Sigmoid	24	0.4198	0.6950	0.6914	0.3410	-0.0623
C38	Sigmoid	17	0.4494	0.6831	0.6793	0.3562	-0.0110
C39	Sine	8	0.2074	0.9289	0.9280	0.1656	-0.0571
C40	RBF	15	0.3836	0.7703	0.7676	0.3057	-0.0275
C41	RBF	18	0.4517	0.6726	0.6688	0.3599	-0.0531
C42	RBF	19	0.4943	0.5877	0.5828	0.4010	-0.0240
C43	RBF	20	0.2409	0.8662	0.8654	0.2033	-0.0300
C44	Sine	9	0.2017	0.9353	0.9349	0.1634	0.0528
C45	Sine	10	0.6948	0.1482	0.1432	0.5616	0.0064
C46	RBF	44	0.2654	0.8432	0.8423	0.2253	-0.0442
C47	RBF	8	0.5604	0.5019	0.4990	0.4418	-0.0121
C48	RBF	23	0.6229	0.3724	0.3688	0.5070	-0.1041
C49	RBF	31	0.2868	0.7349	0.7334	0.2422	-0.0251
C50	RBF	8	0.8797	-0.2187	-0.2259	0.7064	-0.4051
C51	RBF	35	0.9299	-0.8916	-0.9026	0.7934	-0.1468
C52	RBF	23	0.7024	-0.0763	-0.0826	0.5914	-0.1497
C53	Sigmoid	6	0.2064	0.9311	0.9307	0.1655	-0.0363

Table A-13 (Continued)

C54	Sigmoid	7	0.4044	0.7439	0.7424	0.3257	-0.0468
C55	RBF	8	0.4568	0.6725	0.6706	0.3632	0.0333
C56	Sine	11	0.4920	0.6223	0.6201	0.3938	0.0414
C57	Sine	13	0.5048	0.5956	0.5933	0.4033	-0.0182
C58	Sigmoid	33	0.2540	0.8863	0.8863	0.2111	0.0915
C59	Sine	4	0.8878	-0.2435	-0.2435	0.7067	-0.3710
C60	Sine	21	0.6793	0.2709	0.2709	0.5423	0.0686
C61	RBF	8	0.6670	0.2906	0.2906	0.5364	-0.0308
C62	Sine	1	1.3262	-1.8127	-1.8127	1.0587	-0.3407
C63	Sine	5	0.5052	0.5994	0.5994	0.4030	0.0146

Table A-14: Full Result Performance at Pulau Langkawi station using Bagged ELM.

<b>Input</b>	<b>Best Activation Function</b>	<b>Best Hidden Neurons</b>	<b>RMSE</b>	<b>NSE</b>	<b>ANSE</b>	<b>MAE</b>	<b>MBE</b>
C1	Sigmoid	22	0.2317	0.9477	0.9462	0.2004	0.1518
C2	Sigmoid	19	0.2653	0.9345	0.9330	0.2268	0.1552
C3	Sigmoid	23	0.2383	0.9445	0.9432	0.2062	0.1509
C4	Sine	32	0.2298	0.9470	0.9458	0.2000	0.1568
C5	Sigmoid	21	0.2928	0.9239	0.9221	0.2511	0.1226
C6	Sigmoid	37	0.3486	0.8967	0.8944	0.2933	0.2519
C7	Sine	39	0.5849	0.7292	0.7231	0.4685	0.1238
C8	Sine	13	0.2824	0.9278	0.9266	0.2411	0.1663
C9	Sigmoid	34	0.2682	0.9370	0.9359	0.2287	0.1811
C10	Sine	48	0.3589	0.8854	0.8835	0.3047	0.2263
C11	Sigmoid	18	0.3494	0.8933	0.8915	0.2908	0.2302
C12	RBF	33	0.6278	0.6877	0.6824	0.5000	0.0776
C13	RBF	32	0.2400	0.9434	0.9425	0.2080	0.1550
C14	Sine	19	0.3000	0.9207	0.9193	0.2569	0.1315
C15	Sine	37	0.3701	0.8840	0.8820	0.3083	0.2685
C16	Sine	41	0.6192	0.6960	0.6908	0.4945	0.1224
C17	Sine	45	0.3117	0.9146	0.9131	0.2659	0.1940
C18	Sine	21	0.3547	0.8916	0.8897	0.2976	0.2577
C19	Sine	44	0.6186	0.6947	0.6895	0.4962	0.1056
C20	Sine	21	0.6341	0.6612	0.6555	0.5385	0.4552
C21	Sigmoid	50	0.6670	0.6387	0.6326	0.5304	0.1524
C22	Sigmoid	35	0.6900	0.6212	0.6148	0.5584	0.3076
C23	Sine	42	0.3539	0.8850	0.8837	0.3032	0.2132

Table A-14 (Continued)

C24	Sine	28	0.3450	0.8993	0.8982	0.2896	0.1932
C25	Sigmoid	13	0.3325	0.9087	0.9077	0.2727	0.2076
C26	Sine	17	0.7045	0.6065	0.6021	0.5753	-0.0788
C27	Sine	26	0.3660	0.8861	0.8848	0.3065	0.2200
C28	Sigmoid	19	0.3520	0.8935	0.8923	0.2939	0.2374
C29	Sine	30	0.7684	0.5283	0.5230	0.6157	-0.0076
C30	Sigmoid	16	0.9061	0.3343	0.3268	0.7885	0.7273
C31	Sigmoid	44	0.7971	0.4705	0.4646	0.6389	-0.0155
C32	RBF	30	0.6891	0.6230	0.6188	0.5511	0.1221
C33	Sine	40	0.3363	0.8987	0.8976	0.2915	0.2017
C34	Sigmoid	15	0.4021	0.8613	0.8598	0.3378	0.2965
C35	RBF	38	0.6112	0.7039	0.7006	0.4913	0.0994
C36	RBF	40	0.6891	0.6056	0.6012	0.5999	0.5175
C37	Sigmoid	28	0.7197	0.5840	0.5794	0.5839	0.1571
C38	RBF	34	0.7390	0.5484	0.5434	0.6059	0.3279
C39	Sine	14	0.6259	0.6678	0.6641	0.5338	0.4382
C40	Sigmoid	42	0.7288	0.5596	0.5547	0.5858	0.0529
C41	Sigmoid	38	0.6716	0.6425	0.6385	0.5460	0.2009
C42	Sigmoid	34	0.9569	0.2411	0.2326	0.7891	0.4607
C43	Sine	42	0.4891	0.7532	0.7518	0.4204	0.1338
C44	Sine	32	0.4895	0.7775	0.7763	0.4153	0.2848
C45	Sine	13	0.7968	0.4927	0.4899	0.6456	-0.0099
C46	Sigmoid	38	0.9984	0.1427	0.1380	0.8830	0.7924
C47	Sigmoid	44	1.2204	-0.4375	-0.4455	1.0345	0.1076
C48	RBF	17	0.6916	0.6206	0.6185	0.5566	0.0928
C49	Sine	7	1.1457	-0.0368	-0.0425	0.9997	0.9663
C50	RBF	15	1.2453	-0.2480	-0.2549	1.0356	-0.5761
C51	Sine	24	0.8281	0.4391	0.4360	0.6689	0.0250
C52	RBF	15	1.1168	-0.0077	-0.0133	0.9230	0.5447
C53	Sine	31	0.6794	0.6158	0.6136	0.5855	0.4988
C54	Sine	15	0.6927	0.6200	0.6179	0.5558	0.1999
C55	Sigmoid	18	0.6588	0.6585	0.6566	0.5358	0.2336
C56	RBF	22	0.9711	0.2363	0.2321	0.7982	0.5532
C57	Sigmoid	23	0.9794	0.2184	0.2140	0.8081	0.3781
C58	RBF	41	1.2269	-0.1994	-0.1994	1.0861	1.0263
C59	Sine	5	1.3201	-0.4096	-0.4096	1.1207	-0.6622
C60	RBF	11	0.8737	0.3728	0.3728	0.7114	0.0537
C61	RBF	6	1.2395	-0.2234	-0.2234	1.0297	0.7536
C62	RBF	3	1.5638	-0.9472	-0.9472	1.2613	0.0225
C63	RBF	7	0.9354	0.3051	0.3051	0.7634	0.5056

Table A-15: Full Result Performance at Sitiawan station using Bagged ELM.

<b>Input</b>	<b>Best Activation Function</b>	<b>Best Hidden Neurons</b>	<b>RMSE</b>	<b>NSE</b>	<b>ANSE</b>	<b>MAE</b>	<b>MBE</b>
C1	RBF	15	0.3371	0.8052	0.7993	0.2975	0.1963
C2	RBF	19	0.3270	0.8208	0.8165	0.2850	0.1599
C3	Sigmoid	22	0.3271	0.8165	0.8122	0.2868	0.1845
C4	RBF	12	0.3432	0.7974	0.7926	0.3034	0.1943
C5	RBF	12	0.3429	0.7985	0.7937	0.3016	0.1941
C6	Sine	16	0.3453	0.7988	0.7940	0.2991	0.2203
C7	Sine	17	0.5935	0.4104	0.3963	0.5013	0.4229
C8	RBF	46	0.3269	0.8187	0.8155	0.2845	0.1754
C9	Sigmoid	50	0.3272	0.8198	0.8166	0.2852	0.1700
C10	Sine	49	0.3159	0.8297	0.8266	0.2720	0.1693
C11	RBF	14	0.3367	0.8095	0.8061	0.2899	0.1859
C12	RBF	16	0.5755	0.4512	0.4414	0.4755	0.3116
C13	RBF	22	0.3302	0.8124	0.8090	0.2892	0.1863
C14	RBF	9	0.3529	0.7860	0.7822	0.3091	0.2065
C15	RBF	12	0.3274	0.8173	0.8141	0.2813	0.1907
C16	Sigmoid	5	0.5825	0.4170	0.4066	0.4883	0.3056
C17	Sine	22	0.3201	0.8246	0.8215	0.2795	0.1760
C18	RBF	12	0.3349	0.8114	0.8081	0.2891	0.2053
C19	RBF	19	0.6170	0.3672	0.3559	0.5198	0.4294
C20	Sigmoid	41	0.3434	0.7983	0.7947	0.2975	0.2036
C21	Sine	6	0.6303	0.3085	0.2962	0.5394	0.4236
C22	RBF	11	0.6974	0.2039	0.1897	0.5872	0.4807
C23	RBF	15	0.3175	0.8333	0.8313	0.2704	0.1698
C24	Sine	13	0.3229	0.8242	0.8222	0.2783	0.1639
C25	RBF	9	0.3400	0.8067	0.8044	0.2915	0.1666
C26	RBF	6	0.6695	0.2638	0.2551	0.5556	0.3447
C27	RBF	48	0.3219	0.8230	0.8210	0.2760	0.1533
C28	Sigmoid	50	0.3526	0.7922	0.7897	0.3075	0.2078
C29	Sigmoid	5	0.6564	0.2878	0.2794	0.5359	-0.0731
C30	Sine	21	0.3382	0.8046	0.8022	0.2899	0.1848
C31	Sine	10	0.5864	0.4306	0.4238	0.4820	0.3055
C32	Sigmoid	5	0.6456	0.3216	0.3136	0.5269	0.2553
C33	Sine	10	0.3313	0.8083	0.8061	0.2888	0.1876
C34	Sigmoid	8	0.3269	0.8201	0.8180	0.2804	0.2007
C35	RBF	13	0.6497	0.3091	0.3010	0.5476	0.4620
C36	RBF	38	0.3334	0.8108	0.8086	0.2881	0.1727
C37	RBF	19	0.6651	0.2612	0.2525	0.5575	0.3911

Table A-15 (Continued)

C38	Sigmoid	23	0.6897	0.2203	0.2111	0.5716	0.3602
C39	RBF	42	0.3202	0.8242	0.8221	0.2739	0.1731
C40	RBF	14	0.6067	0.3846	0.3773	0.5041	0.3902
C41	Sigmoid	47	0.7441	0.0431	0.0319	0.6288	0.2694
C42	RBF	8	0.7085	0.1734	0.1637	0.5979	0.4822
C43	RBF	10	0.3342	0.8127	0.8116	0.2846	0.1831
C44	Sine	6	0.3493	0.8036	0.8024	0.2975	0.2109
C45	Sine	4	0.6532	0.3058	0.3017	0.5316	0.1015
C46	RBF	38	0.3837	0.7102	0.7086	0.3364	0.1900
C47	Sine	12	0.7638	0.0276	0.0219	0.6404	0.3455
C48	Sine	11	0.7522	0.0850	0.0796	0.6173	0.3914
C49	Sigmoid	25	0.3672	0.7623	0.7609	0.3169	0.2043
C50	Sigmoid	21	1.0065	-0.8611	-0.8720	0.8321	-0.0988
C51	RBF	16	0.7896	-0.0178	-0.0238	0.6449	0.3380
C52	Sine	3	0.7300	0.0643	0.0588	0.6056	0.1948
C53	Sine	24	0.3355	0.7981	0.7969	0.2887	0.1961
C54	Sigmoid	12	0.6552	0.2921	0.2880	0.5446	0.3981
C55	Sigmoid	3	0.6381	0.3271	0.3231	0.5233	0.3015
C56	Sigmoid	28	0.9200	-0.5221	-0.5310	0.7929	0.4972
C57	Sigmoid	6	0.7094	0.1743	0.1694	0.5913	0.4597
C58	Sigmoid	27	0.4002	0.7331	0.7331	0.3449	0.2660
C59	RBF	7	0.8927	-0.2989	-0.2989	0.7051	0.1866
C60	Sine	5	0.8348	-0.1328	-0.1328	0.6876	0.4960
C61	Sine	2	0.7802	-0.0139	-0.0139	0.6265	0.0607
C62	Sigmoid	2	1.2704	-1.6969	-1.6969	1.0331	-0.0135
C63	RBF	3	0.8234	-0.1202	-0.1202	0.6993	0.5933

Table A-16: Full Result Performance at Subang station using Bagged ELM.

<b>Input</b>	<b>Best Activation Function</b>	<b>Best Hidden Neurons</b>	<b>RMSE</b>	<b>NSE</b>	<b>ANSE</b>	<b>MAE</b>	<b>MBE</b>
C1	Sine	38	0.2517	0.9207	0.9184	0.2098	0.0555
C2	Sigmoid	10	0.2534	0.9270	0.9254	0.2051	0.0464
C3	Sine	41	0.2645	0.9175	0.9156	0.2235	0.0452
C4	RBF	45	0.2643	0.9146	0.9126	0.2254	0.0467
C5	RBF	45	0.2557	0.9207	0.9189	0.2122	0.0512
C6	Sine	18	0.2745	0.9156	0.9137	0.2195	0.0498
C7	RBF	47	0.9314	0.0889	0.0683	0.7685	0.5147
C8	Sine	19	0.2802	0.9115	0.9100	0.2340	0.0780
C9	RBF	13	0.2435	0.9317	0.9305	0.1951	0.0558

Table A-16 (Continued)

C10	RBF	16	0.2825	0.9110	0.9095	0.2325	0.0621
C11	RBF	21	0.2843	0.9124	0.9109	0.2308	0.0574
C12	RBF	26	0.9299	0.0975	0.0823	0.7649	0.3539
C13	RBF	15	0.2660	0.9083	0.9067	0.2200	0.1037
C14	Sigmoid	48	0.2634	0.9192	0.9178	0.2192	0.0580
C15	Sigmoid	9	0.2765	0.9164	0.9150	0.2201	0.0923
C16	Sigmoid	38	0.9396	0.0577	0.0418	0.7903	0.5742
C17	RBF	15	0.2570	0.9216	0.9203	0.2131	0.0721
C18	RBF	24	0.2715	0.9177	0.9163	0.2181	0.0393
C19	Sigmoid	47	0.8771	0.1912	0.1775	0.7237	0.4770
C20	Sigmoid	13	0.2746	0.9170	0.9156	0.2210	0.0538
C21	Sigmoid	29	0.9464	0.0485	0.0324	0.7882	0.5385
C22	RBF	7	0.9419	0.0172	0.0006	0.7890	0.5195
C23	Sigmoid	10	0.2958	0.9038	0.9027	0.2435	0.0847
C24	RBF	22	0.2831	0.9101	0.9091	0.2333	0.0539
C25	RBF	17	0.3015	0.9020	0.9009	0.2450	0.0683
C26	Sigmoid	47	0.8984	0.1552	0.1457	0.7297	0.2827
C27	Sigmoid	6	0.2678	0.9217	0.9208	0.2160	0.0080
C28	Sine	7	0.2781	0.9164	0.9155	0.2237	0.0426
C29	Sine	32	0.9259	0.0939	0.0838	0.7423	0.1537
C30	Sigmoid	6	0.2991	0.9039	0.9028	0.2442	0.0507
C31	Sigmoid	9	0.9938	-0.0295	-0.0410	0.8176	0.3709
C32	RBF	5	0.9445	0.0697	0.0593	0.7665	0.2633
C33	Sigmoid	44	0.2625	0.9194	0.9185	0.2168	0.0226
C34	Sigmoid	38	0.3041	0.8986	0.8974	0.2460	0.0895
C35	RBF	48	0.9027	0.1354	0.1257	0.7434	0.4837
C36	RBF	15	0.2924	0.9056	0.9045	0.2369	0.0837
C37	RBF	42	0.9514	0.0124	0.0013	0.7958	0.4710
C38	Sine	6	0.9581	0.0345	0.0237	0.8020	0.5611
C39	RBF	12	0.2790	0.9128	0.9119	0.2257	0.0295
C40	Sine	15	0.9418	0.0642	0.0537	0.7919	0.5637
C41	Sigmoid	4	0.9096	0.1207	0.1109	0.7467	0.3026
C42	Sine	9	1.0851	-0.2179	-0.2315	0.9279	0.7660
C43	Sigmoid	4	0.3107	0.8964	0.8958	0.2510	0.0121
C44	Sigmoid	6	0.3348	0.8798	0.8792	0.2713	0.1522
C45	Sine	12	0.9611	0.0446	0.0392	0.7775	0.2868
C46	RBF	6	0.3086	0.8973	0.8967	0.2519	0.0971
C47	Sigmoid	34	1.0373	-0.1207	-0.1269	0.8435	0.2389
C48	Sigmoid	3	0.9827	0.0053	-0.0003	0.7927	0.1586
C49	Sigmoid	5	0.2863	0.9118	0.9113	0.2272	0.0168

Table A-16 (Continued)

C50	RBF	28	1.1345	-0.3424	-0.3498	0.9190	-0.0462
C51	Sigmoid	4	1.0419	-0.1228	-0.1290	0.8416	-0.1699
C52	Sine	5	1.0435	-0.1274	-0.1337	0.8470	0.5191
C53	Sine	18	0.3244	0.8848	0.8841	0.2641	0.0948
C54	RBF	15	0.9324	0.0763	0.0712	0.7780	0.4970
C55	Sigmoid	3	1.0055	-0.0779	-0.0839	0.8515	0.6604
C56	Sine	5	1.1346	-0.3349	-0.3423	0.9708	0.7899
C57	Sine	40	1.1102	-0.3019	-0.3091	0.9322	0.5582
C58	Sine	5	0.3795	0.8466	0.8466	0.3105	0.1288
C59	Sine	4	1.3120	-0.7716	-0.7716	1.0524	0.2843
C60	Sine	2	1.0305	-0.1045	-0.1045	0.8332	-0.1764
C61	Sigmoid	5	1.2379	-0.5964	-0.5964	1.0277	0.7749
C62	Sine	2	1.5384	-1.4703	-1.4703	1.2552	0.2625
C63	Sigmoid	3	1.2039	-0.5171	-0.5171	1.0398	0.8523